Development and biomedical applications of solid phase micro-extraction (bio-SPME) chemical biopsy devices

by

Runshan Will Jiang

A thesis
presented to the University of Waterloo
in fulfilment of the
thesis requirement for the degree of
Doctor of Philosophy
in
Chemistry

Waterloo, Ontario, Canada, 2024

© Runshan Will Jiang 2024

Examining committee membership

The following served on the Examining Committee for this thesis. The decision of the Examining Committee is by majority vote.

External Examiner	Prof. Jonathan V. Sweedler Professor, Chair, and Acting Head Department of Chemistry, University of Illinois Editor-in-Chief, Analytical Chemistry, ACS
Supervisor	Prof. Janusz Pawliszyn Professor and Canada Research Chair Department of Chemistry, University of Waterloo
Internal Member	Prof. Jean Duhamel Professor and Director, The Institute for Polymer Research Department of Chemistry, University of Waterloo
Internal Member	Dr. Richard Smith Senior Manager, University of Waterloo Mass Spectrometry Facility Department of Chemistry, University of Waterloo
Internal-external Member	Prof. Andrew Doxey Associate Professor, University Research Chair, and Director, Biology Core Facility Department of Biology, University of Waterloo

Author's declaration

This thesis consists of material all of which I authored or co-authored: see Statement of Contributions included in the thesis. This is a true copy of the thesis, including any required final revisions, as accepted by my examiners.

I understand that my thesis may be made electronically available to the public.

Statement of contributions

Chapter 1: Runshan Will Jiang was the sole author under the supervision of Prof. Pawliszyn.

Chapter 2: Runshan Will Jiang was the primary investigator for the method development, fabrication, and validation of the in vivo recessed SPME and push-pull SPME sampling devices including the optimization of the synthesis of the wHLB extraction phase particles. Clinical and Pre-clinical applications of in vivo SPME sampling took place at Princess Margaret Cancer Centre, (Toronto General Hospital, University Health Network) and Roswell Park Comprehensive Cancer Center. Runshan will Jiang was the sole writing author of this chapter. The fabrication of the devices and some proof-of-concept studies have already been published as a US utility patent.

Publication number: US 2023/0273195 A1.

https://image-ppubs.uspto.gov/dirsearch-public/print/downloadPdf/20230273195

Chapter 3: Runshan Will Jiang and Dr. Jaroch were the primary co-investigators for the experimental design and experimentation under the supervision of Prof. Pawliszyn; Runshan Will Jiang was the sole writing author of this chapter. Content of this chapter is already published in the Journal of Pharmaceutical Analysis.

Jiang RW, Jaroch K, Pawliszyn J. Solid-phase microextraction of endogenous metabolites from intact tissue validated using a Biocrates standard reference method kit. J. Pharm. Anal. 2023. DOI: 10.1016/j.jpha.2022.09.002

Chapter 4: Runshan Will Jiang was the primary investigator for the fabrication of SPME sampling devices; Runshan Will Jiang, Prof. Marin and Dr. Jaroch were co-investigators in the experimental design of the study presented in this chapter. Prof. Marin was the primary investigator for the sampling and data collection at the College of Dentistry (University of Saskatchewan). The study was conducted under the co-supervision of Prof. Siqueira and Prof. Pawliszyn. Runshan Will Jiang was the sole writing author of this chapter which contains contents already submitted to Analytical Chemistry (under journal editorial review).

Chapter 5: Runshan Will Jiang was the primary investigator for the fabrication of SPME sampling devices, ex vivo experiments, and SPME training at Toronto General Hospital (University Health Network). Clinical sampling took place at Princess Margaret Cancer Centre (Toronto General Hospital, University Health Network). Runshan Will Jiang was the sole writing author of this chapter. This chapter contains material already submitted to Journal of thoracic oncology (under journal editorial review).

Abstract

Micro-sampling is a vital component in modern diagnostics and personalized medicine. In vivo SPME is a novel branch of biomedical applications of SPME (Bio-SPME) that offers unique advantages complementary to existing in vivo micro-sampling techniques such as micro tissue biopsy and microdialysis. When coupled with powerful modern detection methods, such as mass spectrometry, the minimally invasiveness and convenient sample-cleanup of in vivo chemical biopsy SPME enable the rapid analysis of exogenous and endogenous analytes from a biological system in vivo. In vivo SPME has seen success in numerous clinical applications from therapeutic drug monitoring (TDM) to untargeted metabolomic/lipidomic fingerprinting. While the scope of theoretical considerations extends deep into the realm of complex physical chemistry, bio-SPME and in vivo SPME can still be executed by medical personnel with limited theoretical knowledge as long as a few key experimental parameters are controlled, such as extraction time. Chapter 2 details the fabrication of a novel recessed SPME chemical biopsy probe and a push-pull microsyringe sampling device. Compared to conventional in vivo sampling tools, the latest devices offer superior physical robustness with a convenient chemical sorbent that does not require solvent activation. Such devices have been successfully implemented in human in vivo studies which are also included in this chapter. Chapter 3 presents a proof-of-concept study showing the importance of non-destructive sampling (ie. in vivo SPME) in untargeted metabolomics using ovine lung tissue as a model coupled with a commercial metabolomics kit. Chapter 4 is another

proof-of-concept study which explores the applicability of bio-SPME in proteomics which was thought to be impossible. Various sample preparation and device fabrication strategies such as protein digestion and porous coating were employed to achieve protein identification in clinical SARS-CoV-2 patient saliva samples. Chapter 5 of the thesis addresses some of the flaws with previous in vivo applications of SPME, provides strategies to overcome them, and showcases numerous clinical in vivo applications with the improved calibration strategies. In short, this thesis work offers a comprehensive strategy for various in vivo and ex vivo bio-SPME applications.

Acknowledgements

I would like to give my most sincere gratitude to the following individuals who were vital to the completion of this PhD thesis. Lists are in chronological order.

Supervisor

Prof. Janusz Pawliszyn

PhD Advisory Committee

Prof. Andrew Doxey, Prof. Jean Duhamel, Dr. Richard Smith

Previous PhD Advisory Committee members

Prof. Michael Palmer, Prof. Wojciech Gabryelski

External Committee

Prof. Jonathan V. Sweedler

Medical Collaborators

Toronto General Hospital (Prof. Marcelo Cypel's and Prof. Carlos Ibarra's teams)

College of Dentistry, University of Saskatchewan (Prof. Walter Siqueira's team)

Roswell Park Cancer Center (Dr. Todd Demmy and Dr. Gal Shafirstein's team)

UW Science Technical Services

Hiruy Haile, Krunomir Dvorski, Andrew Dube, and Jason Dekorte

Bionanotechnology & Interfaces Laboratory

Prof. Juewen Liu and Dr. Mohamad Zandieh

Pawliszyn Research Group

Dr. Nikita Looby, Dr. Sofia Lendor, Alexander Kasperkiewicz (MSc), Dr. Varoon Singh, Dr. Emir Nazdrajic, Dr. Hernando Rosales, Dr. Karol Jaroch, and Dr. Wei Zhou.

Table of contents

Examining committee membership.....ii

Author's declaration.....iii

Statement of contributions.....iv

Abstract.....vi

Acknowledgements.....viii

List of figures.....xiv

List of tables.....xxi

List of abbreviations.....xxii

Chapter 1. Introduction.....1

1.1 In vivo Sampling.....1

1.2 Fundamentals of bio-SPME.....4

1.3 Extraction kinetics of bio-SPME.....6

1.4 Quantification and calibration of in vivo SPME.....9

1.5 In vivo SPME device and extraction phase coating.....11

1.6 Thesis statement.....14

Chapter 2. Minimally invasive solid-phase microextraction (SPME) chemical biopsy devices for in vivo biomedical applications.....15

2.1 Preamble.....15

2.2 Introduction.....15

2.3 Materials and methods.....19

2.3.1 Materials and chemicals.....19

2.3.2 Particle characterization.....20

2.3.3 Etching.....20
2.3.4 Coating.....21
2.3.5 Push-pull bio-SPME microsyringe.....22
2.3.6 Cleaning.....23
2.3.7 Matrix-matched calibrations.....24
2.3.8 Extraction parameters.....24
2.3.9 Liquid chromatography and mass spectrometry (LC-MS).....26
2.3.10 Microfluidic open interface (MOI)-MS.....26
2.4 Results and discussion.....27
2.4.1 Creating the recess….....27
2.4.2 Puncturing test.....28
2.4.3 Autoclaved coating performance.....30
2.4.4 Synthesis and characterization of wHLB.....31
2.4.5 Clinical and pre-clinical applications.....37
2.4.6 Coupling with direct-MS.....40
2.4.7 Push-pull SPME microsyringe.....43
2.5 Conclusion.....45
Chapter 3. Solid-phase microextraction (SPME) of endogenous metabolites from intact tissue validated using a Biocrates standard reference method kit.....47
3.1 Preamble.....47
3.2 Introduction.....47
3.3 Materials and methods.....52

3.3.1 Materials and chemicals.....52
3.3.2 Liquid chromatography-mass spectrometry (LC-MS), flow injection analysis (FIA).....53
3.3.3 Sample preparations.....54
3.3.4 SLE- and SPME- AbsoluteIDQ p180 kit protocols.....55
3.3.5 Data processing and statistical analysis.....56
3.4 Results and discussion.....57
3.4.1 LC-MS results.....57
3.4.2 Statistical analysis.....65
3.5 Conclusion.....75
Chapter 4. Analysis of endogenous and SARS-CoV-2 viral proteins in human saliva via solid-phase microextraction coupled with liquid chromatography-mass spectrometry......76
4.1 Preamble.....76
4.2 Introduction.....76
4.3 Materials and methods.....79
4.3.1 Materials and chemicals.....79
4.3.2 SPME devices.....80
4.3.3 Sampling and analytical protocol.....81
4.4 Results and discussion.....83
4.4.1 Untargeted analysis.....83
4.4.2 Protein identification.....85
4.4.3 SARS-CoV-2 proteins.....99

4.4.4 Peptide characteristics via bio-SPME.....101

4.5 Conclusion.....102

Chapter 5. In vivo chemotherapeutic drug monitoring of doxorubicin during in vivo lung perfusion via solid phase microextraction.....104

5.1 Preamble.....104

5.2 Introduction.....105

5.3 Materials and methods.....108

5.3.1 Reagents and SPME devices.....108

5.3.2 SPME extraction characteristics.....108

5.3.3 Matrix-matched calibration(MMC).....109

5.3.4 Patient selection.....110

5.3.5 IVLP with DOX.....110

5.3.6 In vivo SPME.....110

5.3.7 Liquid chromatography-Mass spectrometry analysis (LC-MS).....111

5.4 Results and discussion.....112

5.4.1 Extraction time profile of DOX.....112

5.4.2 Extraction temperature.....113

5.4.3 Activation-dependent extraction phase performance.....116

5.4.4 Matrix-matched calibration (MMC).....118

5.4.5 Analyte matrix-binding and biostability.....120

5.4.6 Quantitative therapeutic drug monitoring via in vivo SPME.....121

5.5 Conclusion.....125

Chapter 6. Thesis conclusion and future perspectives.....126

6.1 Thesis conclusion.....126

6.2 Future perspectives.....128

Letter of copyright permission.....131

References.....132

List of figures

Figure 1.2 General extraction time profile of SPME over time. n/n^{eq} is the fraction of total extractable amount of analyte at equilibrium obtained at t (arb.units).....8

Figure 2.1 The outside (left) and inside (right) designs of the etching station. The center piece holding the 4 acid-resistant rubbers is slotted right in the center that protect the tips of the needles during etching.....21

Figure 2.2 Coating removal device. The copper tubes are of fixed lengths so that only 1.5 mm (tip length) of a given needle is sanded.....22

Figure 2.3 From left to right: recessed bio-SPME chemical biopsy probes with (a) 3 cm and (b) 6 cm needle lengths, (c) push-pull bio-SPME microsyringe and (d) its sheath-microtubing in lieu of the probe insert. The sheath is about 4.8 cm in length to allow the entire coated portion of the probe to be exposed to the sample matrix.....23

Figure 2.4 Microscopic image of the push-pull bio-SPME microsyringe. The white coating contains the wHLB/PAN extraction phase deposited in the recess of the probe insert.....23

Figure 2.5. Cross-sectional diagram of the etching station.....28

Figure 2.6 (a) Duck gizzard, (b) cow heart, and (c) lamb lung used for the repeated puncturing test of recessed bio-SPME probes. (d) Before and (e) after microscopic images of the coating showing no observable damage or discoloration of the coating.....29

Figure 2.7 Extraction efficiency of common drugs of abuse (DOA) by conventional HLB sorbent (blue) with and (orange) without solvent activation

(autoclaved). Sample matrix: human plasma, [DOA] = 10 ng/mL, 1000 rpm benchtop agitation, extraction time = 20 min.....30

Figure 2.8 Extraction efficiency of common drugs of abuse (DOA) by commercial MM sorbent (blue) with and (orange) without solvent activation (autoclaved). Sample matrix: human plasma, [DOA] = 10 ng/mL, 1000 rpm benchtop agitation, extraction time = 20 min.....31

Figure 2.9 SEM images of (a) HLB particle coalescence in ACN and (b) HLB particles separated in EtOH.....33

Figure 2.10 Dynamic Light Scattering (DLS) of wHLB particles suspended in water.....33

Figure 2.11 Extraction efficiency of common drugs of abuse (DOA) by wHLB sorbent (blue) with and (orange) without solvent activation (autoclaved). Sample matrix: human plasma, [DOA] = 10 ng/mL, 1000 rpm benchtop agitation, extraction time = 20 min.....35

Figure 2.12 Extraction efficiency of common drugs of abuse (DOA) by wHLB sorbent (blue) with and (orange) without solvent activation (autoclaved). Sample matrices: (a) human whole blood, (b) homogenized lamb lung [DOA] = (a) 20 ng/mL, (b) 50 ng/mL, 1000 rpm benchtop agitation, extraction time = 20 min.....36

Figure 2.13 In vivo SPME chemical biopsy probe sampling from patient's left lung during IVLP with oxaliplatin for secondary lung cancer.....37

Figure 2.14 Time-resolved between-lobe oxaliplatin concentrations of upper and lower lobes of the left lung during IVLP via in vivo SPME-LCMS.....38

Figure 2.15 Woodchuck liver tumor and tissue DOX concentrations quantified via

recessed bio-SPME chemical biopsy probes during immuno-photodynamic therapy (iPDT) with Doxil.....40

Figure 2.16 Determination of tissue doxorubicin (DOX) concentration via recessed SPME chemical biopsy probes coupled with microfluidic open interface-mass spectrometry (MOI-MS). DOX was scanned in SIM mode for 1 min following the 10-second desorption.....41

Figure 2.17 Matrix-matched calibration of doxorubicin (DOX) in homogenized ovine lung tissue via R-SPME-AN coupled to MOI-MS. Red points denote test samples from a separate experiment.....42

Figure 2.18 MOI-MS chromatogram of DOX by recessed bio-SPME probes coupled with MOI-MS. Y-axis is the instrumental response in arb. units. Desorption volume = 10 µL, ~ 30-second gaps were allocated between each MOI desorption event.....43

Figure 2.19 Amounts of NTs and DOAs extracted via Push-pull wHLB/PAN SPME microsyringe from agarose gel. Initial [NT] = 200 ng/g, initial [DOA] = 10 ng/g. The numerical values under the x-axis are the corresponding logP of each analyte.....43

Figure 2.20 Complementary analyte coverage in untargeted metabolomics of bovine brain tissue via recessed SPME wHLB/PAN chemical biopsy probe coupled with push-pull microsyringe. Rinse: water rinse of coating surface post-extraction; Push-pull: aspirated aqueous PBS extraction phase; SPME: wHLB/PAN extraction phase. Reverse-phase LC-MS features were processed via XCMS online.....44

Figure 3.1 Exemplary TICs: *) Analysis, ESI polarity, sample, intensity (a) LCMS, positive, THB, 7.62e6 (b) LCMS, positive, THSB, 3.34E6 (c) LCMS, positive, ITSB, 3.14E6 (d) FIA, positive, THB, 3.46E6 (e) FIA, negative, THB, 1.37E3 (f) FIA, Positive, THSB, 9.14E6 (g) FIA, negative, THSB, 5.18E3 (h) FIA, positive, ITSB, 9.12E6 (i) FIA, negative, ITSB, 4.68E3.....64

Figure 3.2 Principal component analysis of THB, THSB, and ITSB sample preparation techniques. THB: tissue homogenization followed by solid-liquid extraction (SLE) coupled to the Biocrates kit; THSB: tissue homogenization followed by SPME coupled to the Biocrates kit; ITSB: intact tissue extraction via SPME coupled to the Biocrates kit.....65

Figure 3.3 Compounds increased/released during tissue homogenization. Note: Y-axis values were preprocessed with Metaboanalyst 5.0 online software. The legend lists the compounds in descending order, corresponding to their appearance on the graph from left to right.....69

Figure 3.4 Compounds decreased/lost during tissue homogenization. Note: Y-axis values were preprocessed with Metaboanalyst 5.0 online software. The legend lists the compounds in descending order corresponding to their appearance on the graph from left to right.....70

Figure 3.5 Compounds with similar amounts detected by solid-phase microextraction (THSB) and solid-liquid extraction (THB) from homogenized tissue. Note: Y-axis values were preprocessed with Metaboanalyst 5.0 online software. The legend lists the compounds in descending order corresponding to their appearance on the graph from left to right.....72

Figure 3.6 Compounds better detected by solid-phase microextraction (THSB) than solid-liquid extraction (SLE). Note: Y-axis values were pre-processed with Metaboanalyst 5.0 online software.....74

Figure 4.1 A stainless-steel blade coated with C18/PAN bio-compatible extraction phase. Coating length: 1 cm. Blade dimensions: 4.5 cm × 3 mm × 400 µm. Blade material: 304-grade stainless steel.....81

Figure 4.2 Exemplary untargeted LCMS total ion chromatograms (TIC) of desorption solutions from (a) healthy control and (a*)* SARS-CoV-2-positive participants. Each chromatogram is from an individual participant.....84

Figure 4.3 Calculated isoelectric point and molecular weight of peptides derived from SARS-CoV-2 proteins identified in whole saliva (n = 10) via a) HLB\PAN-blades and (b) C18/PAN-blades. (c) pI and MW of all viral and endogenous peptides in whole saliva (n = 30) via C18/PAN-blades.....102

Figure 5.1 SPME probes using sharpened nitinol fibers coated with mixed-mode extraction phase.....107

Figure 5.2 Mixed-mode SPME probe extraction time profile of DOX from ovine lung homogenate at 50 µg/g and at 35 °C. Static-mode extraction time = 20 min, 4 replicates (N = 28), RSD < 5% for all data points.....112

Figure 5.3 Extraction time profiles of 11 DOAs and DOX in homogenized lung tissue at: (a) room temperature (20 °C), (b) physiological temperature (37 °C), and (c) 60 °C. Except for DOX (logP ≈ 1.3), analytes are sorted from top to bottom by decreasing polarity.....116

Figure 5.4 Mixed-mode SPME probe extraction efficiency of DOX with and

without solvent activation from ovine lung homogenate at 100 µg/g and at 35 °C. Static-mode extraction time = 20 min, 4 replicates (N = 8), RSD < 5% for all data points.....117

Fig 5.5 In-house HLB SPME probe extraction efficiency of DOX with and without solvent-activation from ovine lung homogenate at 100 µg/g and at 35 °C. Static-mode extraction time = 20 min, 4 replicates (N = 8), RSD < 10% for all data points.....118

Figure 5.6 Matrix-matched calibration using homogenized ovine lung tissue spiked with doxorubicin via SPME. Static mode extraction time = 20 min, extraction temperature = 35 °C, 4 replicates (N = 32), RSD < 10% for all data points, with the exception of 1000-ppm-level data points.....119

Figure 5.7 Spiking time extraction profile from homogenized ovine lung tissue spiked to 50 and 100 µg/g DOX. Static mode extraction time = 20 min, extraction temperature = 30 °C, 3 replicates (N = 40), RSD < 20% for all data points.....121

Figure 5.8 Doxorubicin levels in IVLP perfusate (including serum) and tissue. (a-b) determined via standard procedure: solvent extraction of lung tissue biopsies/perfusate, protein precipitation and filtration, HPLC. (c-e) determined by in vivo SPME-LC-MS.....124

List of tables

Table 2.1 Elemental Analysis of HLB particles synthesized from varying monomer reaction ratios at 80 °C.....34

Table 2.2 DOX levels in porcine left lung during chemo-suffusion via recessed bio-SPME chemical biopsy probes. (*) 30 min suffusion (^) 10 min reperfusion.39

Table 3.1 MS analyte-to-internal standard response ratios of compounds detected by each sample preparation method.....58

Table 4.1 Number, calculated mass (MH+ [Da]), intensity, and calculated pI of Tryp peptides derived from human and SARS-CoV-2 proteins identified in whole saliva from COVID-19-positive individuals (n=10) via HLB/PAN-blades coupled with LC-MS/MS.....88

Table 4.2 Number, calculated mass (MH+ [Da]), intensity, and calculated pI of Tryp peptides derived from human and SARS-CoV-2 proteins identified in whole saliva from COVID-19-positive individuals (n=10) via C18/PAN-blades coupled with LC-MS/MS.....90

Table 4.3 Number, calculated mass (MH+ [Da]), intensity, and calculated pI of Tryp peptides derived from human and SARS-CoV-2 proteins identified in whole saliva supernatant from COVID-19-positive individuals (n=10) via C18/PAN-blades via LC-MS/MS.....94

Table 4.4 List of samples in which peptides derived from SARS-CoV-2 were identified in whole saliva and whole saliva supernatant samples from COVID-19-positive individuals (n=10) using HLB and C18 blades coupled with LC-MS/MS.....100

List of abbreviations (alphabetical)

AC – Acylcarnitines

ACN – Acetonitrile

AIBN – 2,2'-Azobis(2-methylprop-ionitrile)

Al_2O_3 – Aluminum oxide

AmAc – Ammonium acetate

AmF – Ammonium formate

Bio-SPME – Biomedical applications of SPME

C18 – 18-carbon

C8 – 8-carbon

CBS – Coated blade spray

CIHR – Canadian Institutes of Health Research

DART – Direct analysis in real time

DLS – Dynamic light scattering

DMF – Dimethylformamide

DMSO – Dimethyl sulfoxide

DOA – Drugs of abuse

DOX – Doxorubicin

DVB – Divinylbenzene

EtOH – Ethanol

FA – Formic acid

FAO – Fatty acid oxidation

FIA – Flow injection analysis

GC – Gas chromatography

H_2O – Water

H_2O_2 – Hydrogen peroxide

HAc – Acetic acid

HCl – Hydrochloric acid

HDPP – High density polypropylene

HESI – Heated electrospray ionization

HLB – Hydrophilic-lipophilic balanced

HPLC – High-performance liquid chromatography

ID – Internal diameter

IDH – Isocitrate dehydrogenase

IPA – Isopropanol or 2-propanol

iPDT – Interstitial photodynamic therapy

IS – Internal standard

ITSB – Intact tissue extraction via SPME coupled with the Biocrates kit

IVLP – In vivo lung perfusion

LC – Liquid chromatography

LLE – Liquid-liquid extraction

LOD – Limit of detection

LOL – Limit of linearity

LOQ – Limit of quantitation

LPA – Lysophosphatidic acid

LPCAT – Lysophosphatidylcholine acyltransferase

LysoPC – Lysophosphatidylcholines

m/z – Mass-to-charge ratio

MeOH – Methanol

MM – Mixed-mode

MMC – Matrix-matched calibration

MOI – Microfluidic open interface

MS – Mass spectrometry

MWCO – Molecular weight cutoff

NIH – National Institutes of Health

NMR – Nuclear magnetic resonance

NSERC – Natural Sciences and Engineering Research Council

NT – Neurotransmitter

NVP – N-vinylpyrrolidone

OD – Outer diameter

OxPt – Oxaliplatin

PAN – Polyacrylonitrile

PBS – Phosphate buffered saline

PC – Phosphatidylcholines

PCA – Principal component analysis

PCR – Polymerase chain reaction

PEEK – Polyether ketone

pI – Isoelectric point

PITC – Phenylisothiocyanate

PPE – Personal protective equipment

PSD – Particle size distribution

PTFE – Polytetrafluoroethylene

QC – Quality control

RAT – Rapid antigen test

REIMS – Rapid evaporation ionization mass spectrometry

RSD – Relative standard error

RT – Retention time

RT-qPCR – Real time quantitative PCR

S:N – Signal-to-noise ratio

SCX – Strong cationic exchange

SEM – Scanning electron microscopy

SLE – Solid-liquid extraction

SM – Sphingomyelins

SPE – Solid phase extraction

SPME – Solid phase micro-extraction

TDM – Therapeutic drug monitoring

THB – Tissue homogenization followed by SLE coupled with the Biocrates kit

THSB – Tissue homogenization followed by SPME coupled with the Biocrates kit

TIC – Total ion chromatogram

TOF – Time-of-flight

Tryp – Trypsin

UHPLC-HRMS – Ultra-high-performance liquid chromatography coupled with high-resolution mass spectrometry

USask – University of Saskatchewan

UW – University of Waterloo

wHLB – Wettable HLB

Chapter 1. Introduction

1.1 In vivo sampling

In the rapidly evolving field of health care, it is widely recognized that personalized medicine stands to play a vital role in further improving quality of care and speed of diagnosis.[1,2] Personalized medicine relies heavily on the monitoring of various therapeutic and endogenous molecules via minimally invasive techniques.[3,4] For such purposes, physical biopsies remain the standard measurement and diagnostic tool. However, in vivo chemical biopsy is a novel alternative that offers considerable advantages by minimizing invasiveness, ex vivo variabilities, and processing time.[5,6,7] At the molecular level, qualitative and quantitative analyses of the human body pose difficult challenges for researchers and health care professionals. From biological sampling to end-point detection, sample preparation of complex biological matrices is often a tedious yet necessary middle step.[8] Even when state-of-art detection techniques such as nuclear magnetic resonance (NMR) spectroscopy and mass spectrometry (MS) are employed for analysis of such matrices, analytical results are often still impacted by insufficient sample preparation. This remains true even when upstream separation techniques such as gas chromatography (GC) and liquid chromatography (LC) are employed prior to detection.[9,10]

There are currently several in vivo sampling techniques capable of providing physiological information about the human body, either in lieu of or complementary to physical biopsies. For example, microbiopsy, as a safer variant

of physical biopsy, requires much smaller amounts (e.g. mg instead of g) of tissue for analysis with the obvious advantage of greatly increased patient safety, but at the cost of greatly reduced information acquisition due to the limited number of tests that can be performed.[11,12,13] In comparison, in vivo chemical biopsy techniques often offer better information-to-invasiveness trade-offs. Microdialysis is one such technique; first introduced in 1966 by Bito et al., it has since undergone many modifications and improvements.[14,15,16] Until recently, microdialysis was deemed the only viable technique to study neurochemistry without inducing substantial trauma.[15] Microdialysis is based on the principle of diffusion; namely, the chemical concentration difference of analytes between the microdialysis fluid and the sample matrix through a semi-permeable membrane.[15,16] The membrane is typically of a non-polar nature and enables the selective extraction of endogenous compounds such as neurotransmitters; once extraction is completed, the resulting perfusion fluid is then collected for downstream analysis.[15,16] While microdialysis has gained substantial popularity as an in vivo sampling technique in the fields of neuroscience, pharmacokinetics, and pharmacodynamics, there are major drawbacks associated with its use. For example, the non-polar membrane often renders microdialysis ineffective for the extraction of a large group of compounds, such as lipids, metabolites, and drugs of a non-polar nature.[17] Additionally, microdialysis requires a continuous supply of fresh dialysate delivered by a pump to maintain the concentration gradient that drives diffusion. This necessitates bulky equipment being present in the operating room, which may obstruct or hinder medical staff during surgery. Moreover,

quantitation of endogenous and exogenous analytes can be problematic due to heavy dilutions.[16] Complementary to microdialysis, newer sampling techniques can address some of these shortcomings. For example, Intelligent Knife (iKnife) coupled with Rapid Evaporation Ionization Mass Spectrometry (REIMS) is a recently developed in vivo sampling technique that analyzes vaporized tissue with an electrosurgical knife by time-of-flight (TOF) MS.[18] This technique is often used as a real-time intraoperative tool to distinguish between cancer cells and healthy cells.[19,20] While this cutting-edge technique has found some success in clinical applications, some shortcomings limit its implementation. First, this vaporization/pyrolysis-based technique requires destructive sampling of tissue, which often hinders downstream histopathological confirmation.[21] Second, when iKnife-REIMS is used to guide surgical decisions, the accuracy of the technique heavily depends on the iKnife MS database; however, a comprehensive database requires a substantial amount of user feedback, which is often limited by the high upfront cost of implementing such a system.[21,22]

In this thesis work, in vivo solid phase microextraction (SPME) is explored as a novel minimally-invasive chemical biopsy technique for rapid quantitation in both targeted and untargeted applications through deployment of simple SPME devices. In vivo SPME is a promising alternative chemical biopsy technique that offers rich chemical and physicochemical information about the sampled biological system while addressing the shortcomings of other techniques.[23] Presented in this thesis are various proof-of-concept studies and biomedical applications of SPME (bio-SPME) in live animal models and human participants.

1.2 Fundamentals of bio-SPME

The “microextraction” aspect of SPME is the essence of bio-SPME. Unlike conventional extraction techniques, such as solid phase extraction, solvent extraction, or exhaustive gas-phase analysis via SPME, bio-SPME is often featured as a non-exhaustive extraction technique in biomedical applications.[23] This typically translates to absolute recoveries of less than 5%, which circumvent any substantial changes to the biological matrix. For instance, absolute recoveries of 1-2% were achieved for in vivo extraction of metabolites in living mice in a prior in vivo SPME study.[24] To achieve non-exhaustive extraction, bio-SPME relies on the miniaturization of the sampling device, as the extracted amount of a given analyte at equilibrium (n_e^{eq}) is determined according to the following equation:[23]

$$n_e^{eq} = \frac{K_{es}V_eV_s}{K_{es}V_e+V_s} C_s^0 \qquad (1)$$

where K_{es} *(=* C_e^{eq} */* C_s^{eq}*)* is the thermodynamic partition coefficient (also known as the distribution coefficient) of an analyte between the extraction phase (C_e^{eq}) and the sample matrix (C_s^{eq}) at equilibrium, and V_e and V_s are the volumes of the extraction phase and sample matrix, respectively. Miniaturization of the bio-SPME sampling device causes V_e to be miniscule relative to V_s, such that $K_{es}V_e << V_s$; therefore, n_e^{eq} can be estimated by the new equation derived from eq 1 with respect to the initial analyte concentration in the sample matrix (C_s^0):[25]

$$n_e^{eq} = K_{es}V_eC_s^0 \qquad (2)$$

Here, the key advantage is that when absolute recovery is minimal due to the small V_e, the amount of analyte extracted is largely independent on the volume of the sample matrix. It is important to note that a low absolute recovery does not translate to low analytical sensitivity, as a small desorption solution volume can be used to achieve an enrichment factor (E) over multiple orders of magnitude.[23]

$$E = \frac{C_e^{eq}}{C_s^0} = \frac{n_e^{eq}}{n_s^0} \times \frac{V_s}{V_e} \qquad (3)$$

As seen in eq. 3, E is the ratio of analyte concentration of the extraction phase (C_e^{eq}) to initial analyte concentration of the sample (C_s^0). Assuming a reasonable K_{es} exists between the extraction phase and the sample, E is largely affected by V_s / V_e. Small injection volumes in liquid chromatography (LC) enable the desorption of analytes to be in the micro-liter range, thus resulting in $V_s >> V_e$ and consequently, a large value for E.[23]

Equations listed thus far assume extraction equilibrium is reached; in other words, the amount of any extracted analyte is solely determined by the thermodynamic distribution constant between a given sample and a given extraction phase. In practice, extraction equilibrium is rarely reached, especially for in vivo applications of bio-SPME.[25] As such, the rate of mass transfer from the bulk of the sample matrix to the extraction phase becomes an important factor for pre-equilibrium extractions. What prevents most analytes from rapidly reaching K_{es} at equilibrium is the existence of a boundary layer between the bulk sample

matrix and the extraction phase during static extraction. This was shown via an experimentally validated computational model by Alam et al.[26]

1.3 Extraction kinetics of bio-SPME

Fick's first law of diffusion is the basis for generating the computational model:

$$F = -DA_e \frac{dC}{dx} \qquad (4)$$

where flux (*F*) is the mass transfer of an analyte through the boundary layer as a function of the diffusion coefficient (*D*), and a concentration gradient (*dC/dx*) over distance *x* perpendicular to the cross-sectional area of the boundary layer (A_e). Complex mathematical models can be derived from here to estimate the amount of analyte collected in the extraction phase (N_e) via a typical cylindrical fiber geometry based on sample concentration, C_s:

$$C_s = \frac{N_e b}{ERe^m Sc^{1/3} A_e D_s t} \qquad (5)$$

$$C_s = \frac{N_e Ln(\frac{b+\delta_s}{b})}{2\pi D_s L t} \qquad (6)$$

Eq. 5 best models a scenario where there is a sample fluid flow perpendicular to the fiber.[27] In eq. 5, *b* is the outer diameter of the fiber. *Re* is the Reynolds number calculated by *ud / v*, where u is the linear velocity of the sample and *v* is the kinetic viscosity of the sample fluid over a distance, *d*. *Sc* is the Schmidt number calculated from *v / D*. D_s is the diffusion coefficient of an

analyte in the sample matrix, and *t* is time. *E* and *m* are constants dependent on *Re* and are available in the literature.[27] In bio-SPME, a similar alternative model should be established for biofluid analysis, such as blood and urine, when a benchtop vortex sample mixer or a Concept 96 SPME station is employed. In such scenarios, a stationary SPME device is lowered into a moving sample for extraction, thus causing the sample to form a vortex flow around the extraction phase that effectively disrupts the boundary layer.[28] On the other hand, Eq 6 is a suitable model for static-mode extractions using an SPME fiber, such as in vivo SPME. While fluid velocity and viscosity exert much less influence on N_e, mass transfer (analyte diffusion) through the boundary layer becomes significant since it is not heavily disturbed. As such, the volume of the boundary layer is an important parameter and is dependent on *b* and *L*, which are the outer diameter and length of the fiber, respectively, as well as δ, which is the total distance of the boundary layer through which analytes must travel to reach the extraction phase.

In practice, many variables in eq. 5 and 6 are not under the control of the experimenter, such as the viscosity of biofluids or the boundary layer during in vivo SPME. There is also limited room for optimization of the geometric dimensions of the SPME fiber as a balance must be reached between the physical robustness and non-invasiveness of bio-SPME devices.[29] Further, there are many factors that prevent extraction equilibrium from being reached in bio-SPME applications, such as time constraints during clinical operations and unknown equilibrium times for untargeted -omics studies (metabolomics, lipidomics, proteomics, etc.). As such, extraction time (*t*) remains one of the most

important factors in determining the amount of analyte extracted (*n*). Ai derived the following non-linear equation that models the extraction time profile of SPME during the linear kinetic extraction regime, as well as the equilibrium extraction regime:[30]

$$n = [1 - \exp(-a_e t)] \frac{K_{es} V_e V_s}{K_{es} V_e + V_s} C_s^0 \qquad (7)$$

where a_e is the extraction rate constant indicative of how fast equilibrium can be reached and is dependent on V_e, V_s, K_{es}, surface area of the extractant, and overall mass transfer coefficient (k_0). This equation shows that as extraction reaches thermodynamic equilibrium, n can be expectedly predicted mostly by eq.1 since $[1 - exp(-a_e t)] \approx 1$. More importantly, when Eq. 1 and 7 are combined, a general full extraction time profile can be obtained from the resulting relationship:

$$\frac{n}{n^{eq}} = 1 - \exp(-a_e t) \qquad (8)$$

where n / n^{eq} is the fraction of total extractable amount of analyte at equilibrium at any given time. Therefore, a typical extraction time profile should look like this:

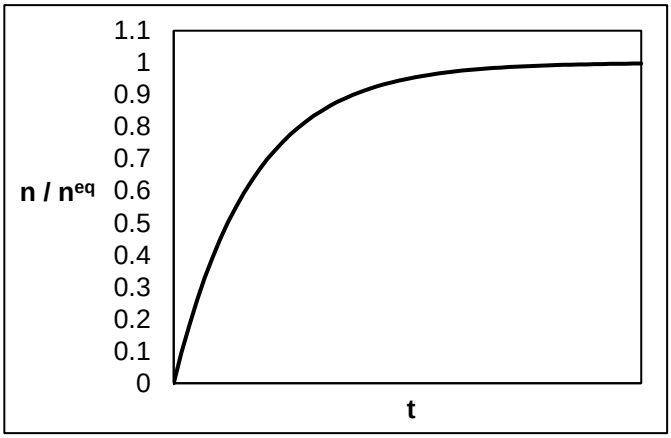


Figure 1.2 General extraction time profile of SPME over time. n/n^{eq} is the fraction of total extractable amount of analyte at equilibrium obtained at t (arb. units).

Fig. 1.2 shows that initial analyte uptake by the extraction phase is largely time dependent (linear kinetic extraction regime) and mostly independent of K_{es}. This also means that controlling extraction time is key to analytical accuracy and precision during bio-SPME, especially given that sampling time is often limited during in vivo applications.[31] Conveniently, a reasonable n/n^{eq} (near-equilibrium extraction) can often achieved for tissue and in vivo SPME with a drastically shorter extraction time compared to static mode matrix-free extractions. Matrix-binding accelerates the extraction kinetics and thus shortens equilibrium time as the local depletion of an analyte (via SPME) is rapidly compensated by the matrix-bound portion.[78]

1.4 Quantification and calibration of in vivo SPME

A n_e independent from V_s, a large enrichment factor (multiple orders of magnitude), and careful control of t enable rapid relative quantification of any extractable analyte via in vivo SPME with low limit of detection (LOD). This has already seen pre-clinical success; for instance, in a comparison of in vivo concentrations of oxylipin in different regions of a living rat brain.[32] Absolute quantification can also be achieved via various calibration techniques, such as the preloading of isotopically labeled internal standards (IS) for analytes of interest in the extraction phase.[23] This technique, based on the equal and opposite desorption time profile mirroring the extraction time profile, is referred to as “in-fiber standardization” and has excellent analytical accuracy due to its robustness against factors that affect extraction parameters – the symmetry of absorption (of a target analyte) and desorption (of its IS) conveniently takes

temperature and agitation into consideration during extraction.[23] However, the in-fiber calibration technique has various limitations for bio-SPME applications. One common issue associated with all IS-based calibration techniques is that a suitable IS is often expensive and has limited target compounds.[33] Additionally, in vivo applications often forbid the introduction of exogenous substances due to safety concerns.[34] Alternatively, employment of matrix-matched calibration (MMC), an ex vivo calibration approach that bypasses the need for isotope-labeled IS for exogenous analytes, provides a useful solution in cases where IS loading is unfeasible. This technique works well with in vivo clinical applications such as therapeutic drug monitoring (TDM), where animal tissue models that sufficiently represent in vivo conditions can be used for calibration in lieu of in vivo samples.[35,36] For example, Roszkowska et al. demonstrated that the amounts of Doxorubicin (DOX) extracted from homogenized porcine lung samples in vitro were comparable to amounts extracted from live porcine lungs during in vivo lung perfusion (IVLP) surgery.[35] Since the homogenization of the model tissue did not affect matrix-binding of DOX, the same technique was later used for in vivo quantitative TDM of DOX during human IVLP.[36] Chapter 5 discusses the shortcomings of the MMC technique applied in previous studies and strategies to improve the reliability of MMC for in vivo applications of bio-SPME, backed with data from numerous clinical cases of IVLP. While MMC eliminates the requirement for IS when quantitating exogenous compounds in various in vivo SPME applications, it is unsuitable for quantitation of endogenous compounds unless additional calibration techniques are employed. Chapter 3

introduces in vivo SPME in untargeted analysis of endogenous analytes and its advantages over conventional extraction techniques.[33] When coupled to a commercial metabolomics assay, semi-untargeted metabolomics with rapid quantitative results can be achieved via bio-SPME using unit-resolution mass spectrometers (MS) instead of costly high-resolution MS conventionally required for untargeted metabolomics.[34]

1.5 In vivo SPME device and extraction phase coating

In vivo SPME has distinguished itself as a novel branch of bio-SPME due to the combination of unique challenges associated with creating suitable in vivo devices. Ideally, such devices should be minimally invasive, physically robust, chemically inert, and easy to handle for medical personnel.[23,25,31] In previous studies, a coated nitinol fiber was selected for in vivo TDM of a chemoagent in lung cancer patients owing to its physical and chemical inertness.[36] A commercial 8-carbon sulfonate strong cationic exchange (C8-SCX) extraction phase (also known as mixed-mode) was bound to the tip of the fiber by a porous and biocompatible binder, polyacrylonitrile (PAN). PAN is considered biocompatible due to its non-toxic nature and size-exclusion against macromolecules and cells.[37] The latter enables metabolism quenching and prevents biofouling as proteins (enzymes) and microbial cells are prevented from reaching the extraction phase.[37,38] The biocompatible size-exclusion property of PAN also conveniently reduces matrix effects as the bulk of unwanted elements present in the sampled biological system is prevented from entering the extraction phase.[25] The mixed-mode (MM) extraction phase is popular in many in vivo SPME

applications due to its ability to extract a wide range of analytes, including nonpolar, nonionizable polar, and cationic analytes.[17,36,39] It is vital for non-exhaustive techniques such as SPME to maintain a balanced coverage when aiming for the recovery of a wide range of analytes while ensuring reasonable detection limits. This is particularly true for untargeted in vivo applications where quantitative calibration of all extracted compounds can be challenging. In this sense, a matrix-compatible binder facilitates the balanced recovery of a broad range of analytes by limiting matrix effects to a degree, while the chemistry of the extraction phase, together with matrix binding, often play a bigger role in achieving balanced analyte coverage independent of logP.[23,25.] Chapter 2 encompasses the development of a recessed bio-SPME chemical biopsy probe that is substantially more physically robust and easier to handle than the nitinol-based SPME fiber device. This novel device is also equipped with a modified, wettable version of hydrophilic-lipophilic balanced particles (wHLB) that eliminates the need for solvent activation, thus making it autoclave-compatible for in vivo SPME applications. The copolymeric wHLB extraction phase is also capable of extracting analytes from a wide range of logP values. Compared to MM, advantages of HLB-type extraction phases include the ease of in-house synthesis and “softer” polar interactions when compared to ion exchange extraction phases, thus resulting in less biased and/or irreversible extractions of highly polar analytes[40,41] Finally, the recessed wHLB/PAN chemical biopsy probes can be coupled with microfluidic open interface (MOI), a direct-MS technique, to provide immediate point-of-care feedback to surgeons and general

physicians. Additionally, a microtubing can be employed as a sheath for the probe, forming a microsyringe that enables aqueous phase extraction of highly polar analytes in addition to bio-SPME.

To understand how SPME, a non-exhaustive extraction technique with limited extraction capacity, can be used to extract a wide range of analytes from complex biological matrices, a few key fundamental concepts must be explained. Bio-SPME extracts via free concentration (water soluble portion) in biological matrices where the matrix-bound portion of a given analyte is not in direct contact with the extraction phase via the aqueous portion of the sample matrix.[42] Considering the diffusion-controlled mass transfer during the kinetic extraction regime, one can expect preferential extraction of polar (and smaller) analytes during the initial uptake due to their abundance in the aqueous portion of a biological matrix over nonpolar (and larger) analytes. This can pose a problem as the saturation effect would prevent the extraction of nonpolar analytes in bio-SPME (since $K_{es}V_e << V_s$). Fortunately, this can be circumvented by employing a mixed mode extraction phase (such as C8-ion exchange and HLB) that favors nonpolar interactions (K_{es} of nonpolar analytes > K_{es} of polar analytes), so that the bias for small and nonpolar analytes is reduced, and the eventual displacement effect can balance the coverage of both polar and nonpolar analytes.[43,44] In a biological matrix, prior studies found that the matrix-binding constant (K_a) can be assumed to be inversely proportional to the polarity of a given analyte; that is, $logK_a \approx -logP$. [45] The authors also stated that the desorption rate constant (k_r) is proportional to K_a as the overall extractant-sample

distribution constant (K_{es}) is a balance between the analyte's affinities toward both the extraction phase and the binding matrix.[45] However, regardless of k_r's dependence on K_a, a balanced coverage is expected due to the interplay between K_{es} and K_a as long as an extraction phase of a nonpolar nature is employed.[45] Huq et al. also experimentally demonstrated this intricate interplay between an analyte's matrix-binding affinity and extraction phase affinity.[78]

Lastly, Chapter 4 demonstrates the feasibility of bio-SPME in clinical peptidomics/proteomics from SARS-CoV-2 patient saliva samples for the first time. Proteomics was thought to be impossible via SPME due to the size-exclusion property of the PAN binder. On the contrary, in this novel application of SPME, a Trypsin digestion step prior to extraction and introducing porosity to the C18/PAN coating enabled extraction of the digested peptides and even protein identification via bio-SPME.

1.6 Thesis statement

This thesis work provides comprehensive strategies to implement bio-SPME and in vivo SPME, including device fabrication, clinical applications, end-point detection, and quantification. Devices presented in this thesis offer drastic improvements to the solid support and extraction phase of conventional bio-SPME devices; proof-of-concept studies presented in this thesis demonstrate the advantage and validity of bio-SPME in biofluid and biomass analysis in vitro as well as tissue analysis in vivo.

Chapter 2. Minimally invasive solid-phase microextraction (SPME) chemical biopsy devices for in vivo biomedical applications.

2.1 Preamble

The devices presented in this chapter have been used in various clinical and preclinical applications including therapeutic drug monitoring (TDM) of chemoagents during in vivo lung perfusion (IVLP) in humans and in animal models. The devices will also be used for untargeted metabolomics from patients and animals afflicted with malignant hyperthermia (MH), brain tumors, and other conditions. The devices and some applications presented in this chapter have been published as a US utility patent (Publication number: US 2023/0273195 A1) in a collaborative effort between Dr. Zhou, Prof. Pawliszyn and me. The content presented in this chapter has been formatted for submission to *Nature Methods* upon the collection and analysis of more clinical samples. Please see *Statement of contributions* for more information. We would like to thank the following organizations for their generous fundings: Natural Sciences and Engineering Research Council (NSERC) of Canada, Canadian Institutes of Health Research (CIHR), National Institutes of Health (NIH), and the University of Waterloo.

2.2 Introduction

Surgical biopsy of soft tissue is currently a standard procedure performed for acquisition of diverse diagnostic and physiological information, such as

therapeutic drug monitoring (TDM), biomarker screening, and metabolic profiling.[46] To reduce the area of the infection-prone sampling site and the extent of trauma from tissue biopsy, techniques such as fine-needle aspiration biopsy can be used instead of core biopsy.[46] This technique typically employs a 23 – 25 gauge needle (0.52 – 0.64 mm OD) that is inserted into the location of interest to extract a small tissue biopsy (few mg), which can then be used for standard histological studies or biochemical tests.[47] Metabolomics and biomarker discovery represent relatively new biopsy-based approaches to diagnostics. Significant (i.e. $p < 0.05$) metabolomic differences associated with physiological changes can be used to distinguish between healthy and afflicted tissue. The metabolic profiles of the tissue biopsy are often obtained via high-resolution magnetic resonance or mass spectrometry following liquid extraction of the tissue sample.[48]

Biomedical applications of solid phase microextraction (bio-SPME), such as in vivo SPME, are techniques that combine sampling, sample clean-up, metabolism quenching, and sample enrichment (concentration) into one streamlined process.[45] Given the wide range of chemical sorbents that can be affixed onto an SPME device, in vivo SPME often doubles as a tool for untargeted metabolomics and biomarker discovery in addition to targeted analysis.[25] When a mixed-mode sorbent is used, such as hydrophilic-lipophilic balanced (HLB) and C8-sulfonate (C8-SCX), a balanced recovery of analytes via in vivo SPME is expected across a wide range of logP values with a short sampling time prior to extraction equilibrium.[45] Polyacrylonitrile (PAN) is often

used as a binder for bio-SPME devices due to its biocompatibility and chemical and mechanical stability. In addition to securing the extraction phase onto an SPME device, binders serve to prevent the extraction of macromolecules and microorganisms, thus ensuring metabolism quenching and preventing biofouling.[49]

Fiber and needle geometries of SPME are often employed to safely perform both targeted and untargeted analyses in vivo. This is one of the prominent advantages of in vivo SPME probes – minimal invasiveness during sampling. In vivo SPME devices have been successfully implemented in numerous live animal and clinical studies in vivo. For example, to enable in vivo sampling of fish tissue protected by tough scales, Poole et al. utilized stainless steel rods with a recess behind the tip for the deposition of the extraction phase. The rods were then fired through fish scale for in vivo metabolite extractions in live fish.[29] In another live animal study, a stainless steel SPME probe coated a hydrophilic-lipophilic balanced (HLB) sorbent was coupled to a supporting sheath to extract target neurotransmitters from live macaque brains.[50] In humans, nitinol-based SPME fibers coated with a C8-sulfonate mixed-mode extraction phase were used for in vivo chemotherapeutic drug monitoring during in vivo lung perfusion (IVLP) with doxorubicin (DOX).[36,51] The authors were able to estimate local DOX concentrations inside the patients' lungs at multiple time points throughout the chemotherapeutic process. The validity of the spatial and temporal resolution in the TDM of DOX by in vivo SPME was proven in a prior

study by Roszkowska et al. utilizing a live porcine model and ex vivo matrix-matched calibration.[35]

Still, current designs of in vivo SPME devices are burdened by some limitations. For example, most of the devices used in the aforementioned studies lack a protective tip to avoid potential coating abrasion and stripping when applied to more physically resilient tissue such as heart muscles. While Poole et al. took advantage of a recessed stainless steel rod design capable of protecting the sorptive coating when puncturing fish scale, such rods boast a thick outer diameter (OD) of almost 600 µm, which could cause trauma in delicate organs and tissues. On the other hand, although the nitinol fibers used in the IVLP studies had a tiny OD (< 250 µm) and were inert, they lacked the stiffness of stainless steel and were difficult to track during surgery. These caused a great deal of inconvenience for the medical team to handle during IVLP. As for chemical sorbents, the conventional HLB and C8-sulfonate extraction phases are commonly used for bio-SPME and require prior organic solvent activation and storage to ensure adequate extraction efficiency. These requirements present an obstacle for many clinical applications as steam-sterilization (autoclaving) of medical devices is a common clinical practice that would deactivate the sorbent via evaporation.

The present study introduces a recessed SPME chemical biopsy probe made from stainless steel acupuncture needles with a wettable HLB (wHLB) extraction phase in the recess that does not require solvent activation. The featured miniature bio-SPME probes are minimally invasive due to their small

size (250 µm OD) and physically robust thanks to their stainless-steel support and recess-protected coating. Additionally, the extraction phase offers a wide range of analyte coverage without the need for solvent activation, making it autoclave-compatible. When coupled with a sheath, the resulting push-pull SPME sampling microsyringe also enables aqueous phase extraction of highly polar analytes. Both devices are also compatible with the microfluidic open interface (MOI) direct-MS technique, thus enabling the potential for rapid point-of-care in vivo therapeutic drug monitoring.

2.3 Materials and methods

2.3.1 Materials and chemicals

Seirin Laser SL2560 and SL2530 stainless-steel acupuncture needles were purchased from Eastern Currents (Vancouver, BC, Canada). Stainless-steel microtubings were purchased from McMaster Carr (Elmhurst, IL, USA). All drug of abuse (DOA) standards were purchased from Cerilliant Corporation (Round Rock, TX, USA). All neurotransmitter (NT) standards were purchased from Toronto Research Chemicals (Toronto, ON, Canada). Acetonitrile (ACS grade), toluene (ACS grade), divinylbenzene (DVB), N-vinylpyrrolidone (NVP), 2,2'-Azobis(2-methylprop-ionitrile) (AIBN), polyacrylonitrile (PAN), dimethylformamide (DMF), and phosphate buffered saline pellets were purchased from MilliporeSigma (Oakville, ON, Canada). Formic acid (FA), acetic acid (HAc), ammonium formate (AmF), hydrochloric acid (HCl), sodium hydroxide, LC-MS grade methanol (MeOH), ethanol (EtOH), acetonitrile (ACN), 2-propanol (IPA), toluene, and water were purchased from Fischer Scientific (Mississauga, ON,

Canada). C8-SCX mixed mode fibers were kindly provided by Supelco (Milwaukee, PA, USA). Doxorubicin (DOX) and oxaliplatin (OxPt) were purchased from Toronto Research Chemicals (Toronto, ON, Canada). Human plasma (pooled gender) was purchased from BiolVT (Westbury, NY, USA). Fresh ovine lungs were purchased from a local butcher shop (Waterloo, ON, Canada). Anhydrous ethanol (EtOH) (99.9%) was purchased from Chem Store (University of Waterloo, ON, Canada).

2.3.2 Particle characterization

A FEI Quanta Feg 250 ESEM (Hillsboro, OR, USA) was used for scanning electron microscopy (SEM) imaging. A Malvern Zetasizer nano series was used for dynamic light scattering (DLS) analysis (Malvern, UK). A Costech 4010 Elemental Analyzer (Dar es Salaam, Tanzania) coupled to an Isochrom continuous flow isotope ratio mass spectrometer (Micromass, UK) was used for the C and N elemental analysis.

2.3.3 Etching

An etching station was manufactured by precision machining, using high-density polypropylene (HDPP), polyoxymethylene (Acetal), poly ether ketone (PEEK), and acid-resistant rubber (white vinyl) (Fig. 2.1). 20 needles were inserted into the station and subjected to acid etching using ~75 mL of HCl (37% w/w) for 30 minutes at room temperature (20 °C) to achieve a ~15 µm recess (250 µm OD to 220 µm OD). After removing the etchant, the recessed needles were then briefly rinsed with water, sonicated in MeOH for 15 minutes, and dried

by N_2 prior to coating. Different sizes of etching stations were made to accommodate different needle lengths (30 mm and 60 mm).

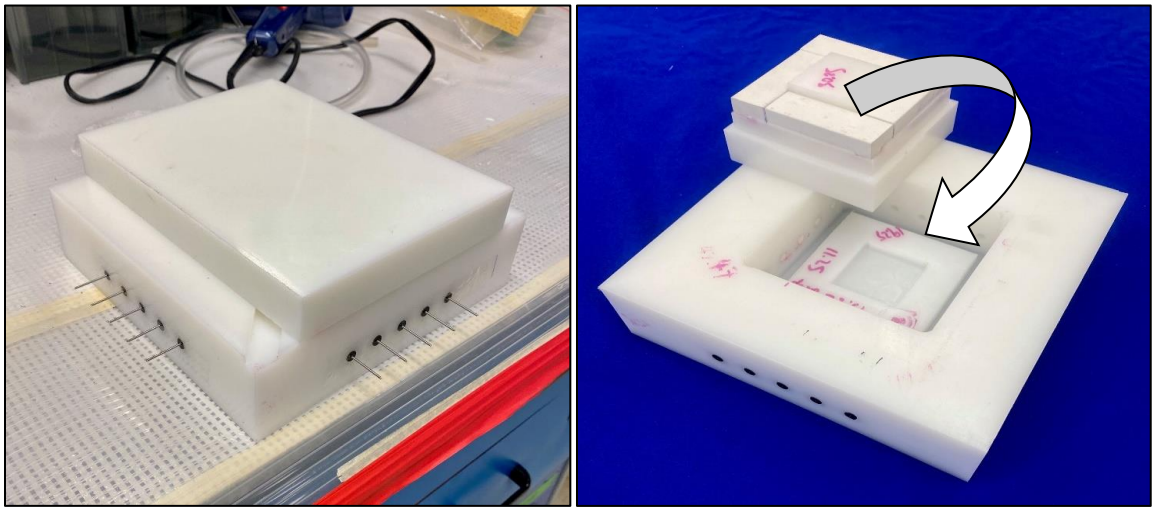


Figure 2.1 The outside (left) and inside (right) designs of the etching station. The center piece holding the 4 acid-resistant rubbers is slotted right in the center which protects the tips of the needles during etching.

2.3.4 Coating

Wettable HLB (wHLB) particles were synthesized via precipitation polymerization. In a 200-mL Teflon Polytetrafluoroethylene (PTFE) cylindrical reaction vessel, 80 mL EtOH was added as the solvent and 20 mL of toluene was added as the porogen. The mixture was heated to 80 °C then purged with a low N_2 flow for 30 min while mixed with a magnetic stir bar at 150 rpm. Next, 2 mL of filtered (through aluminum oxide) DVB crosslinker, 6 mL of filtered NVP hydrophilic functional monomer, and 20 mg of AIBN initiator were added to the mixture. The reaction mixture was then kept at 80°C and mixed at 150 rpm under N_2 purging in the head space for 22 hours. Following, the polymer particles formed were filtered through a 50-micron stainless steel sieve to remove large agglomerates, and subsequently washed/collected via centrifugation 3 times with

~250 mL of EtOH. The resulting wHLB particles were then dried at 60 °C under N_2-purged vacuum overnight. The coating slurry was prepared in a ~7% w/v polyacrylonitrile binder dissolved at 80 °C in DMF. Once cooled, 10% (w/w) particles were added to the binder, and the slurry was kept under mixing by stir bar until use. The chemical sorbent was deposited into the recess by dip-coating, and coating on the tip of the needle was removed using a simple sanding device, as shown in Fig. 2.2, to obtain the final recessed product (Fig 2.3). Mixed-mode (MM) C8-sulfonate and conventional in-house HLB (HLB) slurries were prepared to the same ratio in PAN.

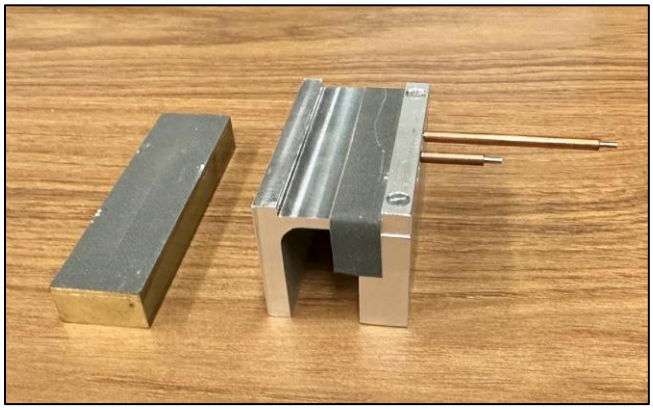


Figure 2.2 Coating removal device. The copper tubes are of fixed lengths so that only 1.5 mm (tip length) of a given needle is sanded.

2.3.5 Push-pull bio-SPME microsyringe

The coated recessed-coating bio-SPME probes can be inserted into a microtubing with a slightly larger (~4µm) internal diameter (ID) than the OD of the probes. The assembly functions as a microsyringe that can push out a pre-deposited aqueous extraction phase, such as PBS, in vivo to perform aqueous phase extraction. The stainless-steel sheath has a wall thickness of 1 µm, resulting in an OD of ~450 µm. The specific length and sharpened tip of the

sheath were attained with a diamond wheel cutter. A microscopic view of the push-pull microsyringe is shown in Fig. 2.4 below.

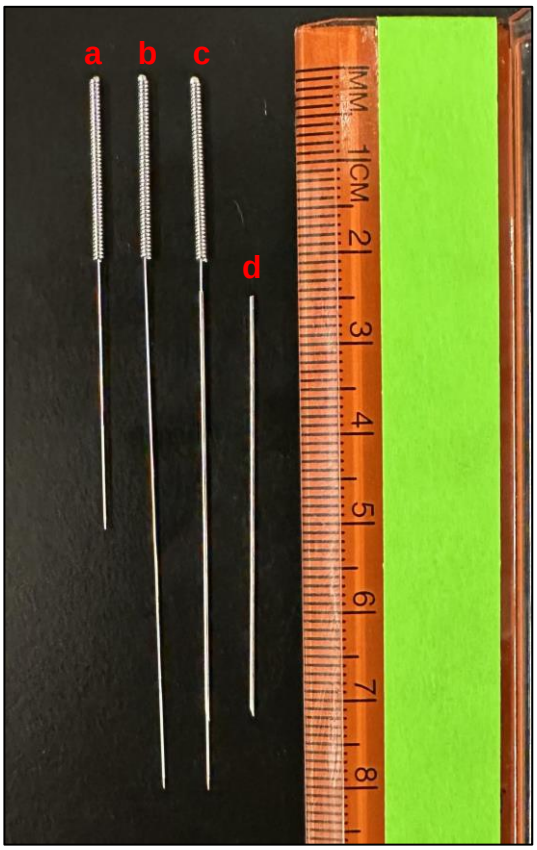


Figure 2.3 From left to right: recessed bio-SPME chemical biopsy probes with (a) 3 cm and (b) 6 cm needle lengths, (c) push-pull bio-SPME microsyringe and (d) its sheath-microtubing in lieu of the probe insert. The sheath is about 4.8 cm in length to allow the entire coated portion of the probe to be exposed to the sample matrix.

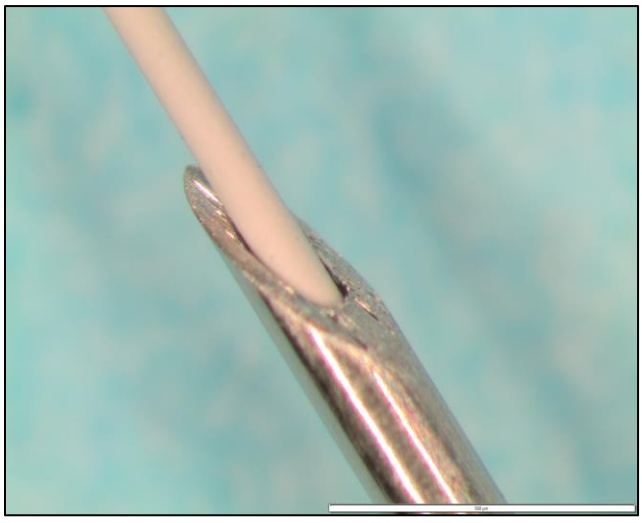


Figure 2.4 Microscopic image of the push-pull bio-SPME microsyringe. The white coating contains the wHLB/PAN extraction phase deposited in the recess of the probe insert.

2.3.6 Cleaning

The probes and microsyringes were submerged in a cleaning solution, constituted with 3:3:3:1 ACN/MeOH/IPA/H_2O (by volume), on a benchtop vortexer at 500 rpm for 60 minutes. When applicable, chemical sorbents were activated using a preconditioning solution (70% ethanol) that also doubled as a storage solution until use. When applicable, a standard medical sterilization procedure was adopted where SPME devices were subjected to steam sterilization (autoclave) at 121 °C for 45 minutes. The autoclaved SPME probes were then dried by N_2 and stored in glass vials until use.

2.3.7 Matrix-matched calibrations

Human plasma, human blood, and ovine lungs were used as model matrices for ex vivo matrix-matched calibrations. Ovine lungs were chilled to 4°C, diced up to remove large ventricles, and homogenized using a blender. Working tissue homogenate samples were prepared by adding 1.5 mL of PBS (pH 7.4) to 13.5 g of tissue in a 20-mL glass vial.[35] Standards of the target analytes DOA and DOX were spiked into each glass vial of tissue homogenate according to the protocol adapted from Roszkowska et al.[35]

2.3.8 Extraction parameters

Unless otherwise specified, the extraction parameters were generally kept as follows: 5-second water wash to remove surface organic solvent (when applicable), 20-minute static mode extraction at room temperature (20 °C), 5-second water wash post-extraction to remove matrix particulates on the needles,

60-minute desorption (except for MOI-MS) with agitation (500 rpm via a benchtop vortexer) in 7:2:1 MeOH/ACN/H_2O + 0.1% FA (by volume). 4 µL of PBS was used as the aqueous extraction phase for push-pull SPME microsyringe.

2.3.9 Liquid chromatography and mass spectrometry (LC-MS)

A Thermo Vanquish UHPLC was coupled with a Thermo TSQ Vantage or a Thermo TSQ Quantiva MS/MS via heated ESI (HESI) (San Jose, CA, USA) for all targeted analyses. A Phenomenex Kinetex reverse-phase PFP (10 cm x 2.1 mm, 1.7 µm) column was used for LC separation (Torrance, CA, USA). Mobile phase A was water (0.1% FA), B was ACN (0.1% FA), and flow rate was 0.4 mL/min throughout. Generally, the gradient started with 0.5 minutes of 10% B, increased to 95% B linearly over 6 minutes, stayed at 95% B for 2 minutes before dropping back down to 10% B in 0.5 minutes, where it was kept for 2 minutes for column equilibration (11 min total). Oxaliplatin (OxPt) was analyzed via normal-phase LC-MS/MS using a Phenomenex Luna HILIC (7.5 cm x 4.6 mm, 3 µm) column (Torrance, CA, USA). Mobile phase A was water (5 mM AmF), B was ACN, and flow rate was 0.4 mL/min throughout. Generally, the gradient started with 0.3 minutes of 95% B, decreased to 40% B linearly over 1 minute, and stayed at 40% B for 1.7 minutes before increasing back up to 95% B in 0.5 minutes, where it was kept for 2.5 minutes for column equilibration (6 min total). LC gradients were adopted and reoptimized for specific column and LC-MS combinations.[12] The MS/MS SRM transitions and respective conditions (S-lens voltage and collision energy) were adopted from prior works. [35,62,128] Analyte SRM transitions and parameters were re-optimized via direct-infusion into the MS

following a change in instrumental calibration protocol to accommodate for slight mass changes thus ensuring maximum sensitivity.

A Thermo Vanquish UHPLC was coupled with a Thermo Exactive Orbitrap high-resolution MS via HESI for all untargeted analyses. A Supelco Discovery reverse-phase HS F5-3 (10 cm x 2.1 mm, 2.6 µm) column was used for LC separation (Milwaukee, PA, USA). Mobile phase A was water (0.2% FA for positive mode, 0.02% HAc for negative mode), B was ACN (0.2% FA / 0,02% HAc), and the flow rate was kept at 0.3 mL/min throughout. The gradient started with 2 minutes of 10% B, increased to 95% B linearly over 45 minutes, and stayed at 95% B for 10 minutes before dropping back down to 10% B in 1 minute, where it was kept for 2 minutes for column equilibration (60 min total). The Orbitrap method employed a full-scan over the range of 84 – 1000 m/z with lock-masses of 391.28429 (positive mode) and 255.23295 (negative mode), resolution set to “high”, and automatic gain control (AGC) target set to “Balanced”.

2.3.10 Microfluidic open interface

The MOI interface (Waterloo, ON, Canada) was coupled to a generic syringe pump and a Shimadzu 8060 triple quadrupole mass spectrometer via a HESI ion source.[14] All MOI desorptions were carried out for 10 seconds in static-mode inside the MOI chamber with 10 µL of 7:2:1 MeOH/ACN/H_2O + 0.1% v/v FA following a 5-second water rinse after each extraction. The desorption solution was then directly sprayed into the MS inlet to continuously scan for compound-specific transitions. The MOI-MS system was calibrated each time before use by injecting ~5 µL of DOA standard into the MOI chamber.

2.4 Results and Discussion

2.4.1 Creating the recess

Prior attempts to create a recess on stainless-steel needles with simpler approaches proved to be inefficient and unreliable. For example, covering the tip and body of a needle for both acid- and electro-etching was tedious and yielded > 30% between-needle relative standard deviations (RSD) in recess depths (N = 20). As such, an etching station was created by precision machining to ensure quick and uniform acid-etching of large batches of needles (N = 20 / batch). The 30-min etching time was optimized to yield a 15 µm recess using 80 mL of concentrated HCl at 20°C that was kept under agitation with an orbital shaker at 85 rpm. A cross-sectional diagram of the etching station is shown below (Fig. 2.5). Four acid-resistant rubbers are fixed in the center of the etching station at a fixed distance away from the handle, as shown in Fig. 2.1, so that the needle tip (1.5 mm) is protected during the acid-etching process. A small piece of rubber is also secured in the opening on the interior of the high-density polypropylene (HDPP) block to prevent HCl from etching the body of the needle. The channel between the two rubber pieces determines the length of the recess and therefore the coating length. The etching station was machined with great precision to minimize dimensional deviations between the needles, which would in turn affect the coating length and consequently, analytical precision.

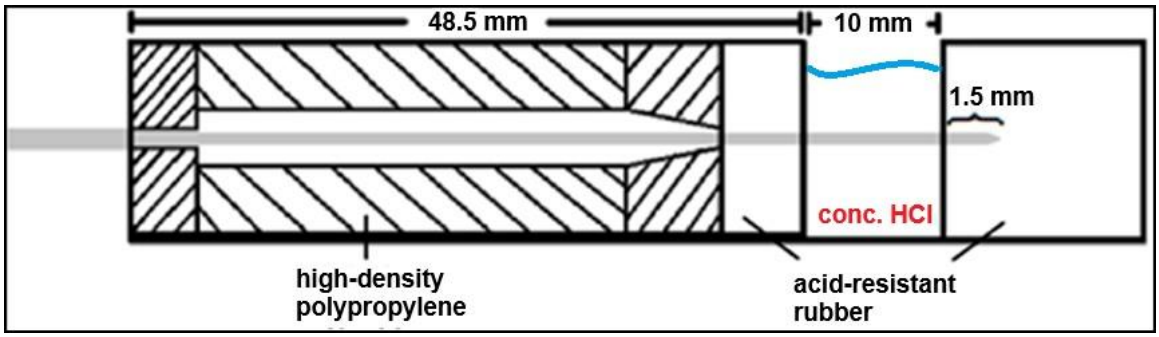


Figure 2.5. Cross-sectional diagram of the etching station.

2.4.2 Puncturing test

To ensure the physical integrity of the recessed bio-SPME chemical biopsy probes, 5 probes prepared according to the coating and clean-up steps outlined in the Methods section were subjected to repeated puncturing tests using three types of animal organs, as shown in Fig. 2.6 a – c (5 punctures each, totaling 15 punctures for each probe), with no visible damage observed in any coating (representative before and after images are shown in Fig. 2.6 d – e).

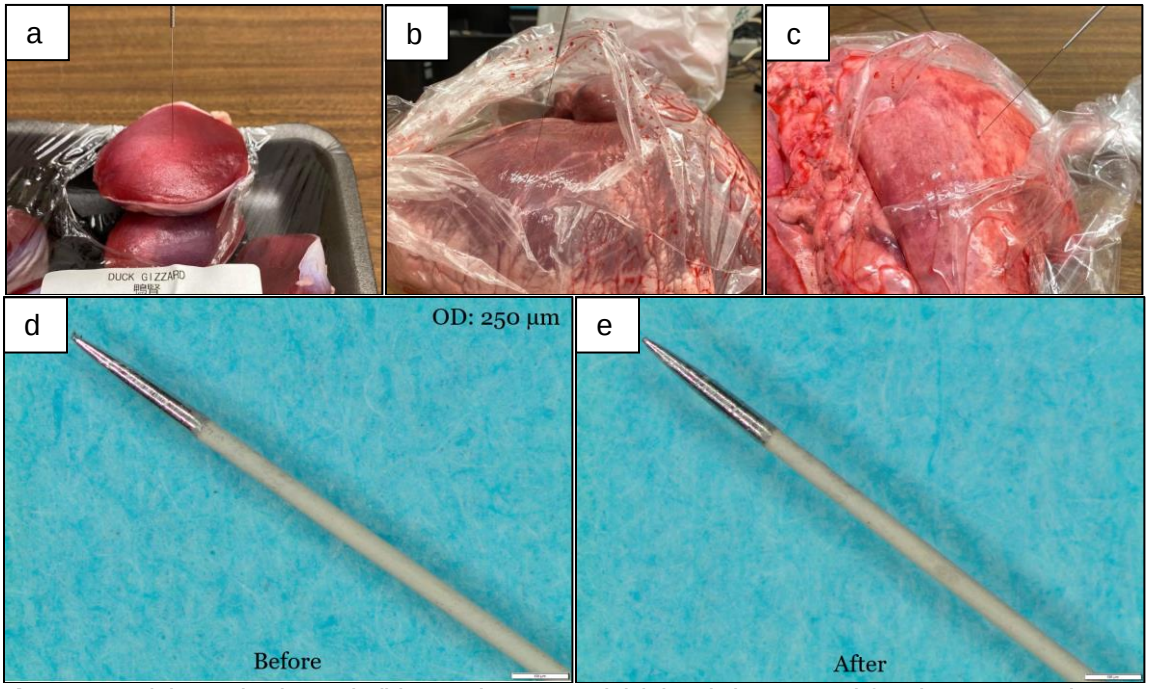


Figure 2.6 (a) Duck gizzard, (b) cow heart, and (c) lamb lung used for the repeated puncturing test of recessed bio-SPME probes. (d) Before and (e) after microscopic images of the coating showing no observable damage or discoloration of the coating.

Various tissue sampling scenarios were considered: duck gizzard was selected due to its firmness, cow heart was used to assess performance against tough muscle tissue, while lamb lungs represented a soft but puncture-resilient tissue due to its elastic pleural membrane. In addition, no discoloration of the coating (i.e., blood) was observed, confirming the size-exclusion feature of the biocompatible PAN binder.

2.4.3 Autoclaved coating performance

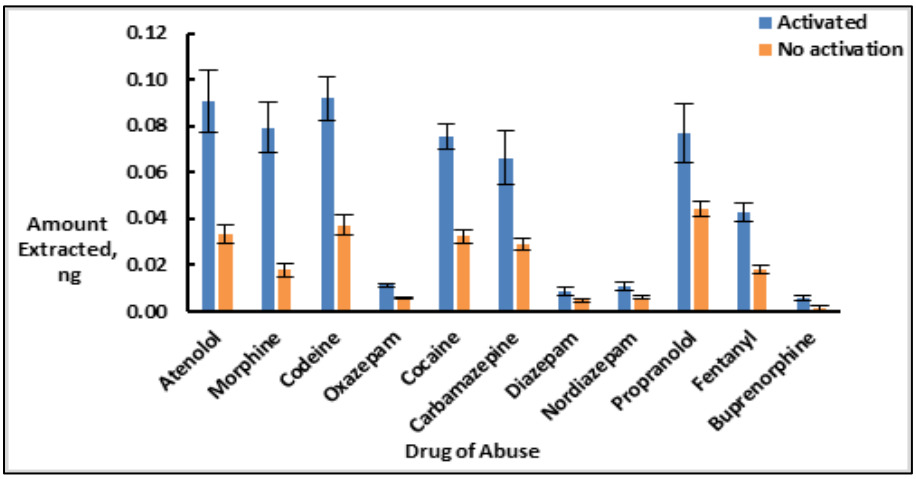


Figure 2.7 Extraction efficiency of common drugs of abuse (DOA) by conventional HLB sorbent (blue) with and (orange) without solvent activation (autoclaved). Sample matrix: human plasma, [DOA] = 10 ng/mL, 1000 rpm benchtop agitation, extraction time = 20 min.

Due to the incompatibility of solvent activation for clinical in vivo applications (solvent evaporation),[52] the extraction efficiency of autoclaved HLB/ PAN SPME probes was investigated, as shown in Fig. 2.7. As expected, the conventional HLB extraction phase showed greatly reduced extraction efficiency for DOAs over a wide range of logP values ($LogP_{atenolol}$ = 0.2, $LogP_{buprenorphine}$ = 5.0, PubChem). The same experiment was performed for the commercial mixed-mode C8-sulfonate extraction phase and the same pattern (deduced extraction efficiency) was observed, apart from highly non-polar analytes (Fig. 2.8). It is currently unclear why the extraction efficiency of non-polar analytes was less affected by autoclave-deactivation of the C8-sulfonate extraction phase. Further studies should investigate this phenomenon to better understand the mechanism of mass transfer between the sample matrix and the extraction phase.

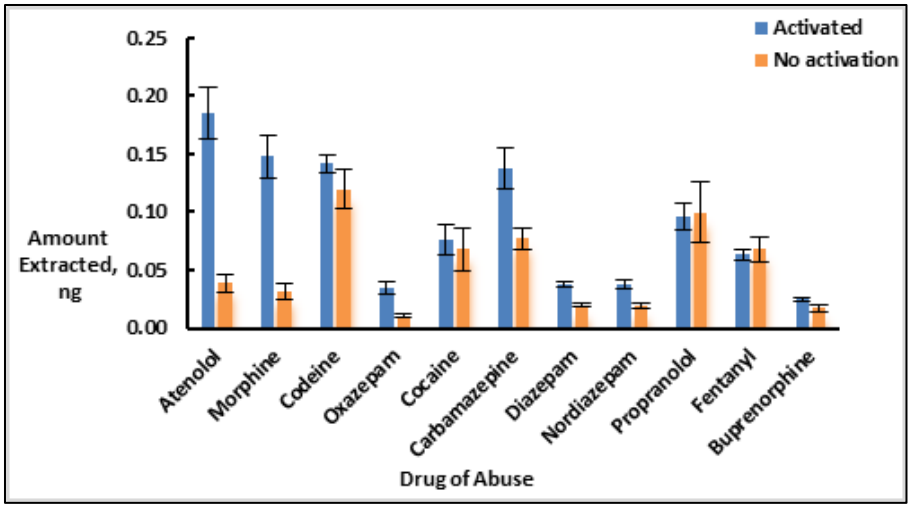


Figure 2.8 Extraction efficiency of common drugs of abuse (DOA) by commercial MM sorbent (blue) with and (orange) without solvent activation (autoclaved). Sample matrix: human plasma, [DOA] = 10 ng/mL, 1000 rpm benchtop agitation, extraction time = 20 min.

2.4.4 Synthesis and characterization of wHLB

We hypothesized that hydrophilic particles would rapidly establish the aqueous medium that facilitates analyte mass transfer between the sample and the extraction phase. As such, the journey to synthesizing a wettable version of the HLB extraction phase began. The finalized protocol for the synthesis of the wHLB particles (in Methods) was the fruit of various synthesis parameter optimization experiments. The in-house synthesis protocol of the conventional HLB particle was adopted as a starting point.[53] Since NVP is the hydrophilic functional monomer in the synthesis of HLB particles (NVP-DVB copolymer), the effect of increasing the NVP:DVB mole ratio was first investigated. Due to the drastic difference in the reactivity ratios for NVP (r_1) and DVB (r_2) where $r_2 >> r_1$, doubling the NVP:DVB reaction mole ratio from 1:4 to 1:2 (by doubling nNVP; nDVB remained the same) did not affect the extraction efficiency of HLB yielding

results identical to Fig. 2.7 above.[127] During the batch-syntheses, drastically different yields and discolorations (yellow) of the HLB particles were obtained, which were later found to correlate with the slightly (within ±3°C) different reaction temperatures associated with different silicone oil bath setups. Reaction temperature has numerous effects in free radical copolymerization and vinyl polymerization reactions, such as monomer reactivity ratios and rates of reaction.[55,56] Similarly, reaction solvent also plays a vital role in monomer reactivity.[55,57] As such, two externally calibrated and elevated reaction temperatures (75 and 80 °C) as well as a few mildly polar to polar solvents were investigated (ACN, EtOH, water). Particle yield and discoloration were inconsistent at 75 °C in all solvents and at 80 °C in water. 80 °C was then chosen as the reaction temperature while ACN and EtOH were investigated as potential solvents. Between ACN and EtOH, particle coalescence was often observed for HLB particles synthesized with ACN as the solvent, and to a lesser extent, with EtOH as the solvent. An example of this is shown in the SEM image below (Fig. 2.9a). This was reasoned to be due to the particles adhering to the reaction glass vessel during synthesis, as less adherence was observed when EtOH was used as a solvent. The extent of particle adherence to the reaction vessel was further reduced when a Teflon reaction vessel was used instead of a glass one (Fig. 2.9b).

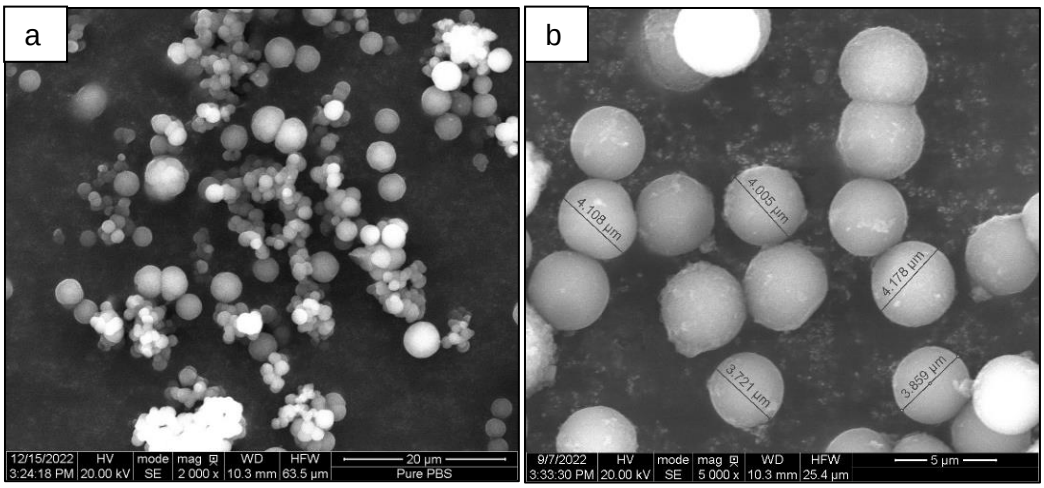


Figure 2.9 SEM images of (a) wHLB particle coalescence in ACN and (b) wHLB particles separated in EtOH.

In addition to the reduced degree of particle coalescence, HLB particles synthesized in EtOH were also uniform in size at around 4 µm in diameter. This was an unintended yet welcomed outcome. The particle size distribution (PSD) was characterized via Dynamic Light Scattering (DLS) dispersed in water and is shown below (Fig 2.10).

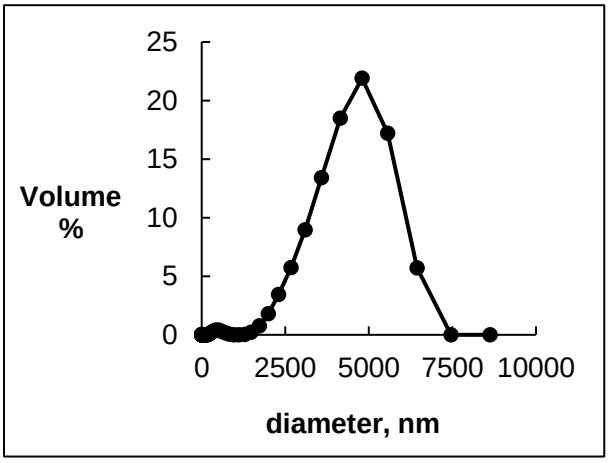


Figure 2.10 Dynamic Light Scattering (DLS) of wHLB particles suspended in water.

A more uniform PSD often correlates to improved reproducibility in separation science due to the increased uniformity in matrix flow and mass

transfer.[58] Moreover, an even and smooth SPME coating can be achieved when uniform-sized particles are used in the coating slurry, as shown in Fig. 2.4. This minimizes analytical deviations associated with physical irregularities of the coating as well.

Table 2.1 shows the elemental composition of HLB particles synthesized with various reaction monomer ratios at 80 °C in EtOH.

Table 2.1 Elemental Analysis of HLB particles synthesized from varying monomer reaction ratios at 80 °C.

Copolymer Particle	Total elemental composition (%wt.)			
	%C	±%C	%N	±%N
1:4 NVP:DVB (HLB)	89.1	0.3	0.92	0.03
1:2 NVP:DVB	87.5	0.2	0.87	0.01
1:1 NVP:DVB	88.4	0.3	1.13	0.01
2:1 NVP:DVB	87.6	0.1	1.34	0.01
3:1 NVP:DVB	86.7	0.2	1.59	0.02
4:1 NVP:DVB	86.7	0.1	1.76	0.01
5:1 NVP:DVB (wHLB)	84.7	0.2	2.59	0.01

The NVP:DVB reaction mole ratio was optimized by step-wise increases until a desired experimental outcome was reached. SPME probes coated with each resulting copolymer particles were subjected to the same DOA extraction efficiency experiment previously carried out for MM and conventional HLB probes. The extraction efficiency of the resulting wHLB sorbent at a 5:1 NVP:DVB mole ratio remained the same when the sorbent coating was autoclaved (Fig. 2.11). A reaction time optimization experiment was later performed, and 22 hours was determined to be the minimum reaction time required to produce effective wHLB particles. Reaction times of 12, 16, 20, 22, 24 hours were tested.

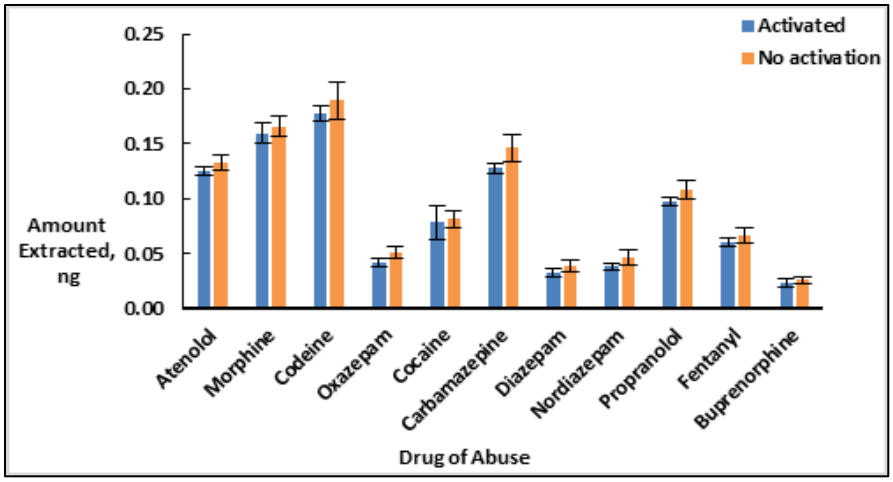


Figure 2.11 Extraction efficiency of common drugs of abuse (DOA) by wHLB sorbent (blue) with and (orange) without solvent activation (autoclaved). Sample matrix: human plasma, [DOA] = 10 ng/mL, 1000 rpm benchtop agitation, extraction time = 20 min.

Based on the weight% of N, the molar NVP content of wHLB can be estimated using the molecular formulae of NVP and DVB:

$$N\%_{wt.} = 0.0259 = \frac{14.0067\, n_{NVP}}{130.19\, n_{DVB} + 111.14\, n_{NVP}}$$

$$n_{NVP} = 0.303\, n_{DVB} = \frac{0.233}{n_{NVP} + n_{DVB}}$$

Similarly, using weight% of C:

$$C\%_{wt.} = 0.847 = \frac{10 \times 12.011\, n_{DVB} + 6 \times 12.011\, n_{NVP}}{130.19\, n_{DVB} + 111.14\, n_{NVP}}$$

$$n_{NVP} = 0.453\, n_{DVB} = \frac{0.312}{n_{NVP} + n_{DVB}}$$

Solving the equation with the measured total $N\%_{wt.}$ and $C\%_{wt.}$ in the particles shows wHLB contains somewhere between 23 – 31% molar content of NVP. Excess NVP remained in the reaction mixture due to the different reaction ratios.

Intuitively, the wettability of the sorbent should also depend on the availability of water in the sample. Figures 2.12 a – b below show that the extraction efficiency of wHLB did not change following autoclaving in more complex matrices than plasma, such as human blood and homogenized ovine lung tissue.

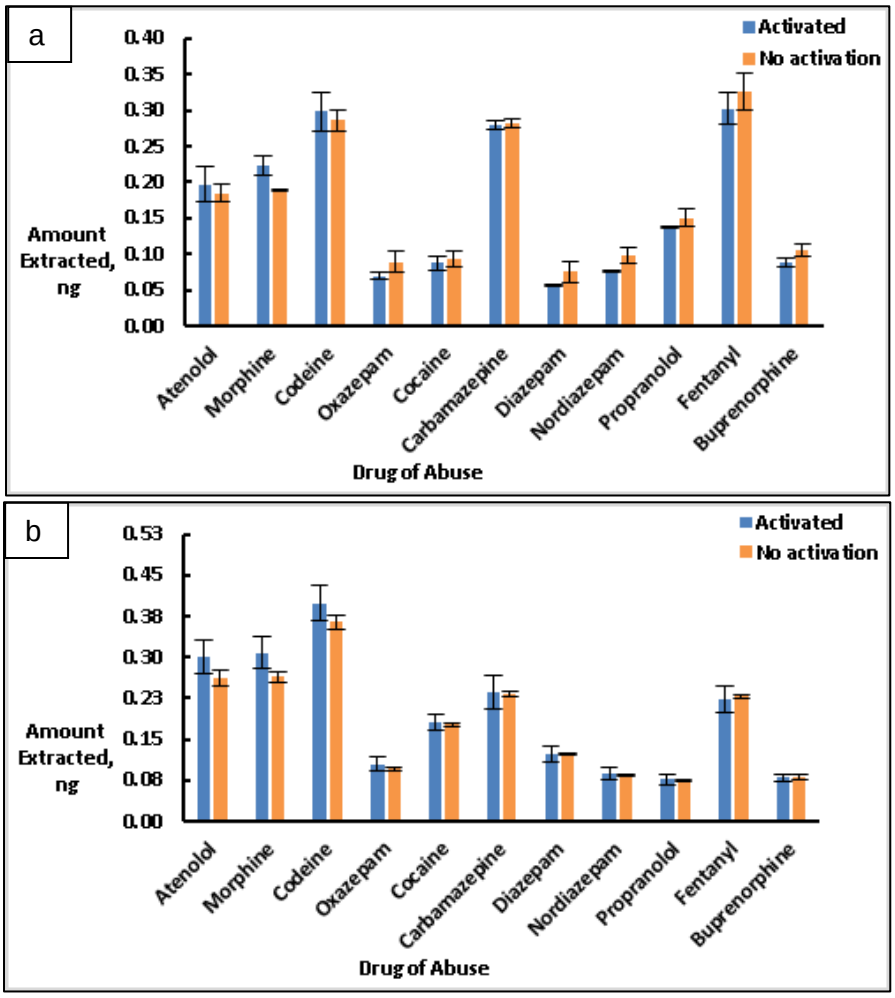


Figure 2.12 Extraction efficiency of common drugs of abuse (DOA) by wHLB sorbent (blue) with and (orange) without solvent activation (autoclaved). Sample matrices: (a) human whole blood, (b) homogenized lamb lung [DOA] = (a) 20 ng/mL, (b) 50 ng/mL, 1000 rpm benchtop agitation, extraction time = 20 min.

The nanogram amounts extracted did not increase proportionally to the increasing spiked DOA concentrations going from a simpler matrix (plasma in Fig.

2.11) to more complex matrices (blood and tissue in Fig. 2.12). This was expected due to reasons such as increased matrix-binding and the balanced recovery feature of SPME accommodating for endogenous compounds.[45] As a result, wHLB/PAN was used as the extraction phase in the finalized recessed bio-SPME probes submitted to clinical and pre-clinical applications.

2.4.5 Clinical and pre-clinical applications

One of the most notable recent in vivo clinical applications of SPME entails the chemotherapeutic drug monitoring of DOX via in vivo SPME.[36,50,51] In order to quantitatively determine the amount of DOX extracted during in vivo lung perfusion (IVLP), matrix-matched calibration (MMC) was performed using ovine lung homogenate as the tissue model.[36,51] Similarly, another IVLP study with oxaliplatin (OxPt) for lung metastasis took place at Toronto General Hospital (Toronto, ON, CA) where the novel recessed bio-SPME wHLB\PAN chemical biopsy probes were used to monitor OxPt levels in vivo.

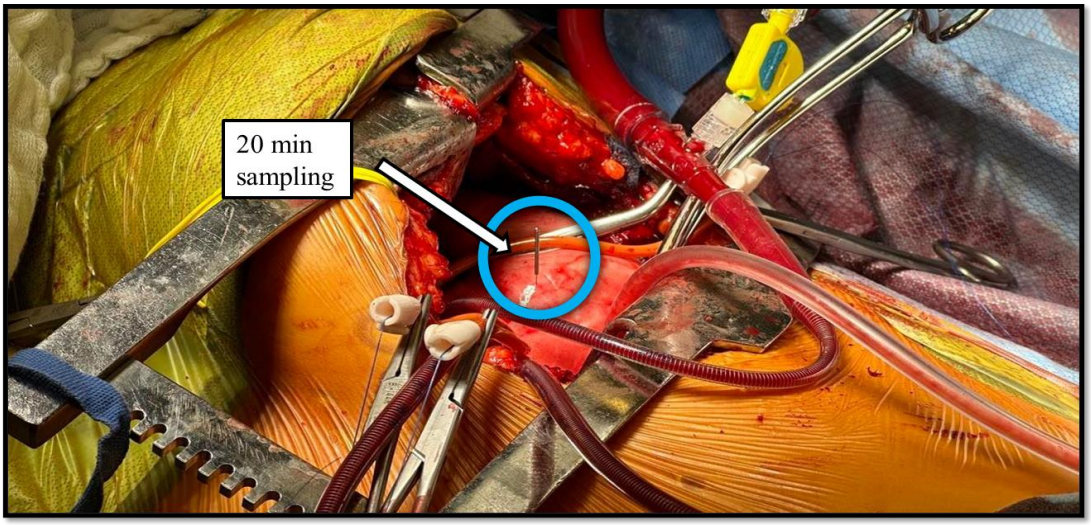


Figure 2.13 In vivo SPME chemical biopsy probe sampling from patient's left lung during IVLP with oxaliplatin for secondary lung cancer.

The temporal and spatial (between-lobe) data from the surgery were obtained via LC-MS/MS endpoint detection and are shown in Fig. 2.14 below.

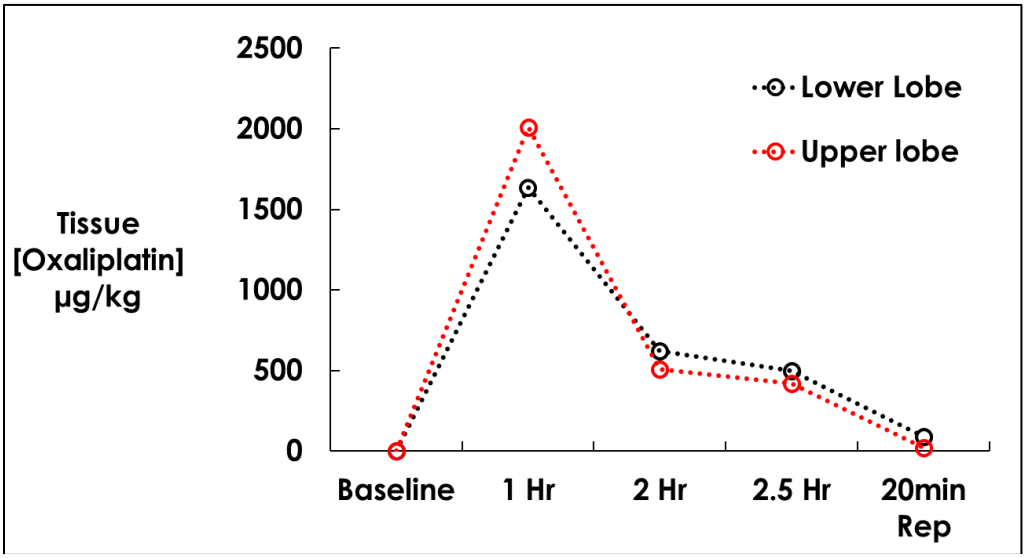


Figure 2.14 Time-resolved between-lobe oxaliplatin concentrations of upper and lower lobes of the left lung during IVLP via in vivo SPME-LCMS. 20min Rep = 20-min of reperfusion following the 2.5-hour IVLP.

The dosage of OxPt was 50 mL at 9 mg OxPt /mL. Five data points were collected: at baseline (before IVLP), at 1, 2, 2.5 Hr of IVLP, and after 20 min blood reperfusion post-IVLP (N = 10). Expected in vivo OxPt levels were obtained where OxPt peaked initially and rapidly decreased over the course of IVLP due to rapid OxPt metabolism.[59] The similar between-lobe DOX levels were also expected due to the high-flow circulation (~500 mL/min) of the chemoagent during IVLP.[50]

In contrast, a chemo-suffusion (no flow) study was conducted at the Roswell Park Comprehensive Cancer Center (Buffalo, NY, USA) where in vivo DOX levels were monitored using the same probes during an open-chest surgery

of a mature live pig. In the left lung, 1 location of each lobe was sampled as baseline and 3 arbitrary locations (top, middle, bottom) of each lobe were sampled at 30 min after suffusion and 10 min after reperfusion (N = 14). The tissue DOX concentration varied drastically between different locations of each lobe and between lobes (Table 2.2), which expectedly reflected the drawback of static-mode (suffusion) chemotherapy. The tissue DOX concentrations determined via probes 3 and 5 far exceeded the upper linearity range of the MMC curve. Based on separate investigations, the upper limit of linearity of 500 – 1000 mg-DOX / kg was found to be due to saturation of tissue binding (Chapter 5), not the capabilities of the MS detector; therefore, these two values were considered overestimations and were not further investigated.

Table 2.2 DOX levels in porcine left lung during chemo-suffusion via recessed bio-SPME chemical biopsy probes. (*) 30 min suffusion (^) 10 min reperfusion.

Probe #	Location	Tissue [DOX], mg/kg
1, 2	Caudal (lower) and Cranial (upper) lobe baseline (pre-treatment)	-
3	Caudal bottom 5-min post-treatment*	1353.9
4	Caudal middle 5-min post-treatment*	479.4
5	Caudal top 5-min post-treatment*	1580.2
6	Cranial bottom 5-min post-treatment*	263.8
7	Cranial middle 5-min post-treatment*	63.9
8	Cranial top 5-min post-treatment*	61.2
9	Caudal bottom 5-min post-reperfusion^	17.7
10	Caudal middle 5-min post-reperfusion^	29.9
11	Caudal top 5-min post-reperfusion^	19.3
12	Cranial bottom 5-min post-reperfusion^	4.7
13	Cranial middle 5-min post-reperfusion^	3.9
14	Cranial top 5-min post-reperfusion^	12.9

Another pre-clinical application of the recessed wHLB/PAN probes was conducted. In this study, Doxorubicin Liposomal (Doxil™) (DOX encapsulated in

lipid nanoparticles) was administered to woodchucks with liver cancer to bioaccumulate in the tumors. DOX was then released within the tumors from the protective lipid shell upon localized photo-activation via interstitial photodynamic therapy (iPDT).[60] The bio-SPME probes were inserted, in triplicates, into each of the two tumors and nearby liver tissue to quantify DOX levels before (Pre-light) and after (Post-light) light-activation. The results (Fig. 2.15) showed that iPDT is an effective technique for local chemotherapy delivery. However, further fine-tuning of the spatial coverage of the DOX-delivery technique may be required as nearby healthy liver tissue also contained high levels of DOX.

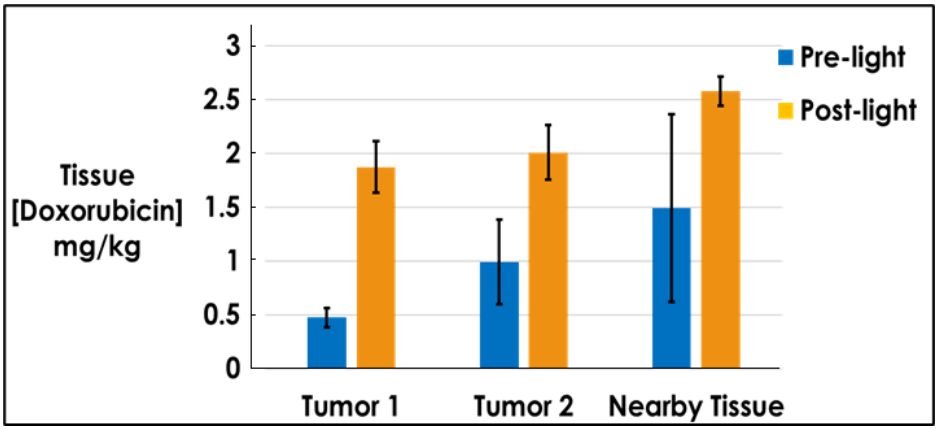


Figure 2.15 Woodchuck liver tumor and tissue DOX concentrations quantified via recessed bio-SPME chemical biopsy probes during immuno-photodynamic therapy (iPDT) with Doxil.

2.4.6 Coupling with direct-MS

Microfluidic open interface (MOI) is a direct-MS interface technology developed by Pawliszyn's group. As a proof-of-concept study, recessed bio-SPME probes coupled with MOI-MS were used for rapid quantification of DOX in homogenized tissue immediately following extractions (Fig. 2.16). 10 µL of desorption solution was used for static-desorption of the recessed bio-SPME

probes. Fluid-flow into the MS inlet was driven by the original Shimadzu heated (100 °C) ESI ion source without external forces applied.[62]

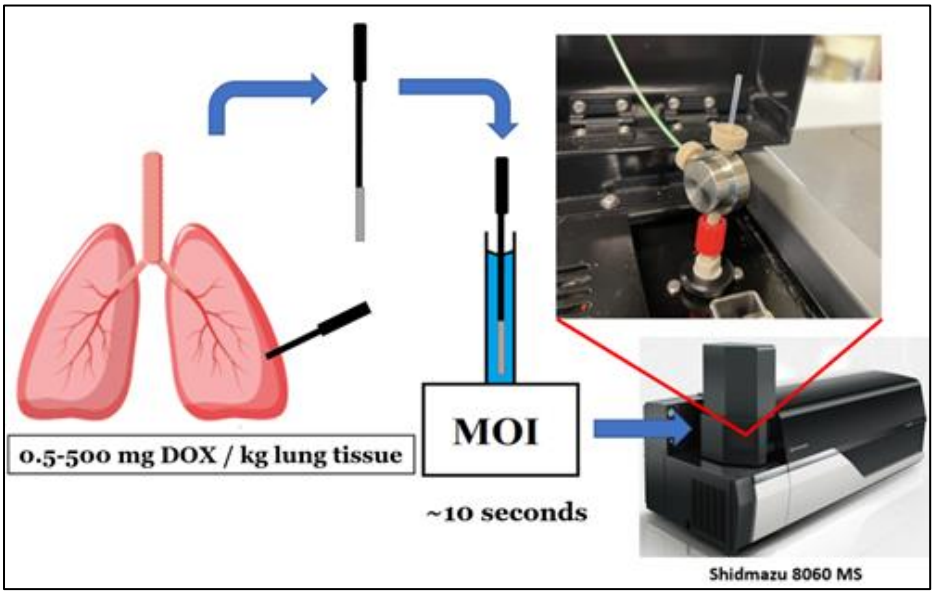


Figure 2.16 Determination of tissue doxorubicin (DOX) concentration via recessed SPME chemical biopsy probes coupled with microfluidic open interface-mass spectrometry (MOI-MS). DOX was scanned in SIM mode for 1 min following the 10-second desorption.

Figure 2.17 shows the lamb lung homogenate MMC curve for DOX via recessed SPME probes coupled to MOI-MS, where a wide linear dynamic range was observed from 1 mg/kg limit of quantitation (LOQ) to 500 mg/kg upper LOL. To validate the absolute quantitation by bio-SPME probes and MOI-MS, two separately prepared samples of known DOX concentrations were used to test the MMC calibration curve (red points). All data points were replicated 4 times (N = 32). The LOD of this method was found to be approximately 0.5 mg-DOX/kg, which was comparable to LC-MS/MS results from previous studies and confirmed in parallel during this study.[50] This result may come as a surprise to many chromatographers as MOI-MS does not have an upstream

chromatography separation. Nevertheless, the sample cleanup of bio-SPME drastically reduces matrix effects commonly associated with biological sample extractions, and the large enrichment factor (due to tiny desorption volume, e.g. 10 µL) ensures analytical sensitivity.[61]

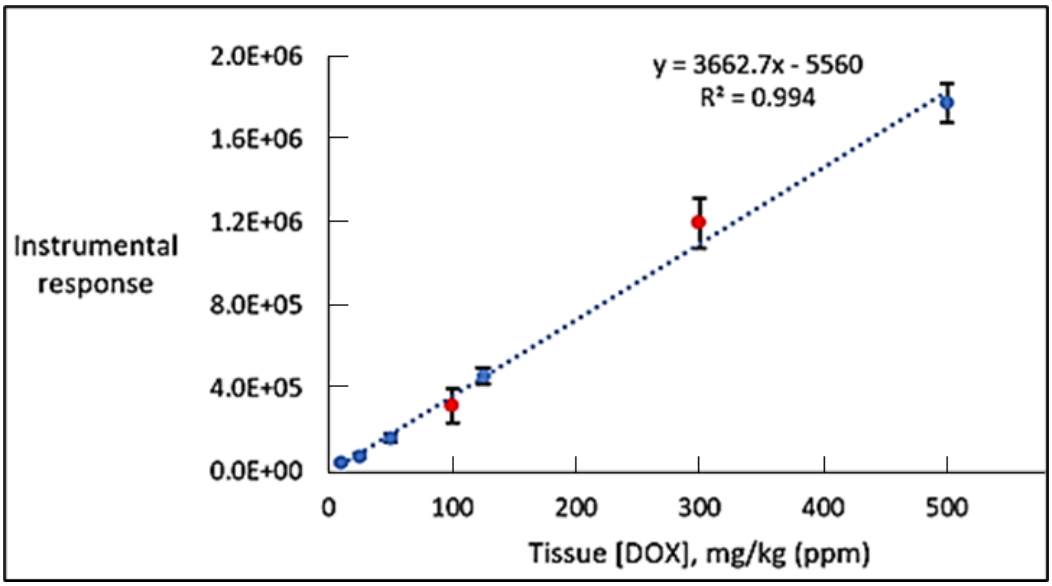


Figure 2.17 Matrix-matched calibration of doxorubicin (DOX) in homogenized ovine lung tissue via R-SPME-AN coupled to MOI-MS. Red points denote test samples from a separate experiment.

Below is the MOI-MS chromatogram containing 8 levels (4 replicates each) of DOX spiked in tissue (n = 32). Reproducible peak areas (RSD < 15%) were obtained for all levels of tissue DOX. While the peak shapes may vary a little due to the handling of the experimenter, the integrated peak areas should remain largely unaffected from samples with tissue [DOX] > 5 mg/kg. With recent advancements in the automation of MOI-MS and portable mass spectrometry, in vivo SPME techniques can be further improved to ensure accuracy and precision in point-of-care analysis for future clinical applications.[62,63]

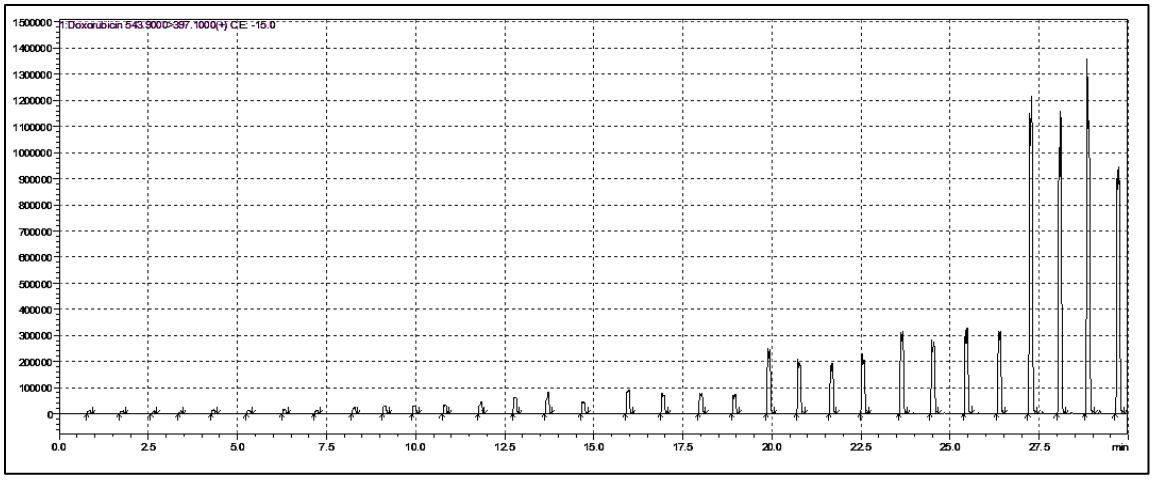


Figure 2.18 MOI-MS chromatogram of DOX by recessed bio-SPME probes coupled with MOI-MS. Y-axis is the instrumental response in arb. units. Desorption volume = 10 µL, ~ 30-second gaps were allocated between each MOI desorption event.

2.4.7 Push-pull SPME microsyringe

Next, the combined analyte coverage of the wHLB/PAN coating and the aqueous extraction phase (PBS) of the push-pull SPME microsyringe was investigated. A 2% agarose gel spiked with polar neurotransmitters (NTs) and non-polar DOAs was used to test the extraction efficiency of the device

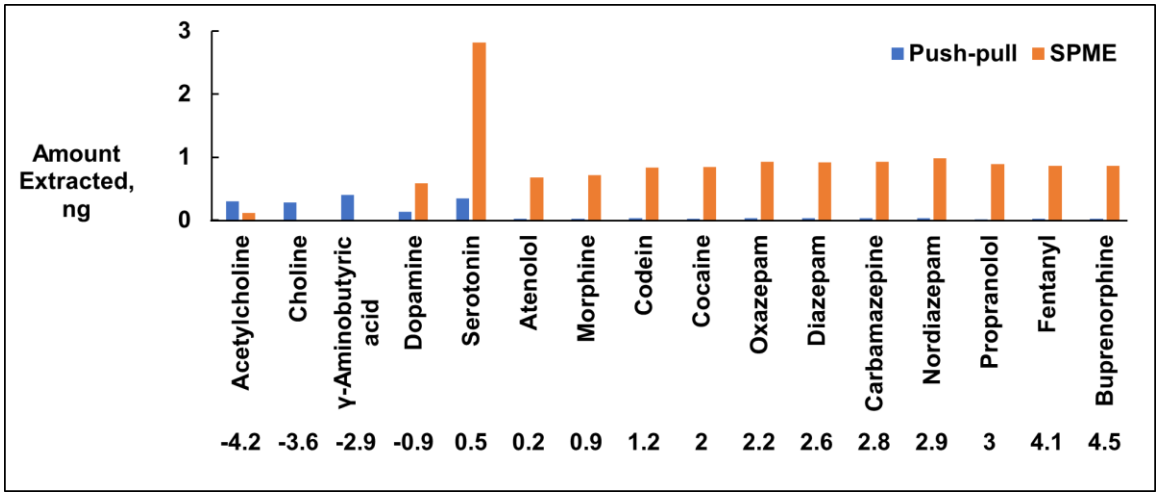


Figure 2.19 Amounts of NTs and DOAs extracted via Push-pull wHLB/PAN SPME microsyringe from agarose gel. Initial [NT] = 200 ng/g, initial [DOA] = 10 ng/g. The numerical values under the x-axis are the corresponding logP of each analyte.

The data above shows complementary analyte coverage between the aqueous extraction phase of the microsyringe and the wHLB/PAN extraction phase of the recessed bio-SPME probe for highly polar and non-polar analytes, respectively. This suggests the extraction of highly polar analytes is possible with one in vivo SPME device, which was thought to be impossible due to most extraction phase chemistries lightly favoring non-polar interactions.

Untargeted metabolomics and lipidomics are great approaches to understand the extent of complementary analyte coverage offered by the push-pull SPME microsyringe as the presence of endogenous compounds provides an unbiased library of potential analytes representative of biological systems. In the following proof-of-concept study, fresh cow brain tissue was used as the model matrix to explore the analyte coverage of SPME (wHLB/PAN), push-pull microsyringe (PBS), as well as the brief water rinse that contains any matrix components bound to the coating surface via unspecific interactions.

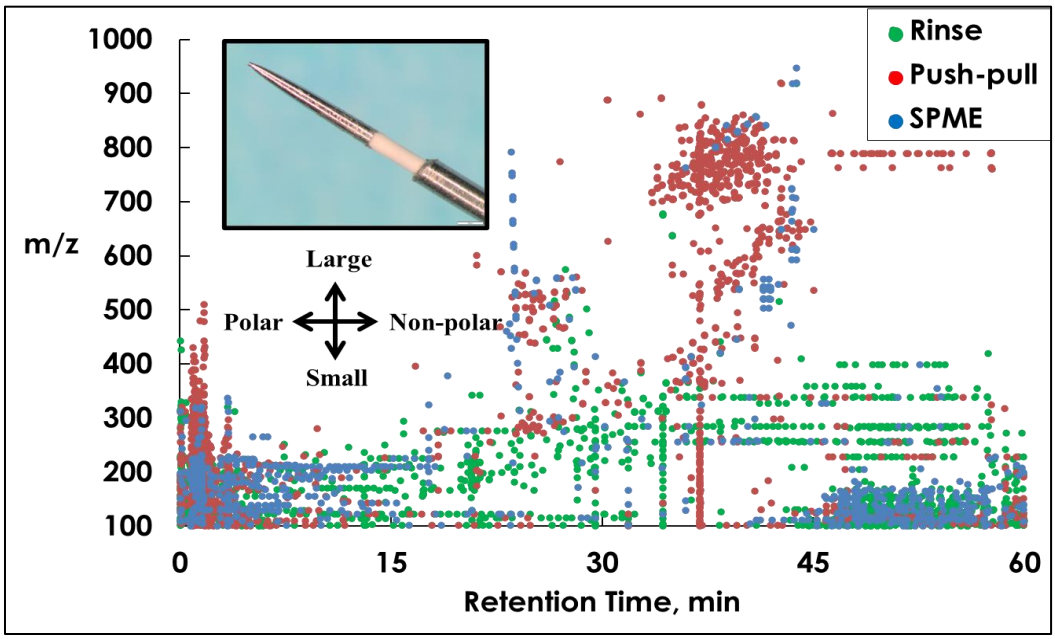


Figure 2.20 Complementary analyte coverage in untargeted metabolomics of bovine brain tissue via recessed SPME wHLB/PAN chemical biopsy probe coupled with push-pull microsyringe. Rinse: water rinse of coating surface post-extraction; Push-pull: aspirated aqueous PBS extraction phase; SPME: wHLB/PAN extraction phase. Reverse-phase LC-MS features were processed via XCMS online.

The most abundant features (by peak area) are plotted in Fig. 2.20 according to the extraction phase. A lower cut-off of 10000 area count was used to declutter the plot. In cases where a feature was detected in more than 1 source, the one with the highest instrumental response was chosen. As expected, the push-pull portion of the microsyringe excelled at capturing polar analytes. As well, larger compounds were also best extracted via push-pull since larger molecules typically struggle to diffuse through the boundary layer around the coating. The post-extraction coating rinse also expectedly captured a wide range of analytes evenly scattered across the retention time. The wHLB/PAN sorbent captured many analytes at both ends of the chromatogram, which is indicative of both polar and non-polar interactions with the extraction phase. The extraction of highly polar and small molecules (based on low RT and m/z) could be potentially explained by the high content of NVP moieties in the wettable version of HLB, but further studies are needed to better understand these specific interactions. Regardless, the untargeted analysis with push-pull microsyringe demonstrated that additional information, complementary to bio-SPME, can be obtained with a miniscule amount of aqueous phase.

2.5 Conclusion

Novel in vivo SPME devices presented in this chapter inherited advantages of existing bio-SPME probes while improving on their flaws for in vivo biomedical applications. The recessed stainless-steel acupuncture needles offer a robust physical support to protect the coating and facilitate insertion for in vivo sampling. The needles come in two lengths (30 and 60 cm) and are equipped

with a handle to improve the convenience of tracking and handling for medical staff. The wettable version of the conventional HLB chemical sorbent, wHLB for short, can extract a wide polarity range of compounds. Such sorbent enables targeted analyte quantification and untargeted metabolomics without the need for prior solvent activation. Furthermore, the recessed bio-SPME probes can be assembled into a push-pull SPME microsyringe when coupled with a sharpened stainless-steel sheath. The pushing and pulling of an aqueous extraction phase by SPME microsyringes can provide untargeted information complementary to that attainable by the wHLB-SPME extraction phase. Beyond the clinical, pre-clinical, and proof-of-concept studies presented in this chapter, further biomedical applications will explore what in vivo SPME can achieve in the realms of personalized care and bioinformatics.

Chapter 3. Solid-phase microextraction (SPME) of endogenous metabolites from intact tissue validated using a Biocrates standard reference method kit.

3.1 Preamble

The findings presented in this chapter were obtained with the help from Biocrates Life Sciences (Innsbruck, Austria). The materials presented in this chapter have been published in the *Journal of Pharmaceutical Analysis* in a collective effort from the following co-authors: Runshan W. Jiang, Karol Jaroch, and Janusz Pawliszyn (DOI: 10.1016/j.jpha.2022.09.002). Please see *Statement of contributions* for more information. We would like to thank the following organizations for their generous fundings: Natural Sciences and Engineering Research Council (NSERC) of Canada and the University of Waterloo.

3.2 Introduction

Metabolomics is the systematic study of low-molecular-weight molecules in a biological system. Typically, the primary aim of metabolomics is to quantify the effects of physiological and biochemical changes on cellular metabolism. For example, metabolomics analysis can be used to assess the survival outcomes of donor lungs in transplant patients.[65] As metabolomics gains more interest in the fields of biology and biomedicine, researchers must contend with new challenges and considerations relating to sample acquisition, storage, and preparation. For

instance, Roszkowska et al.[66] observed differences in the metabolomic coverage provided by ex vivo solid-phase microextraction (SPME) and solid-liquid extraction (SLE) when the two methods were applied to analyze fish tissue. Specifically, they found that SLE resulted in the detection of more lipids due to the release of compounds from protein complexes and the disruption of the bilayer membrane. A similar study showed that metabolomics using in vivo SPME enabled the extraction of unstable fish tissue metabolites that could not be detected by traditional methods. This advantage was enhanced by immediately following up in vivo SPME with instrumental analysis to avoid changes in the sample induced during storage.[67] Even with simpler sample matrices, such as blood, urine, and other biological fluids, numerous preanalytical variables have been shown to result in biases that can adversely impact the outcome of qualitative and quantitative analyses.[68] As such, direct sampling and sample preparation techniques are highly desirable.

When applied in vivo, SPME is a powerful and minimally invasive analytical technique that allows chemical biopsies to be performed directly on a living system. In vivo SPME typically utilizes a miniature fiber geometry, which can be inserted into the target tissue to obtain metabolomic information in its current physiological state without alteration.[24] In addition, SPME's metabolism-quenching effect prolongs the stability of bioactive metabolites which can be stored on-fiber, transported and frozen until analysis.[24,31] SPME is also compatible with several different extraction phases, offering a broad range of analyte coverage,[69] while its non-exhaustive nature helps to minimize changes in

the studied biological system.[31] The latter feature is key in differentiating SPME from exhaustive extraction methods such as liquid-liquid extraction (LLE) and solid-phase extraction (SPE), which typically involve destructive sampling of the studied system. For instance, Napylov et al.[32] successfully extracted up to 52 oxylipins from the brain tissue of live, conscious rats via SPME, which was the largest panel of oxylipins detected in vivo to date. The success of their study was largely due to SPME's ability to overcome the chemical limitations of the membranes used in conventional in vivo microdialysis. Furthermore, Napylov et al.[32] noted that over 24 of the oxylipins had been exclusively detected postmortem, with only 3 having been detected in living rats via in vivo SPME. This observation, combined with the success of Napylov et al.'s study, highlights the prominent advantages of in vivo SPME compared to conventional destructive sampling methods. Further applications of in vivo SPME in animal models yielded interesting findings, such as significantly different ($p < 0.05$) endogenous metabolomes in the brains, livers, kidneys, and muscles of different strains of lab mice.[70] In another study, in vivo SPME was successfully utilized to measure and correlate the local concentrations of the cognitive enhancement drug, donepezil, and its target enhancement metabolite, acetylcholine, for the first time in a live primate (Macaca mulatta).[71] Following years of exploratory work assessing the application of in vivo SPME in animal models, researchers have shifted their attention to explore human clinical applications of this technology in the last decade. In 2021, Bogusiewicz et al. demonstrated, for the first time, the viability of applying SPME to sample brain tissue in a conscious human patient.[72] They

successfully performed chemical biopsies in vivo by inserting four SPME fibers into the patients' brain tissue prior to stereotactic biopsy. This approach enabled them to avoid causing any extra damage, while still allowing the standard procedure to be performed in parallel during the operation. The obtained lipidomic data were characteristic of brain tissue, thus confirming SPME's potential as a complementary tool for collecting information in vivo. Similarly, in vivo SPME has been used for therapeutic drug monitoring (TDM) and metabolomics in the lungs. To this end, SPME fibers coated with a biocompatible C8-sulfonate (mixed-mode) extraction phase were used to quantify concentrations of the chemotherapeutic agent, doxorubicin (DOX), in the lungs undergoing perfusion during localized chemotherapy.[36,51] The desorption solutions obtained from the fibers used in these analyses were then subjected to further untargeted metabolomics analysis via ultra-high-performance liquid chromatography coupled with high-resolution mass spectrometry (UHPLC-HRMS).[36]

SPME enables quantification through kinetic calibration in in vivo experiments, but this ability depends on certain requirements. Typically, internal standards are preloaded onto the fiber and the quantity of target analytes is calculated based on the desorption and adsorption rates of the internal standard and analyte, respectively. To ensure isotropy in the analytes' adsorption and desorption to and from the SPME fiber, the selected internal standards must share similar physicochemical properties with the target analytes; thus, deuterated internal standards of the target analytes are typically the optimal

choice. As a result, kinetic calibration is a suitable method for applications requiring the quantification of a limited number of compounds, such as TDM or pharmacokinetic studies in blood.[73,74] However, since metabolomic profiling deals with an enormous number of compounds in various biological matrices, kinetic quantification using internal standards is often impractical. Additionally, even if analytically suitable standards could be chosen, utilizing internal standards in vivo is challenging for safety reasons. Instead, matrix-matched calibration (MMC) is often an appropriate alternative. Roszkowska et al. demonstrated that comparable analyte responses can be achieved for various chemotherapeutic agents when using lamb tissue homogenate to simulate in vivo conditions.[35] Thus, in vivo SPME can be used as a quantitative analytical technique when coupled with in vitro MMC.

Nonetheless, some challenges remain in untargeted metabolomics, with analytical variation ranking among the most problematic. Instrumental signal variations can occur due to numerous factors, such as inherent imperfections in the analytical instruments and varying ion suppression caused by drastic differences in analyte composition between individual samples. This difference is further exaggerated when handling a large cohort, or inter-batch, inter-day, or inter-laboratory variability.[75,76] In addition, metabolite annotation during data mining is a major bottleneck in untargeted metabolomics. To alleviate this bottleneck, commercial metabolomic assays capable of quantifying hundreds of key metabolites from various compound classes can be used.[76] In this study, an Absolute p180 kit (Biocrates, Innsbruck, Austria) was used for the quantitative

analysis of nearly 200 endogenous compounds, including amino acids, biogenic amines, monosaccharides, acylcarnitines, glycerophospholipids, and sphingolipids. The kit contains a 96-well plate, which is used to introduce internal standards to the unknown samples, as well as calibration standards and three levels of quality control (QC) samples. In this study, we used a Vanquish UHPLC coupled with a Vantage TSQ mass spectrometer (Thermo Fisher Scientific, Waltham, MA, USA) for both the LC-MS and flow injection analysis (FIA) portions of the assay. The LC-MS portion aimed to detect amino acids and biogenic amines, whereas the FIA portion was intended to detect monosaccharides, acylcarnitines, glycerophospholipids, and sphingolipids. Currently, all assays sold by Biocrates are based on liquid extractions, which require homogenization for tissue analysis. As discussed earlier, this process invariably results in changes to the metabolome.

This proof-of-concept study has two primary objectives: 1) to show that SPME can be combined with a Biocrates AbsoluteIDQ kit to detect various analytes in targeted tissue metabolomics and 2) to demonstrate the advantages of intact tissue sampling compared to homogenized tissue sampling.

3.3 Materials and methods

3.3.1 Materials and chemicals

AbsoluteIDQ p180 kit was purchased from Biocrates Life Sciences (Innsbruck, Austria). Further details relating to the contents of the kit can be found at https://biocrates.com/absoluteidq-p180-kit/. P.A.-grade phosphate

buffered saline (PBS) tablets, LC-MS grade ethanol (EtOH), methanol (MeOH), acetonitrile (ACN), and 2-propanol (IPA) were purchased from Thermo Fisher Scientific (Waltham, MA, USA). P.A.-grade phenylisothiocyanate (PITC), pyridine, LC-MS-grade ammonium acetate (AmAc) (Burlington, MA, USA), and formic acid (FA) were purchased from Sigma-Aldrich (St. Louis, MO, USA). Ovine (lamb) lungs were chosen as the target organ tissue and were purchased fresh from a local butcher shop.

3.3.2 Liquid chromatography-mass spectrometry (LC-MS), flow injection analysis (FIA)

Biogenic amines and amino acids were analyzed via Thermo Vanquish Horizon liquid chromatography coupled with a Thermo Vantage TSQ mass spectrometer system (Waltham, MA, USA). The LC-MS system was managed using Thermo Xcalibur 4.0, Chromeleon 7.2.6, and Thermo TSQ Series 2.6 Tune Master instrument control software. The chromatography method was adopted from the AbsoluteIDQ p180 kit with the following modification: the chromatographic separation process was optimized and performed on a C18 reverse-phase HPLC column (100 mm × 2.1 mm, 3 µm particles) at 50 ± 0.5 °C and a C18 reverse-phase HPLC guard column (10 mm × 2.1 mm, 3 µm particles), both were included in the kit. Mobile phase A is ultrapure water with 0.2% v/v FA, and mobile phase B is acetonitrile with 0.2% v/v FA. Separation was achieved using the following multistep gradient: started at 0% B until 0.25 min followed by a linear increase to 12.0% B until 1.5 min, then a linear increase to 17.5% B until 2.7 min. A steep linear increase to 50.0% B took place in 4 min followed by a

steeper increase to 95% B until 4.5 min. B was then maintained at 95% until 5.25 min, followed by a sharp linear decrease back to 0.0% B until 5.4 min. Lastly, the method ends with a 2.6 min equilibration stage at 0.0% B (8 min total). A flow rate of 0.8 mL/min was maintained throughout the gradient for each 5.0 µL injection. All samples were kept at 4 °C in the LC autosampler prior to injection. The autosampler syringe was washed with ACN, MeOH, IPA, and water (50/20/15/15 v/v/v/v) for 5.0 s at 32.0 µL/s before and after each injection.

Acylcarnitines, glycerophospholipids, sphingolipids, and hexoses were analyzed via FIA on the same LC-MS system in both positive and negative modes according to the kit's recommendation. All mobile phases used in the LC-MS and FIA (FIA additive provided in the kit) analyses were degassed via ultrasonication.

3.3.3 Sample preparations

Three sample preparation and extraction methods were tested in this study: 1) tissue homogenization followed by SLE coupled with the Biocrates kit (THB); 2) tissue homogenization followed by SPME coupled with the Biocrates kit (THSB); and 3) intact tissue extraction via SPME coupled with the Biocrates kit (ITSB). In methods 2) and 3), the Biocrates AbsoluteIDQ p180 kit was used for metabolite detection, quantification, and QC for SPME.

Chilled lamb lung tissue samples (4 °C) were diced up to remove the major bronchi and adipose tissue. A uniform suspension was obtained using a generic tabletop blender to homogenize approximately 200 g of the tissue with

small amounts (~10 g) of dry ice to avoid heating. The homogenate was then mixed with 0.01 M PBS at a ratio of 1:3 (mg tissue/µL solvent) on a benchtop vortexer to produce the final homogenate.[77] PBS was chosen as the extraction phase for SLE because organic solvents are generally incompatible with SPME, and PBS offers the added advantage of the favorable extraction of more polar analytes, such as amino acids, biogenic amines, and short-chain lipids compared to organic extraction phases. The supernatant for THB analysis was collected by centrifuging a portion (~10 mL) of each tissue homogenate sample at 10,000 g for 5 min using a swing-bucket rotor inside an Eppendorf Centrifuge 5804R (Hamburg, Germany).

3.3.4 SLE- and SPME- AbsoluteIDQ p180 kit protocols

The in vivo SPME methodology used in this study was adopted from Bojko et al.[36] with minor changes. Specifically, the present study was conducted using nitinol-based SPME fibers coated with a C8-sulfonate strong cationic exchange (SCX) mixed-mode extraction phase (Supelco, Bellefonte, PA, USA). The coated wires were cut into ~4 cm fibers and stripped such that the coating length extended 15 mm from the tip. The fibers were then cleaned with a solution comprised of acetonitrile, methanol, isopropanol, and water (30/30/30/10, V/V/V/V) for 30 min on a Benchmark Scientific BenchMixer Multi-Tube Vortexer (Edison, NJ, U.S.A.) at 1500 rpm. After cleaning, the fibers were placed in a MeOH:water (1:1 v/v) preconditioning solution for 15 min at 1500 rpm, and then stored in a fresh preconditioning solution until use. Four fibers were briefly rinsed with ultrapure water (~ 5 s) to remove any surface solvent and then inserted into

the tissue homogenate prepared in Section 2.3 (THSB). The same rinsing process was applied to an additional four fibers, which were then inserted into intact ovine lungs (ITSB) for 20 min at ~ 18 °C (instrument room temperature) for static extraction. Following extraction, the fibers were removed from the sample, rinsed in ultrapure water for 5 s to remove any particulates and macromolecules that may have attached to the surface of the coating via nonspecific binding, and briefly dried with a Kim wipe. Next, the fibers were desorbed in an 80-µL ACN:water (4/1, v/v) solution for 60 min at 1500 rpm. PBS blanks, 10-µL aliquots of the solvent extraction for THB, and 40 µL of desorption solution from THSB and ITSB were added to the kit plate according to the instructions provided in the user manual. Similarly, the PITC derivatization of amino acids was conducted according to the instructions provided in the user manual. Four replicates were performed for each sample type (n = 4).

3.3.5 Data processing and statistical analysis

The raw instrumental data from the LC-MS and FIA analyses were processed using Biocrates MetIDQ, Version Boron (Innsbruck, Austria), following the directions in Sections 5 and 6 of the user manual (p.180). Due to the changes made to the default kit protocol to accommodate the integration of SPME as an upstream sample preparation and extraction step, the processed raw data (i.e., signal intensity for FIA, peak area, and area:IS ratios for LC-MS) from MetIDQ were subjected to further manual sorting in Excel (Microsoft Office 365, Albuquerque, NM, USA). During this sorting step, compounds were excluded if the IS-corrected data (response of analyte/response of IS) had a signal-to-noise

(S:N) ratio of less than 3 or a relative standard deviation (RSD) exceeding 30%. The sorted LC-MS and FIA data were then combined and uploaded for data preprocessing on Metaboanalyst 5.0. Pareto scaling and log transformation were employed to account for massive values for certain metabolites. Principal component analysis (PCA) was also performed using Metaboanalyst 5.0. Data from all three groups (ITSB, THSB, and THB), were subjected to nonparametric one-way analysis of variance (Kruskal-Wallis test) with $p < 0.05$ on TIBCO Statistica, version 13.3. (Palo Alto, CA, USA).

3. 4 Results and discussion

3.4.1 LC-MS results

A complete table of compounds and their relative abundances can be found in Table 3.1. Exemplary LC-MS and FIA chromatograms for all three method groups can be found in Figures 3.1 a – i. Preliminary total ion chromatograms (TIC) using the kit's standard sample mixture passed the System Suitability tests as part of the Biocrates AbsoluteIDQ p180 kit. This was to ensure the LC-MS system was clean with very little background and sensitive enough to quantitate the target analytes.

Table 3.1 MS analyte-to-internal standard response ratios of compounds detected by each sample preparation method.

#	Compound	Compound Class	Detection Method	P180 kit (THB)	SPME-P180 kit (THSB)	SPME-p180 kit (ITSB)
1	**Met**	**Amino acids**	**LC-MS**	1.5 (1E-1)	0.0009 (1E-1)	ND*
2	**Phe**			3.5 (3E-1)	ND	0.011 (3E-3)
3	**Trp**			0.54 (4E-2)	ND	0.0030 (9E-4)
1	**Serotonin**	**Biogenic Amines**		ND	0.0004 (1E-4)	ND
2	**Taurine**			13.1 (1E-1)	0.032 (8E-3)	ND
1	**AC3-OH**	**Acylcarnitines**	**FIA**	ND	0.006 (1E-3)	0.005 (1E-3)
2	**AC5-M-DC**			0.023 (7E-3)	0.015 (3E-3)	0.022 (7E-3)
3	**AC5:1**			0.019 (6E-3)	0.008 (1E-3)	0.008 (1E-3)
4	**AC8**			0.040 (3E-3)	0.028 (3E-3)	0.026 (1E-3)
5	**AC9**			0.008 (1E-3)	0.0021 (4E-4)	ND
6	**AC10**			0.031 (3E-3)	0.018 (2E-3)	0.0168 (9E-4)
7	**AC10:1**			0.19 (1E-2)	0.17 (1E-2)	0.199 (5E-3)
8	**AC10:2**			ND	0.009 (1E-3)	0.0077 (1E-4)
9	**AC12**			0.23 (2E-2)	0.013 (2E-3)	0.0124 (1E-4)
10	**AC12-DC**			0.050 (5E-3)	0.052 (4E-3)	0.056 (3E-3)

11	**AC12:1**		0.22 (3E-2)	0.19 (3E-2)	0.219 (3E-3)
12	**AC14**		0.014 (E-3)	0.0050 (7E-4)	0.0040 (5E-4)
13	**AC14:2-OH**		0.0025 (3E-4)	ND	0.0016 (5E-4)
14	**AC16:1**		0.013 (3E-3)	0.003 (6E-4)	0.0026 (5E-4)
15	**AC16:2**		ND	0.0030 (9E-4)	0.0034 (1E-3)
16	**AC16:2-OH**		0.006 (1E-3)	ND	0.0029 (5E-4)
1	**lysoPC C14:0**	**Glycero-phospholipids**	0.021 (3E-3)	0.0029 (2E-4)	0.0032 (4E-4)
2	**lysoPC C16:0**		0.31 (4E-2)	0.0051 (8E-4)	0.0104 (7E-4)
3	**lysoPC C16:1**		0.031 (2E-3)	0.0019 (3E-4)	0.0023 (3E-4)
4	**lysoPC C17:0**		0.025 (2E-3)	ND	0.0010 (2E-4)
5	**lysoPC C18:0**		0.10 (1E-2)	0.0029 (3E-4)	0.0041 (3E-4)
6	**lysoPC C18:1**		0.083 (9E-3)	0.0017 (2E-4)	0.0036 (2E-4)
7	**lysoPC C18:2**		0.023 (3E-3)	ND	0.0017 (2E-4)
8	**lysoPC C20:3**		0.0046 (3E-4)	0.0012 (1E-4)	0.0016 (1E-4)
9	**lysoPC C20:4**		0.017 (2E-3)	0.0009 (1E-4)	0.0014 (1E-4)
10	**lysoPC C24:0**		0.008 (1E-3)	ND	0.0011 (2E-4)
11	**lysoPC C26:0**		0.023 (3E-3)	0.0014 (3E-4)	0.0030 (7E-4)
12	**lysoPC C26:1**		0.006 (1E-3)	0.0011 (3E-4)	0.0019 (3E-4)
13	**lysoPC C28:0**		0.022 (2E-3)	ND	0.0023 (1E-4)

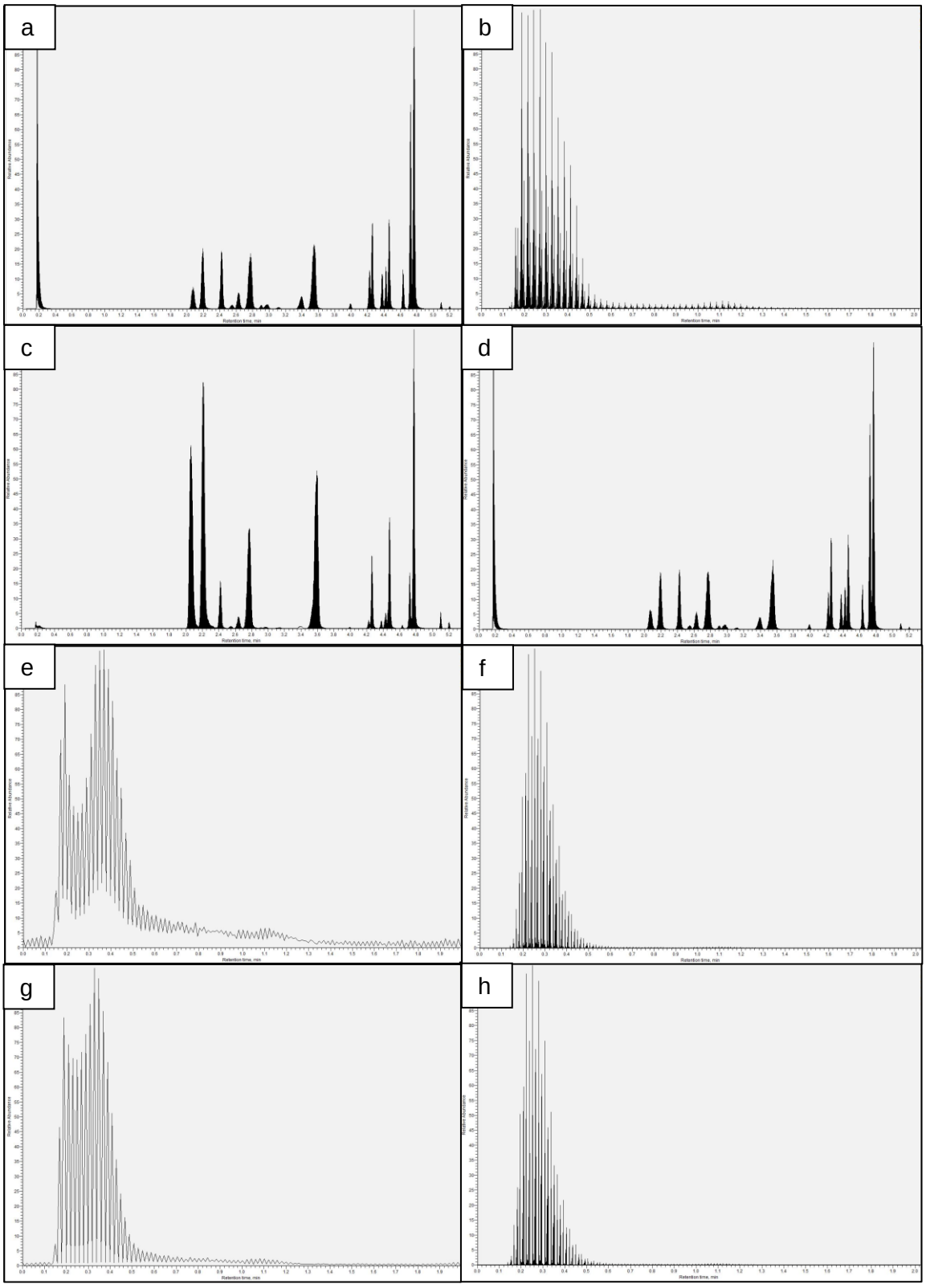
14	**lysoPC C28:1**	0.012 (1E-3)	0.0012 (3E-4)	ND
1	**PC aa C24:0**	0.0058 (7E-4)	0.0008 (2E-4)	0.013 (2E-3)
2	**PC aa C26:0**	0.029 (5E-3)	0.008 (2E-3)	0.013 (2E-3)
3	**PC aa C28:1**	0.012 (1E-3)	0.0013 (3E-4)	0.0018 (4E-4)
4	**PC aa C30:0**	1.12 (8E-2)	0.005 (1E-3)	ND
5	**PC aa C32:0**	2.4 (2E-1)	0.006 (1E-3)	ND
6	**PC aa C32:1**	0.99 (7E-2)	0.0031 (6E-4)	ND
7	**PC aa C32:2**	0.050 (4E-3)	0.0005 (1E-4)	0.0007 (2E-4)
8	**PC aa C32:3**	0.0040 (4E-4)	0.0001 (<E-4)	ND
9	**PC aa C34:1**	0.0040 (4E-4)	0.004 (1E-3)	ND
10	**PC aa C34:2**	1.25 (9E-2)	0.0024 (6E-4)	ND
11	**PC aa C34:3**	0.051 (2E-3)	0.0003 (<E-4)	0.0006 (1E-4)
12	**PC aa C34:4**	0.0103 (7E-4)	0.0002 (<E-4)	0.0002 (<E-4)
13	**PC aa C36:0**	0.0026 (6E-4)	0.0006 (<E-4)	0.0006 (1E-4)
14	**PC aa C36:2**	0.34 (3E-2)	0.0015 (5E-4)	0.0023 (6E-4)
15	**PC aa C36:3**	0.17 (1E-2)	0.0007 (1E-4)	ND
16	**PC aa C36:4**	0.35 (2E-2)	ND	0.0027 (7E-4)
17	**PC aa C36:5**	0.039 (2E-3)	0.0004 (1E-4)	ND
18	**PC aa C36:6**	0.0038 (6E-4)	ND	0.0001 (<E-4)

19	**PC aa C38:0**	0.0054 (3E-4)	ND	0.0001 (<E-4)
20	**PC aa C38:3**	0.052 (4E-4)	0.0003 (<E-4)	ND
21	**PC aa C38:4**	0.18 (1E-2)	0.0007 (2E-4)	ND
22	**PC aa C38:5**	0.122 (8E-3)	0.0007 (2E-4)	ND
23	**PC aa C38:6**	0.029 (2E-3)	ND	0.0007 (2E-4)
24	**PC aa C40:1**	0.0042 (2E-4)	0.0024 (<E-4)	0.0023 (<E-4)
25	**PC aa C40:2**	0.0023 (3E-4)	ND	0.0001 (<E-4)
26	**PC aa C40:4**	0.0133 (5E-4)	0.0002 (1E-4)	0.0002 (1E-4)
27	**PC aa C40:5**	0.023 (1E-3)	0.0001 (<E-4)	ND
28	**PC aa C40:6**	0.018 (1E-3)	0.0009 (2E-4)	0.0010 (2E-4)
29	**PC aa C42:0**	0.0010 (2E-4)	0.0007 (2E-4)	0.0006 (<E-4)
30	**PC aa C42:2**	0.018 (1E-4)	0.0005 (1E-4)	0.0005 (<E-4)
31	**PC aa C42:6**	0.0021 (1E-4)	0.0005 (<E-4)	0.0006 (<E-4)
1	**PC ae C30:0**	0.12 (1E-2)	0.0014 (1E-4)	0.0022 (6e-4)
2	**PC ae C30:2**	0.0023 (6E-4)	0.0002 (<E-4)	0.0003 (<E-4)
3	**PC ae C32:1**	0.091 (9E-3)	0.0005 (1E-4)	ND
4	**PC ae C34:1**	0.27 (2e-32)	0.0009 (2e-4)	0.0025 (7e-4)
5	**PC ae C34:2**	0.04 (3E-3)	0.0003 (<E-4)	ND
6	**PC ae C34:3**	0.0071 (9E-4)	0.0002 (<E-4)	0.0003 (<E-4)

7	**PC ae C36:0**	0.015 (2E-3)	0.0005 (<E-4)	0.0005 (1E-4)
8	**PC ae C36:2**	0.065 (5E-3)	0.0004 (<E-4)	0.0007 (2E-4)
9	**PC ae C36:3**	0.0171 (5E-4)	0.0001 (<E-4)	ND
10	**PC ae C36:4**	0.028 (2E-3)	0.0001 (<E-4)	ND
11	**PC ae C36:5**	0.018 (1E-3)	ND	0.0002 (<E-4)
12	**PC ae C38:0**	0.0055 (1E-4)	0.0012 (<E-4)	0.0013 (1E-4)
13	**PC ae C38:1**	0.0074 (7E-4)	0.0003 (<E-4)	0.0004 (1E-4)
14	**PC ae C38:3**	0.0134 (9E-4)	0.0002 (<E-4)	0.0001 (<E-4)
15	**PC ae C38:4**	0.038 (2E-3)	0.0007 (1E-4)	ND
16	**PC ae C38:5**	0.032 (2E-3)	0.0002 (<E-4)	0.0004 (<E-4)
17	**PC ae C38:6**	0.0090 (6E-4)	1E-4 (<E-4)	ND
18	**PC ae C40:1**	0.004 (1E-4)	0.002 (<E-4)	ND
19	**PC ae C40:4**	0.0083 (7E-4)	0.0003 (<E-4)	0.0003 (<E-4)
20	**PC ae C40:5**	0.009 (1E-3)	0.0001 (<E-4)	0.0001 (<E-4)
21	**PC ae C40:6**	0.0067 (6E-4)	0.0001 (<E-4)	0.0001 (<E-4)
22	**PC ae C42:0**	0.0035 (3E-4)	0.0017 (<E-4)	0.0018 (<E-4)
23	**PC ae C42:1**	0.0029 (6E-4)	0.0002 (<E-4)	0.0003 (<E-4)
24	**PC ae C42:2**	0.0024 (5E-4)	0.0001 (<E-4)	ND
25	**PC ae C42:5**	0.0046 (3E-4)	0.0027 (1E-4)	0.0028 (1E-4)
26	**PC ae C44:3**	0.0004 (<E-4)	0.0027 (1E-4)	0.0028 (1E-4)

27	**PC ae C44:4**		0.0006 (3E-4)	0.0002 (<E-4)	0.0001 (<E-4)
28	**PC ae C44:5**		0.0007 (1E-4)	0.0003 (<E-4)	0.0003 (<E-4)
29	**PC ae C44:6**		0.0011 (<E-4)	0.0005 (1E-4)	0.0005 (>E-4)
1	**SM(OH)C14:1**	**Sphingo-myelins**	0.076 (6E-3)	ND	0.0009 (2E-4)
2	**SM(OH)C16:1**		0.115 (9E-3)	0.0006 (1E-4)	ND
3	**SM(OH)C22:1**		0.20 (2E-2)	ND	0.0007 (2E-4)
4	**SM(OH)C22:2**		0.070 (6E-3)	0.0002 (<E-4)	ND
5	**SM(OH)C24:1**		0.092 (7E-3)	0.0002 (<E-4)	0.0002 (<E-4)
6	**SM C16:0**		1.1 (1E-1)	0.006 (1E-3)	ND
7	**SM C16:1**		0.029 (4E-3)	0.0003 (<E-4)	ND
8	**SM C18:0**		0.122 (7E-3)	0.0005 (1E-4)	ND
9	**SM C18:1**		0.0138 (7E-4)	0.0001 (<E-4)	ND
10	**SM C24:0**		0.45 (3E-2)	0.0007 (2E-4)	ND
11	**SM C24:1**		0.38 (4E-2)	0.0006 (1E-4)	ND

*ND = Not Determined (S:N < 3 or RSD > 30%)


a
b
c
d
e
f
g
h

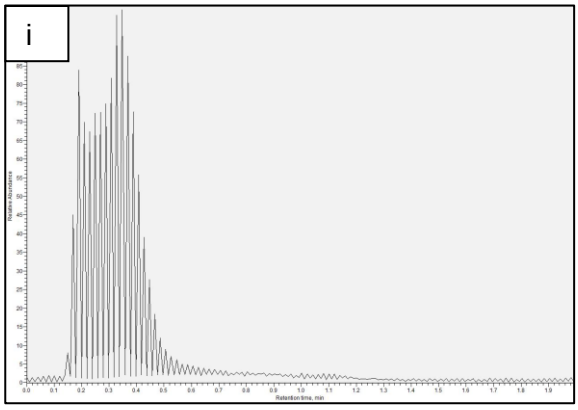


Figure 3.1 Exemplary TICs:
(*) Analysis, ESI polarity, sample, intensity
(a) LCMS, positive, THB, 7.62e6
(b) LCMS, positive, THSB, 3.34E6
(c) LCMS, positive, ITSB, 3.14E6
(d) FIA, positive, THB, 3.46E6
(e) FIA, negative, THB, 1.37E3
(f) FIA, positive, THSB, 9.14E6
(g) FIA, negative, THSB, 5.18E3
(h) FIA, positive, ITSB, 9.12E6
(i) FIA, negative, ITSB, 4.68E3

3.4.2 Statistical analysis

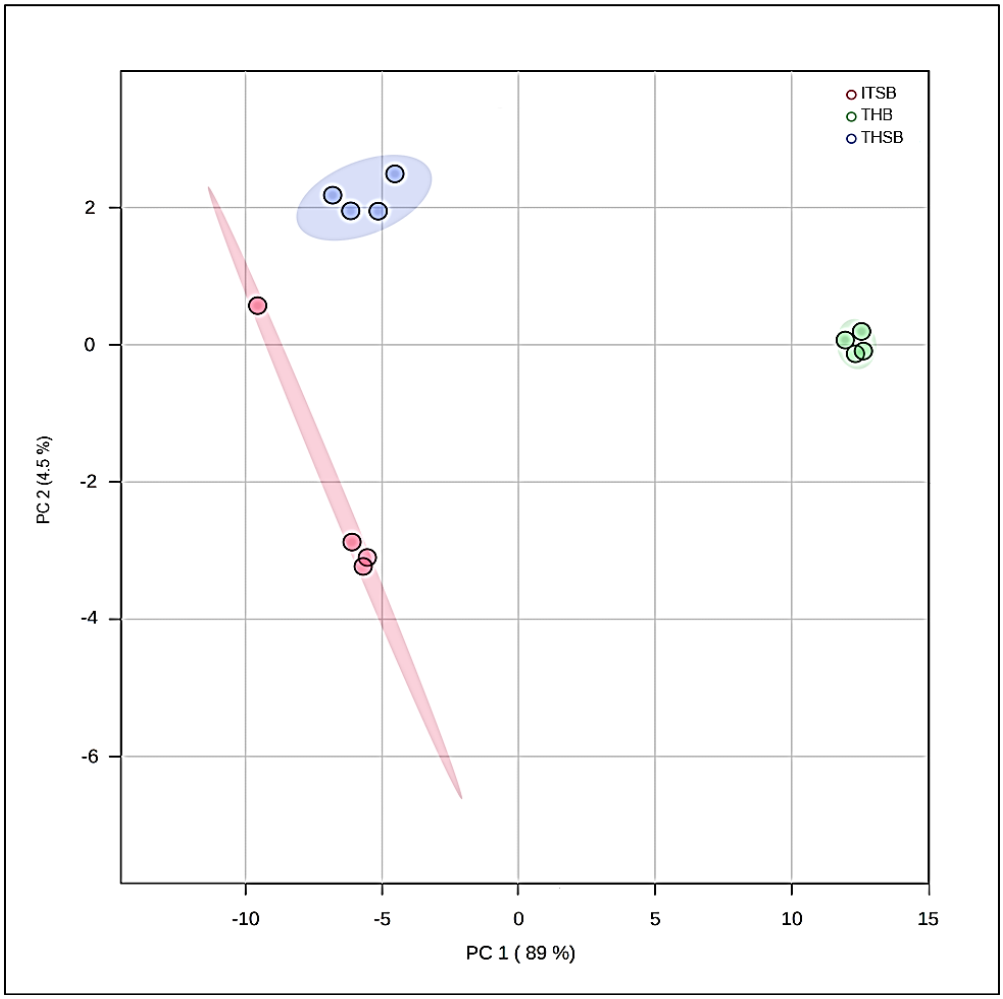


Figure 3.2 Principal component analysis of THB, THSB, and ITSB sample preparation techniques. THB: tissue homogenization followed by solid-liquid extraction (SLE) coupled to the Biocrates kit; THSB: tissue homogenization followed by SPME coupled to the Biocrates kit; ITSB: intact tissue extraction via SPME coupled to the Biocrates kit.

The results of a global PCA revealed distinct separations between the three sample preparation methods (Fig. 3.2). As expected, the biggest separation (along principal component axis 1) was observed for the extractions from homogenized lamb lung tissue via conventional SLE (THB) and the two extractions using SPME fibers (THSB and ITSB). This difference was mostly due to the considerably larger quantity of analytes extracted by the exhaustive SLE method compared to the non-exhaustive SPME technique. More importantly, a clear distinction was also observed between the extractions from intact tissue (ITSB) and homogenized tissue (THSB) using identical SPME methods (along the principal component axis 2). These differences are due to the destructive nature of tissue homogenization which drastically alters the types and amounts of metabolites in a sample. This finding agrees with numerous prior studies, which have speculated that the differences observed in extracted metabolites can be attributed mostly to tissue homogenization.[67,71,72] SPME fibers typically measure no more than 250 µm in outer diameter (OD), which results in minimal damage to the sampled matrix.[24,31] As such, fiber-based SPME can be counted among the novel sample preparation techniques that allow for the direct analysis of intact tissue in vivo. Moreover, SPME extracts analytes via free concentration from the area closely surrounding the fiber, which enables it to determine the spatial resolution of analytes within the organ tissue – information that is generally lost during the homogenization step.[78] Such spatial variation can be seen in Fig. 3.1, where the variance in ITSB was larger than the variance in THSB, and the only difference was the lack of homogenization of the sample tissue. More fibers can

be employed to capture a more representative metabolome profile along with spatially resolved information. Extensive tissue-analyte binding also enables rapid extraction equilibration when using in vivo SPME, which means that quantitative data can be collected in short sampling times.[45] Figures 3.3 and 3.4 illustrate the significant ($p < 0.05$) differences observed for all compounds during extractions from homogenized and intact tissue samples using identical SPME methods. Notably, homogenization resulted in significant ($p < 0.05$) changes in the concentration of small (< 1kDa) metabolites, as well as the lipidome. Specifically, the 30 compounds released by homogenization include phosphatidylcholines (PCs) with aliphatic chains containing 30 to 42 carbons, sphingomyelins (SM) with chains containing 16 to 24 carbons, methionine, and serotonin (Fig. 3.3). In contrast, five lysophosphatidylcholines (LysoPC) with chains containing 17 to 28 carbons, PCs with chains containing 36 to 44 carbons, two acylcarnitines (AC), two SMs, and tryptophan (in total, 17 compounds) decreased or were lost during the tissue disruption protocol (Fig. 3.4). To the best of our knowledge, there exist few studies that have investigated the effect of homogenization on lysoPC levels in tissue, which is likely due to the lack of an approach that allows these compounds to be monitored without destructive sampling/extraction techniques. Given that SPME extracts from the free concentration of analytes,[25] the loss of LysoPC upon tissue homogenization can be potentially explained by several mechanisms. First, lysophosphatidylcholine acyltransferase (LPCAT), which rapidly converts lysoPC to PC as part of the Lands cycle, may be released during the homogenization step. LPCAT is an

intracellular enzyme that can normally access LysoPCs only when it is transported into the cell.[79,80] The loss of LysoPC may also be due to the upregulation of autotaxin, an enzyme that facilitates the hydrolytic conversion of LysoPC to lysophosphatidic acid (LPA). LPA transmits signals calling for cell proliferation and survival, the need for which can be induced by the homogenization step.[79] Similarly, tissue and cellular disruptions can produce a greater free concentration of PCs (especially long-chain PCs) in the lung homogenate. These free long-chain PCs may be created by LPCAT activity discussed above or released from cell membranes during the homogenization process.[81] Further studies are required to confirm these hypotheses. Nevertheless, this study demonstrated a clear metabolome change due to homogenization during sample preparation.

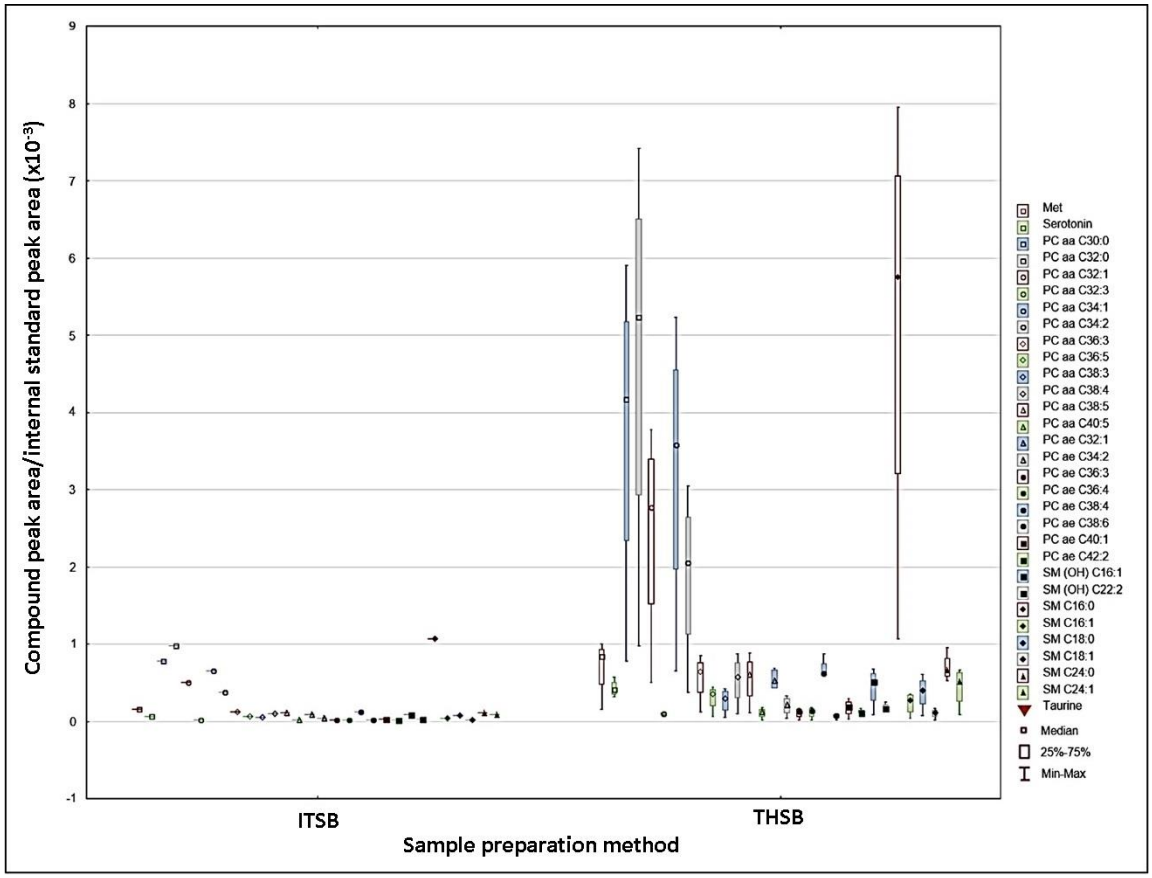


Figure 3.3 Compounds increased/released during tissue homogenization ($p < 0.05$). Note: Y-axis values were preprocessed with Metaboanalyst 5.0 online software. The legend lists the compounds in descending order, corresponding to their appearance on the graph from left to right.

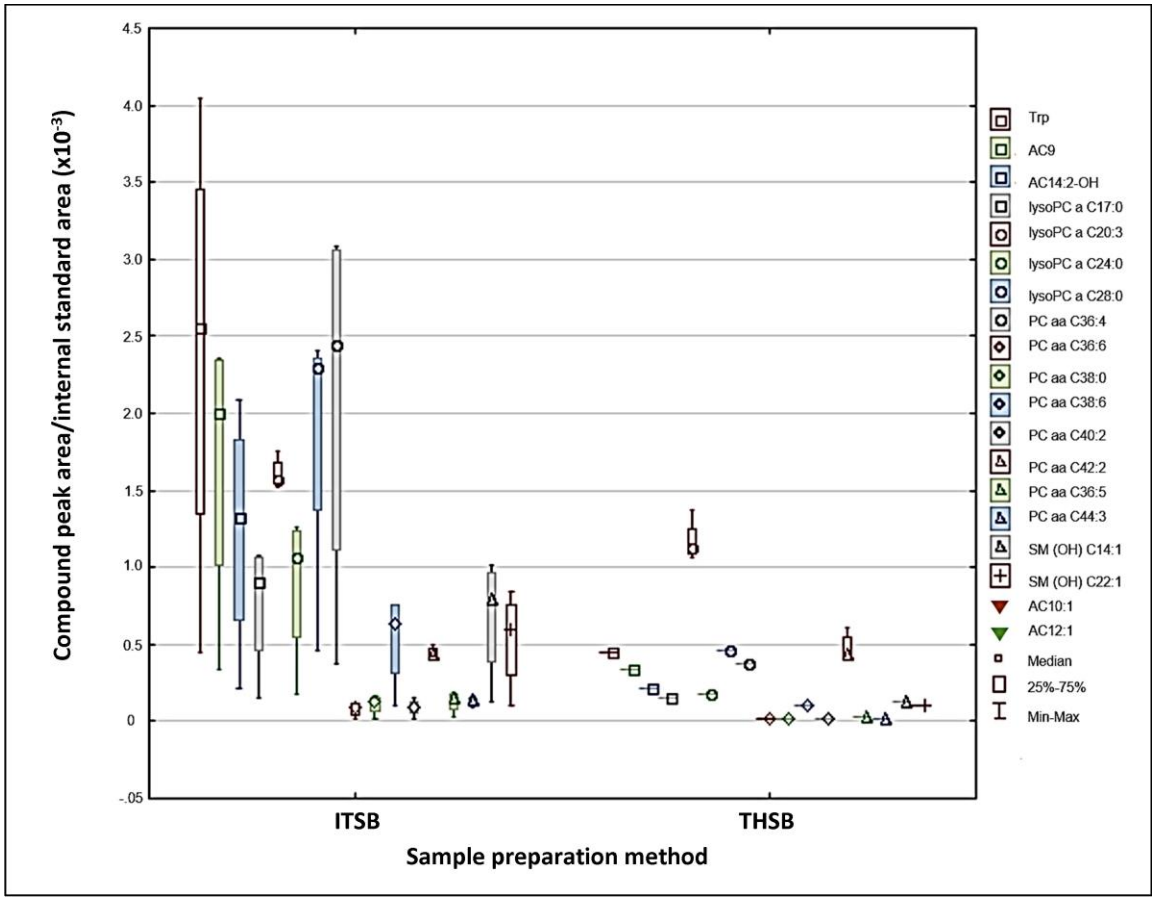


Figure 3.4 Compounds decreased/lost during tissue homogenization ($p < 0.05$). Note: Y-axis values were preprocessed with Metaboanalyst 5.0 online software. The legend lists the compounds in descending order corresponding to their appearance on the graph from left to right.

Shown in Fig. 3.5 below, compounds with similar recoveries between THB and THSB mostly comprised of ACs and a few very long-chain PCs. The similarity in the amounts of long-chain PCs is not surprising, as they are very low in natural abundance; however, the similarity in these ACs was likely due to SPME's enrichment effect on the extracted analytes when using small desorption volumes (e.g. 50 µL).[25] Furthermore, the C8 and the anionic sulfonate functional groups in the mixed-mode extraction phase chemistry also facilitate the extraction of the carnitine head group.[82] Acylcarnitines are intermediate lipid molecules that play a key role in fatty acid transportation in the mitochondria as part of the fatty acid oxidation (FAO) cycle. These molecules are abundant in all biological fluids, especially the liquid portion of blood, and are often screened for the detection of long-chain FAO disorders.[83,84] As such, it was unsurprising that comparable amounts of many acylcarnitine compounds were extracted via SLE and SPME. SPME's ability to extract carnitines has also been demonstrated in a previous study wherein SPME fibers were applied to samples from primary brain tumor tissue. Using SPME, the authors also revealed that higher-grade brain tumors contained higher carnitine levels, and that a relationship exists between carnitine levels and isocitrate dehydrogenase (IDH) mutation status.[72]

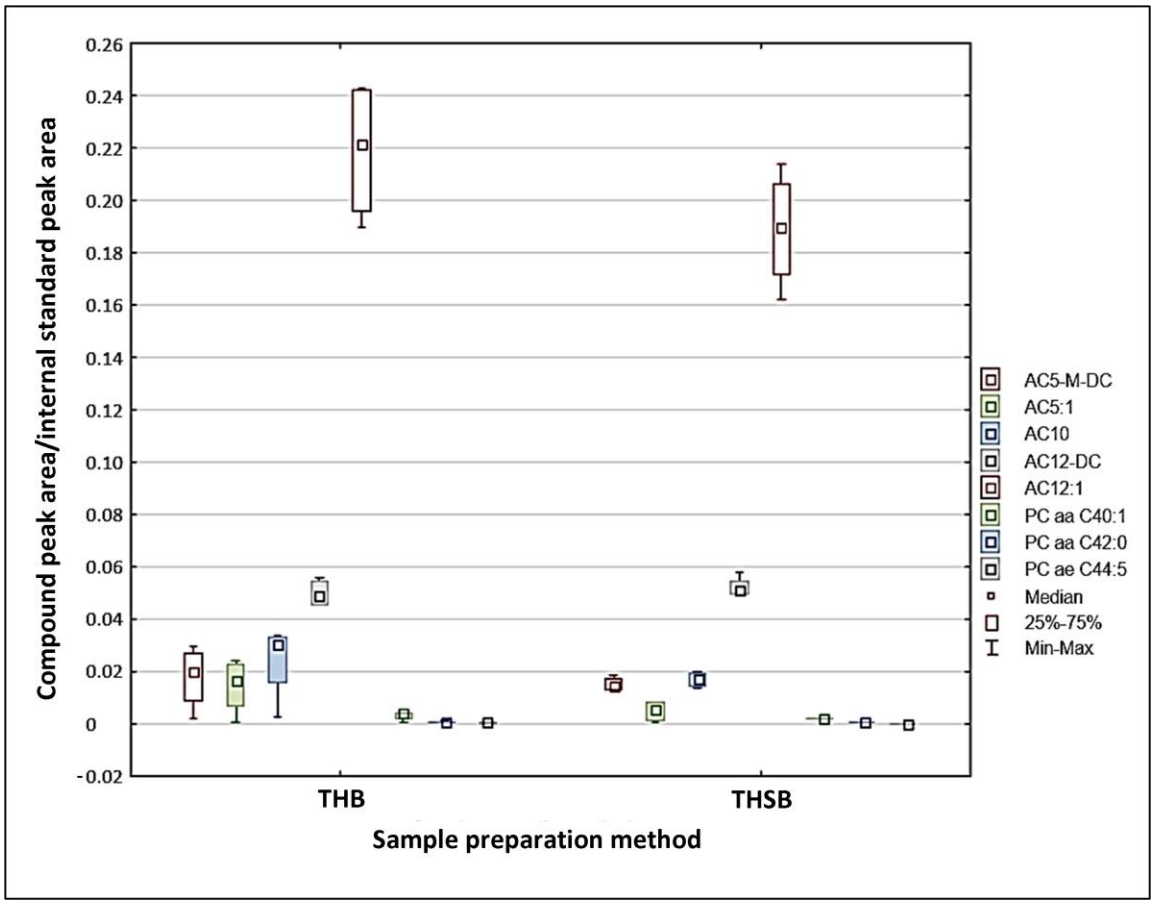


Figure 3.5 Compounds with similar amounts detected by solid-phase microextraction (THSB) and solid-liquid extraction (THB) from homogenized tissue ($p < 0.05$). Note: Y-axis values were preprocessed with Metaboanalyst 5.0 online software. The legend lists the compounds in descending order corresponding to their appearance on the graph from left to right.

Despite SPME's non-exhaustive nature, the wide coverage of endogenous analytes was still expected due to its sample cleanup and concentrating effects.[24,25] SPME analysis can be quantitative despite extracting smaller quantities relative to conventional exhaustive techniques, as chromatographic baseline noise is greatly reduced/near-zero in this technique. Furthermore, the small amount of analytes extracted in SPME also allow for wide analyte coverage in the extraction phase. Sample cleanup was achieved with the biocompatible polyacrylonitrile-based binder in the sorbent coating, which prevented macromolecules from interacting with the extraction phase. This binder also enables metabolism quenching, leading to a much cleaner background compared to the traditional SLE method.[25] In terms of analyte coverage, Birjandi et al.[85] demonstrated the advantage of using SPME for the non-exhaustive extraction of lipids from human hepatocellular carcinoma cells compared to the more conventional SLE method. While SLE extracted a great abundance of phospholipids, SPME provided a more balanced recovery, which greatly reduced matrix effects during LC-MS analysis, thus enabling the detection of a more diverse range of lipid classes. In the present study, the differences between the THSB and THB sample preparation methods were attributable to SPME's non-exhaustive nature, especially in the preequilibrium regime of kinetic extraction (THSB). On the other hand, while the conventional method (THB) could extract an abundance of compounds (Table 3.1), similar analyte coverage was obtained using SPME (THSB), with quantitative signals detected for 102 and 90 compounds for THB and THSB, respectively. Additionally, no significant

differences ($p > 0.05$) between THB and THSB were observed for eight compounds (Fig. 3.6), and four compounds were only reliably detected via the THSB method (P value < 0.05). Notably, these compounds were also detected in THB but with extremely poor reproducibility (RSD >> 30%). Therefore, they were excluded from the results.

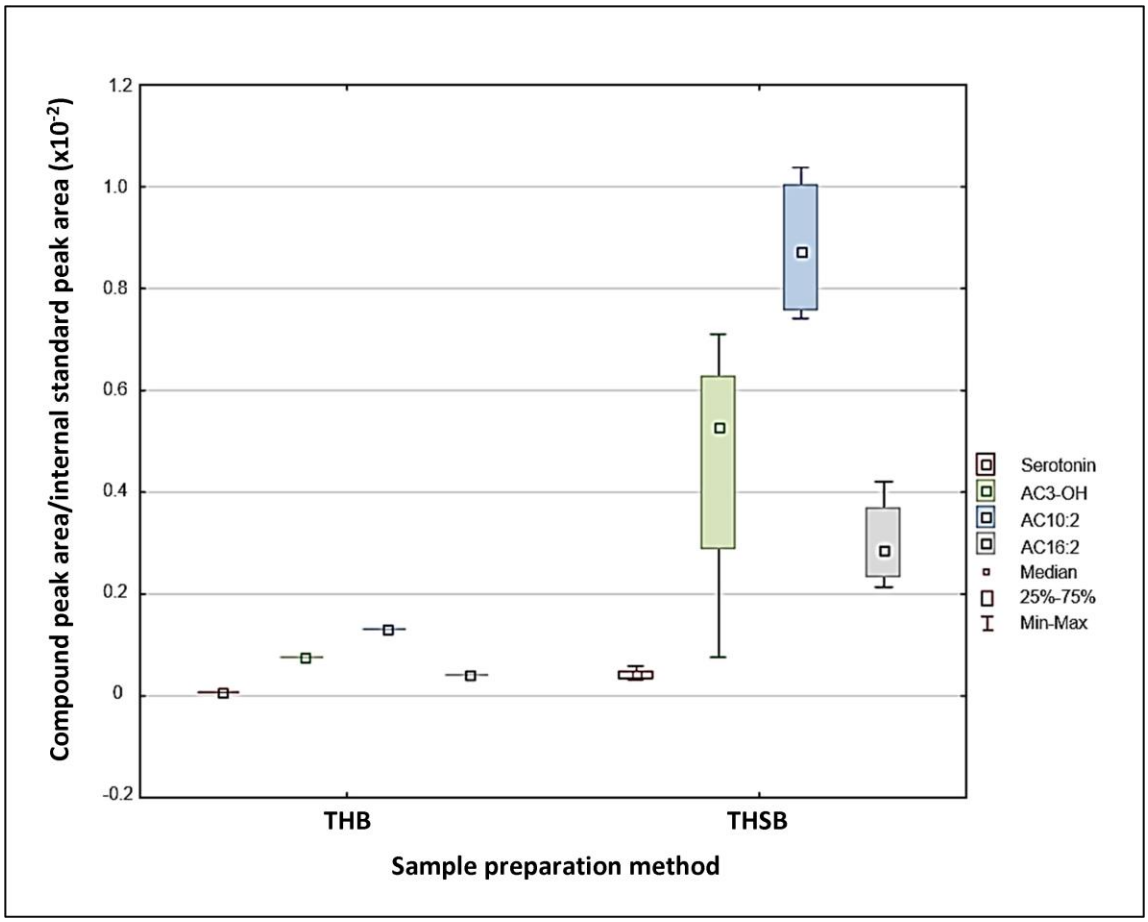


Figure 3.6 Compounds better detected by solid-phase microextraction (THSB) than solid-liquid extraction (SLE). Note: Y-axis values were pre-processed with Metaboanalyst 5.0 online software.

SPME provides more representative metabolomic information by bypassing the disruptive homogenization step (assuming changes do not take place post-extraction). Moreover, various strategies can be employed to further

increase the coverage and detection limits of SPME, such as using multiple fibers and different coating chemistries. For example, Bogusiewicz et al.[72] demonstrated that a single device comprised of multiple fibers with the same coating chemistries can be implemented to perform untargeted metabolomics and lipidomics during intraoperative in vivo sampling. While the authors took advantage of one type of coating chemistry, different coating chemistries can be employed to expand analyte coverage. Desorbing multiple fibers into a single aliquot of desorption solution is also a valid quantitative approach that can drastically boost analyte recovery due to the linear relationship between the amount of analytes extracted and the number of fibers used.[86]

Conclusion

The data reported in this study demonstrated that combining SPME with a well-known metabolomic profiling kit can be a desirable approach for metabolome studies of undisturbed samples. Key findings of this study included the discovery of drastic differences in the metabolomic profiles of intact and homogenized tissues, which had been the subject of much speculation in literature. While exhaustive extraction methods, such as SLE, could recover large quantities of metabolites from homogenized tissue biopsies, these methods often provided metabolomic profiles unrepresentative of living tissues under physiological conditions. In contrast, SPME's ability to provide noninvasive and non-exhaustive analyte recovery made it a valuable tool for applications that involve in vivo metabolomics and without extensive or disruptive sample preparation steps.

Chapter 4. Analysis of endogenous and SARS-CoV-2 viral proteins in human saliva via solid-phase microextraction coupled with liquid chromatography-mass spectrometry.

4.1 Preamble

The findings presented in this chapter were a collaborative effort between University of Waterloo (UW) and University of Saskatchewan (USask). The bio-SPME devices were fabricated at the UW and the clinical sampling took place at the College of Dentistry, USask. The materials presented in this chapter have been submitted for publication in *Analytical Chemistry* with a collective effort from the following co-authors: Runshan W. Jiang, Lina M. Marin, Karol Jaroch, Wei Zhou, Walter L. Siqueira, and Janusz Pawliszyn. Please see *Statement of contributions* for more information. We would like to thank the following organizations for their generous fundings: Natural Sciences and Engineering Research Council (NSERC) of Canada, Canadian Institutes of Health Research (CIHR), University of Waterloo, and University of Saskatchewan.

4.2 Introduction

The Chinese Centre for Disease Control and Prevention promptly published the SARS-CoV-2 viral genome in international databanks, such as GenBank, early into the outbreak which has proven useful for the detection of SARS-CoV-2 across the globe.[87] As a result, polymerase chain reaction (PCR) based screening techniques such as real time quantitative PCR (RT-qPCR) have

been mainly used for the detection of SARS-CoV-2 virus at a hospital.[88] The sampling variability and facility availability concerns associated with RT-qPCR then led to the adoption of protein-based tests, such as the rapid antigen test (RAT).[89] While RATs can be conveniently done at home or local clinics, suffer from sampling variability and outdated kits as the viruses mutate.[90] Alternatively, Siqueira et al. were able to successfully detect SARS-CoV-2 viral proteins in human saliva samples via LC-MS.[5] Saliva is a convenient and non-invasive matrix suitable for screening as viral peptides were detected even weeks after infection.[91,92] Human saliva is a complex biological matrix that requires sample clean-up and/or analyte extraction prior to LC-MS analysis. Solid-phase microextraction (SPME) is a technique that is able to achieve both steps while only requiring small sample volumes (less than 1 mL per sample).[93] From a clinical perspective, the small sample volumes required for biomedical applications of SPME (bio-SPME) are a key advantage, as the collection of large quantities (e.g. > 5 mL) of human saliva can be very difficult and uncomfortable for the patient.[93,94]

SPME is a non-exhaustive extraction technique that excels in the extraction of small molecules from various sample matrices. SPME sampling devices typically utilize small geometries, such as stainless-steel coated blades (also known as thin films) or pins, which can be employed in a 96-well plate format to achieve high-throughput quantitative analysis. Moreover, SPME is essentially solvent-free (a few mL) compared to traditional liquid-based extraction techniques and incorporates sample cleanup into the extraction step, allowing for

convenient 1-step sample preparation and extraction prior to desorption and detection.[94] Although SPME currently offers a wide range of analyte coverage, researchers are continuously exploring strategies to expand it. For example, C8-sulfonate (mixed mode) and hydrophilic-lipophilic balanced (HLB) coating chemistries offer wide coverage based on affinity.[25] However, SPME extraction phases typically favor medium-to-low polarity analytes, which tend to have stronger matrix binding affinity; this poses a problem, as the stronger matrix binding affinity limits the mass transfer of these analytes from the matrix to the extraction phase. Nonetheless, balanced extraction efficiency for both high- and low-polarity analytes can be achieved by implementing a pre-equilibrium extraction regime.[45] This unique feature (i.e., balanced recovery) conveniently enables the untargeted application of SPME for biomedical applications.[40,95]

Aside from polarity, analyte size can also be a limiting parameter when using SPME. Biomedical applications of SPME typically utilize a porous polyacrylonitrile (PAN) biocompatible binder for the stationary phase, as it excels at preventing biofouling and protein binding. Unfortunately, the use of PAN binder tends to hinder the extraction of small peptides (molecular weight cutoff (MWCO) larger than 1.5 kDa) and prevents the extraction of larger peptides completely.[96] However, Onat et al. were able to increase porosity of the binder and thus improving the extraction of short-chain peptides, such as angiotensins, by incorporating lithium perchlorate as a porogen to create mesopores in the coating of the thin-film SPME device.[97] Alternative strategies like this are necessary for the extraction of larger analytes beyond conventional SPME practices.

Additionally, protein digestion is a common technique employed to reduce the size of large peptides and proteins in quantitative targeted proteomics that can also be exploited for bio-SPME.[98]

In this study, we explored the potential for peptidomics and even proteomics via bio-SPME by combining the newest strategies for peptide extraction and Trypsin (Tryp) digestion. We also investigated the extent of SPME's ability to detect endogenous and viral protein via common bio-SPME extraction phases. The results of this work demonstrated the newfound potential of bio-SPME as a convenient and simple tool for the high through-put analysis of various peptides and even identification of proteins in clinical applications. Automated high-throughput analysis using coated SPME blades in the 96-well plate format has been described elsewhere.[99] The extraction and identification of peptides and proteins are new in bio-SPME, which means that there remains substantial untapped potential in this area. As such, further research focusing on different diseases, biological matrices, sampling logistics, extraction phases, and biocompatible binders will follow.

4.3 Material and methods

4.3.1 Materials and chemicals

C18 sorbent particles with a diameter of 5 µm were purchased from Supelco, Sigma Aldrich (Burlington, MA, USA). LC-MS consumables, including methanol (MeOH), isopropanol (IPA), acetonitrile (ACN) and water were purchased from Fisher Scientific (Hampton, NJ, US). Other bench-top consumables, including polyacrylonitrile (PAN, MW ~ 20kDa), dimethylformamide

(DMF) hydrochloric acid (HCl), formic acid (FA) and 1 × phosphate buffer saline (PBS, pH 7.4) were purchased from Sigma Aldrich (Burlington, MA, USA). Uncoated 304-grade stainless-steel blades were sourced locally. Nano-flow reversed-phase HPLC capillary column (50 µm × 10 cm), which had been packed in the laboratory using a Magic C18 resin (5 µm diameter, 200 Å pore size) was purchased from Michrom BioResources (Auburn, CA, USA). Thermo LTQ-Velos Linear Ion Trap mass spectrometer (Waltham, MA, USA) was used for the LC-MS analysis.

4.3.2 SPME devices

The PAN binder was prepared by first dissolving 5.0 g of polyacrylonitrile in 70 mL of dimethylformamide (DMF) at 85 °C for 1 hour with periodic mixing. The coating slurry was prepared by mixing 10% (w/w) C18 particles and 5% (w/w) lithium perchlorate in PAN binder and then shaking the mixture in a vortexer to form a homogeneous slurry. The resultant slurry could be used for at least a year if stored properly (sealed and constantly stirred with a magnetic stir bar). The stainless-steel blades (4.5 cm × 3 mm × 400 µm) were etched in concentrated hydrochloric acid (HCl) (37% w/w) for 30 min at 200 rpm on a benchtop orbital shaker, followed by a rinsing step with water and sonication in ethanol (EtOH) for 15 min. After sonication, the blades were briefly dried at 80 °C and then dip-coated in the C18 coating slurry. Each blade was dip coated with 2 layers to a length of 1 cm, with a 30-second curing process at 80 °C between the application of each layer. Photos of the coated blades are shown in Fig. S1. For cleaning, the blades were first submerged in ultrapure water overnight to remove any

residual lithium perchlorate salt from the coating. Each blade was subsequently cleaned twice via immersion in 1.5 mL of a cleaning solution comprised of methanol, acetonitrile, isopropanol, and water (25:25:25:25 MeOH/ACN/IPA/H_2O, %v/v/v/v) under 1000 rpm vortex-mixing for 30 min (per step) and then stored in a preconditioning solution (50:50 EtOH/H_2O, %v/v) until use. The image of the final product is shown below.



Figure 4.1 A stainless-steel blade coated with C18/PAN bio-compatible extraction phase. Coating length: 1 cm. Blade dimensions: 4.5 cm × 3 mm × 400 µm. Blade material: 304-grade stainless steel.

4.3.3 Sampling and analytical protocols

Stimulated whole saliva samples were collected from participating male and female individuals diagnosed with COVID-19, as well as healthy individuals. The participants' COVID-19 status (positive/negative) was determined based on rRT-PCR tests performed by the Saskatchewan Health Authority, as described elsewhere.[92] Briefly, saliva samples were self-collected by each participant using a SimplOFy™ salivary collection kit (Oasis Diagnostics® Corporation, Portland, OR, USA) and immediately placed on ice and transported to the Salivary Proteomics Research Laboratory, University of Saskatchewan (Saskatoon, SK, Canada). All saliva samples were heat-inactivated at 60 ºC for 30 min.[100] Following inactivation, a sub-portion of the saliva samples was centrifuged at

14,000 G for 20 min at 4 °C to obtain supernatant samples. 225 µL of the whole and supernatant samples were then transferred to a 0.3 mL insert vial along with 25 µL of PBS spiked with internal standards (deuterated analogues of endogenous compounds present in saliva). All samples were subjected to Tryp-digestion according to standard protocol.

Prior to sampling, the SPME blades were briefly washed (5 s) in ultrapure water to remove residual preconditioning solution. After washing, the blades were submerged in 1 mL of Tryp-digested saliva samples for 1 hour at room temperature (20 °C) under 1000 rpm vortex agitation. After extraction, each blade was briefly washed (5 s) with a 3% v/v hydrogen peroxide (H_2O_2) solution to deactivate any potential pathogens and to remove any particulate from the coating surface. The blade was then desorbed in 250 µL of a solution comprised of ACN/H_2O (80/20, v/v) with 0.1% formic acid (FA) at 1000 rpm for 1 hour. The protein concentration in the desorption solution was measured using a Micro BCA Protein Assay Kit from ThermoFisher Scientific (Waltham, MA, USA), and the remaining protein from each sample was dried in a Labconco SpeedVac (Kansas City, MO, USA) and stored at -80°C. All peptide samples were reconstituted in MS-grade H_2O/ACN/FA (97:3:0.1 v/v) to a final concentration of 0.5 µg/µL. The desorption solutions were introduced, in triplicate (2 µg / injection), to a nano-flow reversed-phase HPLC capillary column (50 µm × 10 cm), which had been packed in the laboratory using a Magic C18 resin (5 µm diameter, 200 Å pore size) purchased from Michrom BioResources (Auburn, CA, USA). The column was coupled with a Thermo LTQ-Velos Linear Ion Trap mass

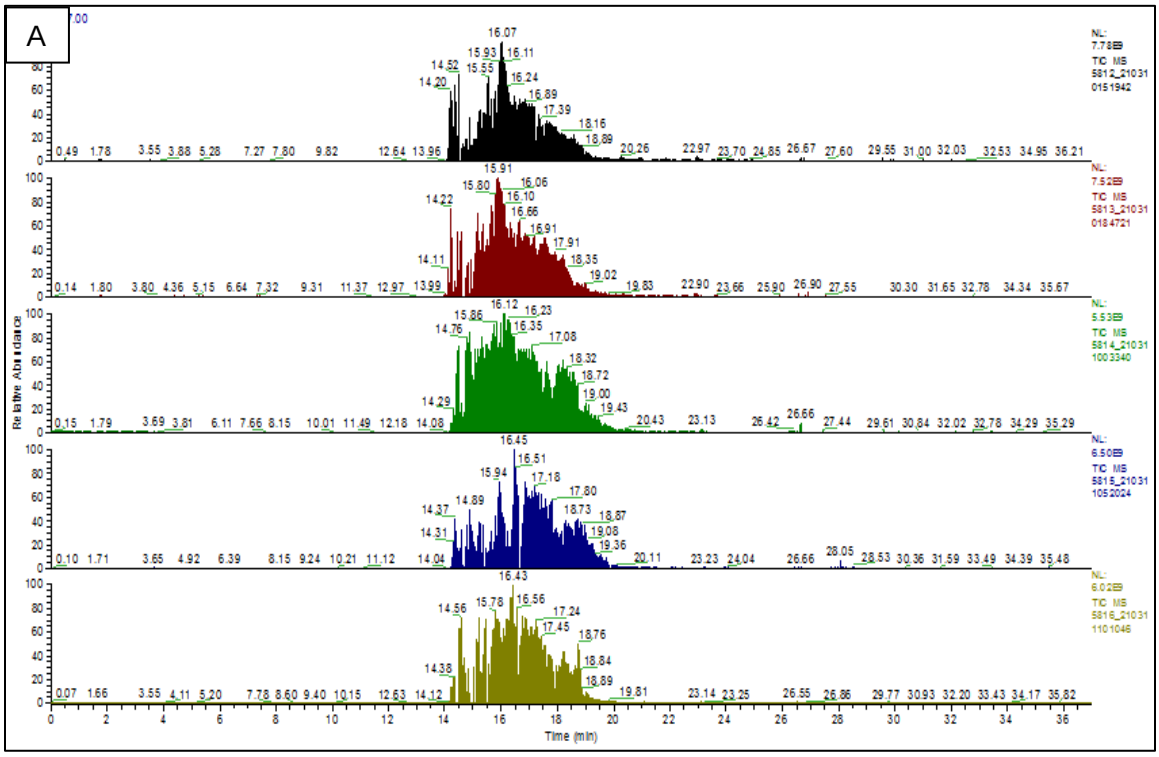
spectrometer (Waltham, MA, USA) for positive mode LC-HESI-MS, with a scan range of 390 – 2000 m/z for tandem MS/MS analysis. Nano-flow LC was developed in a linear 36-min gradient ranging from 0% to 60% of ACN (0.1% v/v FA) with a flow rate of 110 nL/min. The electrospray voltage and ion transfer capillary temperature were set at 1.8 kV and 250 °C, respectively. MS/MS spectral data were collected and queried against a customized COVID-19 and human saliva database—which included Swiss-Prot and TrEMBL (UniProt, downloaded on January 29, 2021) and a total of 212 reviewed proteins—using the SEQUEST algorithm in the Proteome Discoverer 2.4 software package from Thermo Fisher Scientific (Waltham, MA, USA). The Proteome Discoverer results were validated at the peptide and protein levels (1% false discovery rate). For protein identification, each protein group was required to have at least one unique validated peptide. Isoelectric point (pI) values were calculated for each peptide sequence using the Isoelectric Point Calculator (IPC) online.[101]

4.4 Results and discussion

4.4.1 Untargeted analysis

Total ion chromatograms (TICs) obtained from the SPME-LC-MS analysis of healthy controls and SARS-CoV-2-positive patients are shown in Fig. 4.2a and b. The reproducible within-group patterns and the clear between-group differences suggest that proteomic and/or metabolomic changes in the whole saliva samples are highly predictable due to SARS-CoV-2. These results also suggest that bio-SPME can capture clear differences in whole saliva samples

that are positive for SARS-CoV-2 compared to the control despite sampling variations in a clinical setting. Some of the between-sample deviations can be attributed to sample collection, transportation, and preparation steps implemented out of concern for the safety of the research personnel. In general, variability was also expected in such clinical dentistry application since selection criteria, such as age, sex, and diet, were not inplemented.[102]



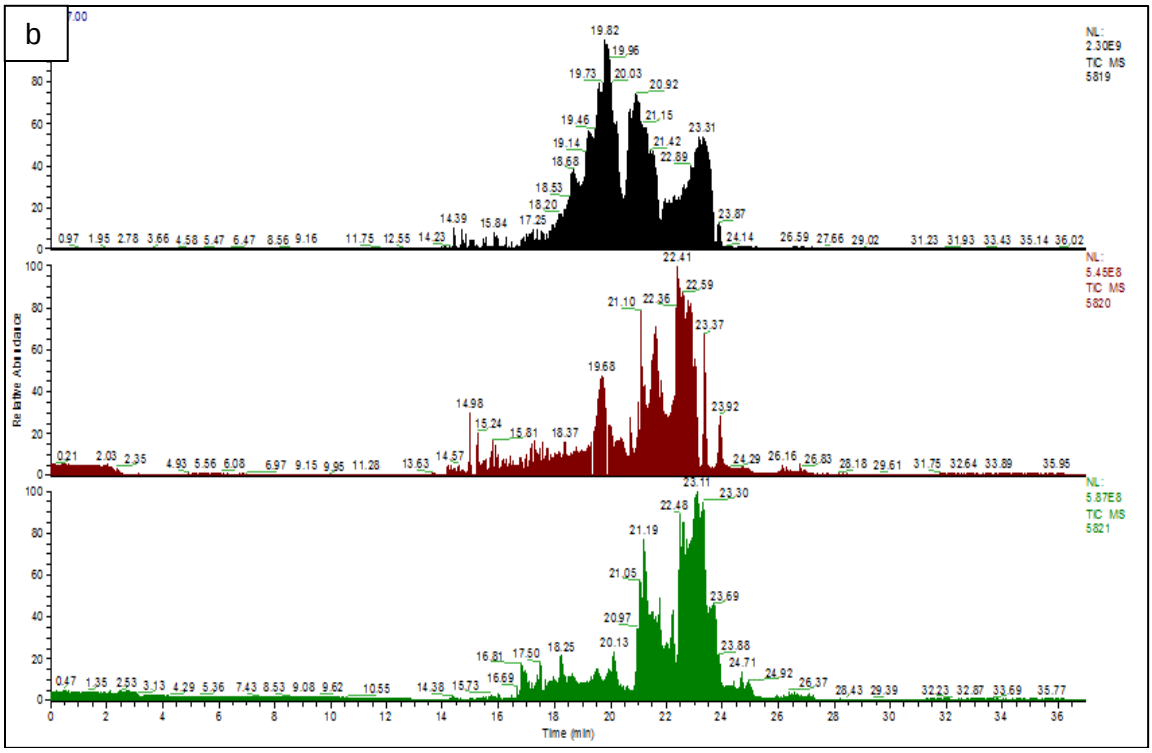


Figure 4.2 Exemplary untargeted LCMS total ion chromatograms (TIC) of desorption solutions from (a) healthy control and (b) SARS-CoV-2-positive participants. Each chromatogram is from an individual participant.

4.4.2 Protein identification

In a subsequent investigation, another 10 randomly selected whole saliva samples from SARS-CoV-2-positive patients were used to test the peptide extraction efficiency of commercial HLB/PAN blades and the porous C18/PAN blades prepared in this study. The proteins identified based on the annotated Tryp-digested peptides extracted by the HLB/PAN blades are summarized in Table 4.1. The table also includes the number of peptides, calculated mass (MH+ [Da]), instrumental response, and calculated pI for each identified protein. As can be seen, 42 proteins were identified, including 3 endogenous proteins detected in all 10 samples: 54 peptides from alpha-amylase 1A, 21 peptides for salivary

acidic proline-rich phosphoprotein 1/2, and 37 peptides for submaxillary gland androgen-regulated protein 3B. Of the 42 identified proteins, 39 were also reasonably high in abundance (instrumental response intensity > 1×10^5), which was expected due to the enrichment effect of SPME when used with a small volume of desorption solution (e.g. 50 µL).[25] The results obtained using the porous C18/PAN blades for the 10 whole saliva samples (and 10 whole saliva supernatants from the same samples) are shown in Tables 4.2 and 4.3. As can be seen, the C18/PAN blades enabled the identification of more proteins (71) compared to the HLB/PAN blades, with 7 being detected in all 10 samples: 42 peptides from alpha-amylase 1A; 16, 64, 22, and 30 peptides from basic salivary proline-rich proteins 1, 2, 3, and 4, respectively; 37 peptides from salivary acidic proline-rich phosphoprotein ½; and 46 peptides from statherin. While the most abundant proteins extracted by both types of blades were largely the same, the porous C18-coated blades were able to extract the common peptides more consistently from whole saliva samples, likely due to a combined effect between increased porosity and the chemical properties of the extraction phase.[40,97] The results of both experiments were very encouraging, as coupling SPME with Tryp digestion enabled the analysis of macromolecules, a feat which previously had been considered impossible for SPME-based approaches.[40,103]

The results of the experiments in which the porous C18/PAN blades were applied to perform extractions from the whole saliva supernatant samples fell somewhere between those of the two previous experiments. However, the ORF3a protein was detected exclusively in a few whole saliva supernatant

samples (Table 4.3). ORF3a is a transmembrane viroporin protein, which could have been partially released from host cells during the separation process used to obtain the whole saliva supernatant.[104] This suggests that further exploration of the role of cell lysis could potentially enable improvements in the detection of viral components.

Table 4.1 Number, calculated mass (MH+ [Da]), intensity, and calculated pI of Tryp peptides derived from human and SARS-CoV-2 proteins identified in whole saliva from COVID-19-positive individuals (n=10) via HLB/PAN-blades coupled with LC-MS/MS.

Access-ion code	Protein name	peptides	MH+ [Da]		Intensity		Calculated pI		Organism	Frequency	
			Mean	S.D.	Mean	S.D.	Mean	S.D.		n	%
P0DUB6	Alpha-amylase 1A	54	1435	488	1.6E+07	2.40E+07	6.0	2.27	Homo sapiens	10	100
P02810	Salivary acidic proline-rich phosphoprotein 1/2	21	1306	387	1.0E+07	2.31E+07	9.2	2.15	Homo sapiens	10	100
P02814	Submaxillary gland androgen-regulated protein 3B	37	1748	701	2.9E+07	4.70E+07	7.5	1.97	Homo sapiens	10	100
P04280	Basic salivary proline-rich protein 1	16	1607	656	5.3E+06	1.19E+07	9.2	1.37	Homo sapiens	9	90
P02808	Statherin	15	1813	820	1.4E+07	1.51E+07	5.1	2.18	Homo sapiens	9	90
P02812	Basic salivary proline-rich protein 2	20	1610	777	3.6E+06	9.45E+06	9.0	1.60	Homo sapiens	8	80
Q96DR5	BPI fold-containing family A member 2	10	1846	691	7.0E+06	8.81E+06	4.8	1.53	Homo sapiens	8	80
Q02487	Desmocollin-2	5	1632	403	1.3E+06	2.39E+06	4.3	1.47	Homo sapiens	8	80
Q04118	Basic salivary proline-rich protein 3	10	1284	449	1.6E+07	3.52E+07	8.7	1.77	Homo sapiens	7	70
Q8TAX7	Mucin-7	6	1389	294	2.0E+07	2.45E+07	5.7	0.85	Homo sapiens	7	70
P23280	Carbonic anhydrase 6	3	1770	360	1.9E+06	1.29E+06	3.1	0.13	Homo sapiens	6	60
P15515	Histatin-1	7	1687	537	1.8E+07	1.21E+07	4.8	1.44	Homo sapiens	6	60
Q6MZM9	Proline-rich protein 27	17	1893	788	1.5E+06	8.83E+05	5.2	2.53	Homo sapiens	6	60
P10163	Basic salivary proline-rich protein 4	11	1034	168	2.6E+07	7.84E+07	9.3	1.18	Homo sapiens	5	50
P32926	Desmoglein-3	3	1634	340	1.6E+06	1.63E+06	3.7	0.59	Homo sapiens	5	50
P15516	Histatin-3	8	1220	328	1.8E+07	3.13E+07	7.5	2.82	Homo sapiens	5	50
Q16378	Proline-rich protein 4	7	1613	404	2.3E+07	4.13E+07	8.3	1.98	Homo sapiens	5	50
P02788	Lactotransferrin	3	1244	122	2.5E+07	1.52E+07	9.0	2.14	Homo	4	40

									sapiens		
P01833	Polymeric immunoglobulin receptor	4	1850	663	8.8E+05	7.51E+05	5.9	3.23	Homo sapiens	4	40
P05814	Beta-casein	2	918	340	1.7E+07	2.05E+07	6.6	0.98	Homo sapiens	3	30
O15554	Intermediate conductance calcium-activated potassium channel protein 4	2	1275	147	2.6E+06	3.67E+06	5.0	N/A	Homo sapiens	3	30
Q6P5S2	Protein LEG1 homolog	2	1722	213	1.6E+05	1.73E+05	3.2	0.14	Homo sapiens	2	20
P25311	Zinc-alpha-2-glycoprotein	2	1461	779	8.1E+05	7.36E+05	4.5	2.02	Homo sapiens	2	20
Q8N4F0	BPI fold-containing family B member 2	1	3101	N/A	1.9E+06	N/A	9.0	N/A	Homo sapiens	1	10
P23560	Brain-derived neurotrophic factor	1	765	N/A	1.2E+04	N/A	3.4	N/A	Homo sapiens	1	10
Q14CN2	Calcium-activated chloride channel regulator 4	1	1264	N/A	2.2E+05	N/A	5.9	N/A	Homo sapiens	1	10
P06731	Carcinoembryonic antigen-related cell adhesion molecule 5	1	1332	N/A	4.1E+06	N/A	7.5	N/A	Homo sapiens	1	10
Q15782	Chitinase-3-like protein 2	1	2051	N/A	2.6E+04	N/A	6.6	N/A	Homo sapiens	1	10
P01034	Cystatin-C	1	910	N/A	1.3E+04	N/A	10.7	N/A	Homo sapiens	1	10
Q9UGM3	Deleted in malignant brain tumors 1 protein	1	765	N/A	2.2E+05	N/A	10.7	N/A	Homo sapiens	1	10
Q8N4Y2	EF-hand calcium-binding domain-containing protein 4A	1	526	N/A	9.4E+03	N/A	9.7	N/A	Homo sapiens	1	10
Q6P3S6	F-box only protein 42	1	2257	N/A	5.7E+04	N/A	9.9	N/A	Homo sapiens	1	10
O15520	Fibroblast growth factor 10	1	779	N/A	2.1E+04	N/A	5.9	N/A	Homo sapiens	1	10
Q08380	Galectin-3-binding protein	1	2806	N/A	1.4E+04	N/A	4.0	N/A	Homo sapiens	1	10
P43026	Growth/differentiation factor 5	1	2174	N/A	2.7E+04	N/A	10.4	N/A	Homo sapiens	1	10
Q9Y6R7	IgGFc-binding protein	1	2197	N/A	4.4E+04	N/A	6.6	N/A	Homo sapiens	1	10
P01877	Immunoglobulin heavy constant alpha 2	1	930	N/A	7.6E+05	N/A	10.5	N/A	Homo sapiens	1	10

P01591	Immunoglobulin J chain	1	1322	N/A	1.1E+03	N/A	11.8	N/A	Homo sapiens	1	10
Q7LBE3	Solute carrier family 26 member 9	1	692	N/A	1.2E+06	N/A	6.0	N/A	Homo sapiens	1	10
P20061	Transcobalamin-1	1	1356	N/A	4.3E+04	N/A	3.6	N/A	Homo sapiens	1	10
P0DTD1	Replicase polyprotein 1ab	7	1660	416	1.7E+06	2.53E+06	5.7	2.42	SARS-CoV-2	6	60
P0DTC5	Membrane protein	1	2050	N/A	1.9E+05	N/A	4.4	N/A	SARS-CoV-2	1	10

Table 4.2 Number, calculated mass (MH+ [Da]), intensity, and calculated pI of Tryp peptides derived from human and SARS-CoV-2 proteins identified in whole saliva from COVID-19-positive individuals (n=10) via C18/PAN-blades coupled with LC-MS/MS.

Access-ion code	Protein name	peptides	MH+ [Da]		Intensity		Calculated pI		Organism	Frequency	
			Mean	S.D.	Mean	S.D.	Mean	S.D.		n	%
P0DUB6	Alpha-amylase 1A	42	1486	800.3	1.4E+07	2.07E+07	6.5	2.16	Homo sapiens	10	100
P04280	Basic salivary proline-rich protein 1	16	1811	825.8	1.0E+07	1.69E+07	9.3	0.96	Homo sapiens	10	100
P02812	Basic salivary proline-rich protein 2	64	1611	804.8	2.9E+06	5.37E+06	8.3	1.98	Homo sapiens	10	100
Q04118	Basic salivary proline-rich protein 3	22	1243	481.4	1.0E+07	2.60E+07	8.7	1.34	Homo sapiens	10	100
P10163	Basic salivary proline-rich protein 4	30	1263	580.8	6.2E+06	1.54E+07	8.1	1.46	Homo sapiens	10	100
P02810	Salivary acidic proline-rich phosphoprotein 1/2	37	1198	445.2	8.4E+06	2.03E+07	7.8	2.52	Homo sapiens	10	100
P02808	Statherin	46	2700	1030.5	1.0E+07	1.49E+07	6.8	2.24	Homo sapiens	10	100
P02814	Submaxillary gland androgen-regulated protein 3B	38	2159	953.8	1.3E+07	1.34E+07	8.2	1.95	Homo sapiens	9	90
Q6MZM9	Proline-rich protein 27	12	1961	905.9	2.2E+06	3.17E+06	7.9	3.54	Homo sapiens	7	70
P15516	Histatin-3	5	1000	193.4	1.2E+06	1.15E+06	6.4	3.08	Homo sapiens	6	60
Q8TAX7	Mucin-7	8	1548	403.9	2.1E+07	2.02E+07	5.5	1.46	Homo sapiens	5	50
Q96DR5	BPI fold-containing family A member 2	5	1579	484.7	3.0E+06	4.27E+06	7.1	2.08	Homo sapiens	4	40

P32926	Desmoglein-3	3	1481	818.9	1.9E+05	3.14E+05	7.6	3.70	Homo sapiens	4	40
Q8NFT8	Delta and notch-like epidermal growth factor-related receptor	3	1360	577.2	4.4E+06	7.54E+06	7.2	3.08	Homo sapiens	3	30
Q02413	Desmoglein-1	5	1598	603.2	3.5E+05	4.74E+05	5.8	1.55	Homo sapiens	3	30
Q8N4Y2	EF-hand calcium-binding domain-containing protein 4A	2	1312	1111.5	6.7E+05	9.44E+05	8.0	1.47	Homo sapiens	3	30
Q96GK7	Fumarylacetoacetate hydrolase domain-containing protein 2A	2	1085	659.4	2.5E+07	7.49E+06	5.0	2.36	Homo sapiens	3	30
Q9Y6R7	IgGFc-binding protein	5	1457	576.5	1.6E+06	3.19E+06	6.1	3.29	Homo sapiens	3	30
Q9P2D0	Inhibitor of Bruton tyrosine kinase	2	1502	1007.9	1.0E+06	1.41E+06	4.9	0.64	Homo sapiens	3	30
P22079	Lactoperoxidase	3	1836	662.1	9.3E+05	1.27E+06	6.8	2.49	Homo sapiens	3	30
Q9HC84	Mucin-5B	4	1737	726.5	9.7E+05	8.63E+05	4.5	1.07	Homo sapiens	3	30
P12273	Prolactin-inducible protein	2	870	632.2	1.0E+06	7.70E+05	3.8	0.93	Homo sapiens	3	30
Q16378	Proline-rich protein 4	4	1426	480.0	3.9E+07	3.07E+07	8.6	2.14	Homo sapiens	3	30
P02787	Serotransferrin	2	1382	319.9	2.6E+06	7.42E+05	7.7	1.53	Homo sapiens	3	30
Q9P2C4	Transmembrane protein 181	3	1184	224.0	2.9E+06	4.55E+06	8.6	2.10	Homo sapiens	3	30
Q8N4F0	BPI fold-containing family B member 2	1	577	N/A	1.6E+06	N/AE+00	10.6	N/A	Homo sapiens	3	30
P60468	Protein transport protein Sec61 subunit beta	1	1118	N/A	5.4E+07	N/AE+00	10.6	N/A	Homo sapiens	3	30
P02765	Alpha-2-HS-glycoprotein	2	1830	326.0	1.9E+06	1.72E+06	7.2	4.45	Homo sapiens	2	20
P02749	Beta-2-glycoprotein 1	2	783	155.4	4.2E+05	5.91E+05	4.1	1.00	Homo sapiens	2	20
Q14CN2	Calcium-activated chloride channel regulator 4	2	1005	358.0	1.8E+06	2.46E+06	3.7	0.68	Homo sapiens	2	20
P23280	Carbonic anhydrase 6	2	2147	1017.0	9.2E+06	9.86E+06	8.5	0.30	Homo sapiens	2	20
P0C0L5	Complement C4-B	2	1554	621.0	1.3E+05	1.09E+05	4.9	2.46	Homo	2	20

									sapiens		
Q9UGM3	Deleted in malignant brain tumors 1 protein	3	1345	621.9	4.9E+04	2.02E+04	9.5	2.03	Homo sapiens	2	20
P15515	Histatin-1	6	1602	512.2	1.2E+07	1.22E+07	4.8	1.51	Homo sapiens	2	20
P01877	Immunoglobulin heavy constant alpha 2	2	1234	982.7	2.7E+07	3.85E+07	4.7	1.43	Homo sapiens	2	20
Q92886	Neurogenin-1	2	1505	595.5	3.4E+06	4.74E+06	4.9	1.54	Homo sapiens	2	20
O43490	Prominin-1	2	1567	538.0	1.3E+06	1.64E+06	4.4	N/A	Homo sapiens	2	20
P07996	Thrombospondin-1	2	1852	53.8	8.7E+06	8.16E+06	5.8	3.14	Homo sapiens	2	20
P11229	Muscarinic acetylcholine receptor M1	1	1115	N/A	1.1E+05	N/AE+00	4.4	N/A	Homo sapiens	2	20
O00472	RNA polymerase II elongation factor ELL2	2	1285	9.6	5.7E+04	2.08E+04	6.0	0.04	Homo sapiens	1	10
Q7LBE3	Solute carrier family 26 member 9	2	1516	104.6	5.5E+06	1.50E+06	3.5	0.23	Homo sapiens	1	10
O95081	Arf-GAP domain and FG repeat-containing protein 2	1	1859	N/A	5.6E+06	N/AE+00	6.0	N/A	Homo sapiens	1	10
P05814	Beta-casein	1	1082	N/A	6.5E+05	N/AE+00	10.5	N/A	Homo sapiens	1	10
P06731	Carcinoembryonic antigen-related cell adhesion molecule 5	1	2879	N/A	3.3E+05	N/AE+00	4.4	N/A	Homo sapiens	1	10
Q15782	Chitinase-3-like protein 2	1	526	N/A	3.8E+03	N/AE+00	6.0	N/A	Homo sapiens	1	10
O60676	Cystatin-8	1	1322	N/A	8.8E+05	N/AE+00	9.4	N/A	Homo sapiens	1	10
P24855	Deoxyribonuclease-1	1	1320	N/A	1.1E+07	N/AE+00	7.4	N/A	Homo sapiens	1	10
Q8TB45	DEP domain-containing mTOR-interacting protein	1	1444	N/A	2.3E+06	N/AE+00	3.4	N/A	Homo sapiens	1	10
O95479	GDH/6PGL endoplasmic bifunctional protein	1	495	N/A	6.3E+03	N/AE+00	6.0	N/A	Homo sapiens	1	10
Q8NBJ4	Golgi membrane protein 1	1	819	N/A	1.6E+06	N/AE+00	4.3	N/A	Homo sapiens	1	10
P43026	Growth/differentiation factor 5	1	915	N/A	3.0E+03	N/AE+00	10.5	N/A	Homo sapiens	1	10

P00738	Haptoglobin	1	2203	N/A	1.6E+06	N/AE+00	3.2	N/A	Homo sapiens	1	10
P02790	Hemopexin	1	3182	N/A	1.1E+07	N/AE+00	4.4	N/A	Homo sapiens	1	10
O15431	High affinity copper uptake protein 1	1	1504	N/A	4.4E+05	N/AE+00	8.8	N/A	Homo sapiens	1	10
P41145	Kappa-type opioid receptor	1	2096	N/A	8.3E+06	N/AE+00	4.2	N/A	Homo sapiens	1	10
P02788	Lactotransferrin	1	2475	N/A	2.8E+06	N/AE+00	9.8	N/A	Homo sapiens	1	10
P05164	Myeloperoxidase	1	1069	N/A	6.3E+04	N/AE+00	6.8	N/A	Homo sapiens	1	10
Q8WV24	Pleckstrin homology-like domain family A member 1	1	1053	N/A	1.2E+06	N/AE+00	6.7	N/A	Homo sapiens	1	10
Q8N271	Prominin-2	1	1785	N/A	2.5E+04	N/AE+00	5.7	N/A	Homo sapiens	1	10
Q8NCL9	Protein APCDD1-like	1	751	N/A	3.0E+06	N/AE+00	7.5	N/A	Homo sapiens	1	10
Q6P5S2	Protein LEG1 homolog	1	1320	N/A	1.1E+07	N/AE+00	10.5	N/A	Homo sapiens	1	10
Q9NQL2	Ras-related GTP-binding protein D	1	1510	N/A	2.2E+06	N/AE+00	8.0	N/A	Homo sapiens	1	10
P55000	Secreted Ly-6/uPAR-related protein 1	1	1084	N/A	1.6E+04	N/AE+00	6.0	N/A	Homo sapiens	1	10
Q9NRA2	Sialin	1	2045	N/A	1.4E+06	N/AE+00	3.6	N/A	Homo sapiens	1	10
P25103	Substance-P receptor	1	1756	N/A	9.9E+05	N/AE+00	3.9	N/A	Homo sapiens	1	10
Q7RTX0	Taste receptor type 1 member 3	1	2306	N/A	1.2E+07	N/AE+00	4.2	N/A	Homo sapiens	1	10
Q969D9	Thymic stromal lymphopoietin	1	2155	N/A	5.6E+06	N/AE+00	10.1	N/A	Homo sapiens	1	10
P00750	Tissue-type plasminogen activator	1	2537	N/A	1.3E+06	N/AE+00	7.4	N/A	Homo sapiens	1	10
P20061	Transcobalamin-1	1	1929	N/A	3.2E+07	N/AE+00	8.8	N/A	Homo sapiens	1	10
P0DTD1	Replicase polyprotein 1ab	5	1126	510.5	7.6E+05	1.37E+06	4.8	0.97	SARS-CoV-2	6	60

Table 4.3 Number, calculated mass (MH+ [Da]), intensity, and calculated pI of Tryp peptides derived from human and SARS-CoV-2 proteins identified in whole saliva supernatant from COVID-19-positive individuals (n=10) via C18/PAN-blades via LC-MS/MS.

Access-ion code	Protein name	peptides	MH+ [Da]		Intensity		Calculated pI		Organism	Frequency	
			Mean	S.D.	Mean	S.D.	Mean	S.D.		n	%
P0DUB6	Alpha-amylase 1A	41	1595	658.4	1.2E+07	1.58E+07	5.6	2.14	Homo sapiens	10	100
Q96DR5	BPI fold-containing family A member 2	24	2076	511.1	5.2E+06	6.00E+06	5.5	2.00	Homo sapiens	10	100
P02810	Salivary acidic proline-rich phosphoprotein 1/2	25	1353	553.4	2.5E+07	3.93E+07	8.4	2.80	Homo sapiens	10	100
P02808	Statherin	42	2405	988.7	3.4E+06	5.26E+06	5.5	2.28	Homo sapiens	10	100
P02814	Submaxillary gland androgen-regulated protein 3B	62	2057	932.0	1.3E+07	3.58E+07	8.1	2.02	Homo sapiens	10	100
P04280	Basic salivary proline-rich protein 1	26	1652	572.3	1.4E+07	1.85E+07	9.5	1.14	Homo sapiens	9	90
P02812	Basic salivary proline-rich protein 2	60	1560	737.0	5.8E+06	8.99E+06	8.6	2.10	Homo sapiens	9	90
P10163	Basic salivary proline-rich protein 4	17	1599	643.1	7.8E+06	8.11E+06	8.0	1.64	Homo sapiens	9	90
Q04118	Basic salivary proline-rich protein 3	17	1547	728.4	7.9E+06	1.65E+07	8.9	2.00	Homo sapiens	8	80
P15515	Histatin-1	9	1486	446.2	8.3E+06	5.72E+06	5.4	2.05	Homo sapiens	8	80
Q9Y6R7	IgGFc-binding protein	9	1711	516.5	3.2E+06	4.46E+06	5.9	0.80	Homo sapiens	8	80
P12273	Prolactin-inducible protein	1	844	N/A	1.7E+07	N/AE+00	4.4	N/A	Homo sapiens	8	80
Q02487	Desmocollin-2	4	1957	780.9	1.6E+06	9.05E+05	5.2	2.42	Homo sapiens	7	70
Q8TAX7	Mucin-7	8	1428	356.5	6.5E+06	5.85E+06	5.5	1.07	Homo sapiens	7	70
P23280	Carbonic anhydrase 6	5	1554	563.0	6.8E+06	5.62E+06	5.6	3.18	Homo sapiens	6	60
P32926	Desmoglein-3	5	1353	383.9	9.6E+05	1.33E+06	5.0	3.09	Homo sapiens	6	60
Q9HC84	Mucin-5B	10	2303	995.7	4.4E+05	7.26E+05	6.8	2.94	Homo sapiens	6	60

P01833	Polymeric immunoglobulin receptor	2	2660	239.1	2.5E+06	1.79E+06	5.3	1.92	Homo sapiens	5	50
Q6MZM9	Proline-rich protein 27	9	2130	943.3	4.6E+06	3.13E+06	8.8	3.21	Homo sapiens	5	50
O95479	GDH/6PGL endoplasmic bifunctional protein	4	998	651.4	6.2E+05	1.02E+06	6.7	2.49	Homo sapiens	4	40
P15516	Histatin-3	6	1172	297.3	1.1E+07	1.64E+07	6.9	2.92	Homo sapiens	4	40
P02788	Lactotransferrin	3	1870	927.0	4.7E+06	7.64E+06	6.4	2.77	Homo sapiens	4	40
Q16378	Proline-rich protein 4	6	1848	1103.5	5.3E+06	4.60E+06	8.1	2.90	Homo sapiens	4	40
P07996	Thrombospondin-1	3	2092	1264.7	4.6E+05	7.20E+05	3.5	0.23	Homo sapiens	4	40
O95479	GDH/6PGL endoplasmic bifunctional protein	1	1863	N/A	2.1E+06	N/AE+00	4.6	N/A	Homo sapiens	4	40
Q15782	Chitinase-3-like protein 2	2	1997	644.5	2.1E+07	1.19E+07	6.9	0.74	Homo sapiens	3	30
Q02413	Desmoglein-1	3	1404	462.7	2.8E+05	4.76E+05	8.1	2.96	Homo sapiens	3	30
Q6P3S6	F-box only protein 42	3	1664	641.8	1.4E+05	1.84E+05	7.4	2.77	Homo sapiens	3	30
Q8N271	Prominin-2	3	1848	1643.7	2.6E+06	3.03E+06	7.2	2.88	Homo sapiens	3	30
Q6P5S2	Protein LEG1 homolog	3	1397	151.7	3.7E+06	5.68E+06	5.8	4.02	Homo sapiens	3	30
Q9P2C4	Transmembrane protein 181	2	1258	261.2	1.9E+06	2.73E+06	7.7	1.93	Homo sapiens	3	30
P25311	Zinc-alpha-2-glycoprotein	3	2280	339.0	3.2E+06	1.05E+06	3.8	0.63	Homo sapiens	3	30
P20309	Muscarinic acetylcholine receptor M3	1	2206	N/A	2.5E+06	N/AE+00	5.6	N/A	Homo sapiens	3	30
P0C0L5	Complement C4-B	3	1309	809.5	9.3E+06	9.14E+06	7.2	1.45	Homo sapiens	2	20
P01034	Cystatin-C	2	1042	254.6	1.4E+06	1.82E+06	7.5	2.19	Homo sapiens	2	20
P54886	Delta-1-pyrroline-5-carboxylate synthase	2	990	50.5	9.6E+05	1.34E+06	8.7	0.53	Homo sapiens	2	20
Q8N4Y2	EF-hand calcium-binding domain-containing protein 4A	2	1038	723.4	3.0E+05	3.54E+05	6.5	3.61	Homo sapiens	2	20

P09958	Furin	2	1867	666.3	1.7E+06	1.53E+06	5.7	3.17	Homo sapiens	2	20
P43026	Growth/differentiation factor 5	2	1129	109.8	1.5E+06	2.09E+06	9.1	0.43	Homo sapiens	2	20
P01877	Immunoglobulin heavy constant alpha 2	3	1596	598.2	3.4E+06	1.38E+06	6.2	3.66	Homo sapiens	2	20
Q6VY07	Phosphofurin acidic cluster sorting protein 1	2	1924	1515.8	8.6E+06	3.10E+06	6.9	3.17	Homo sapiens	2	20
Q9NQL2	Ras-related GTP-binding protein D	2	2357	838.0	6.4E+06	8.92E+06	4.8	2.65	Homo sapiens	2	20
P02787	Serotransferrin	2	1164	14.2	3.0E+06	3.92E+06	7.4	1.09	Homo sapiens	2	20
Q7LBE3	Solute carrier family 26 member 9	2	1071	525.2	4.4E+06	2.83E+06	4.7	1.85	Homo sapiens	2	20
O95081	Arf-GAP domain and FG repeat-containing protein 2	1	927	N/A	6.4E+03	N/AE+00	9.1	N/A	Homo sapiens	2	20
Q8NFT8	Delta and Notch-like epidermal growth factor-related receptor	1	838	N/A	1.2E+04	N/AE+00	4.2	N/A	Homo sapiens	2	20
Q8TB45	DEP domain-containing mTOR-interacting protein	1	1746	N/A	3.0E+06	N/AE+00	5.7	N/A	Homo sapiens	2	20
P01033	Metalloproteinase inhibitor 1	1	1322	N/A	3.3E+06	N/AE+00	6.0	N/A	Homo sapiens	2	20
P05814	Beta-casein	2	1357	197.3	5.4E+05	1.68E+05	7.5	2.19	Homo sapiens	1	10
P02765	Alpha-2-HS-glycoprotein	1	1309	N/A	3.5E+07	N/AE+00	3.5	N/A	Homo sapiens	1	10
P06731	Carcinoembryonic antigen-related cell adhesion molecule 5	1	3045	N/A	1.7E+06	N/AE+00	4.9	N/A	Homo sapiens	1	10
P40199	Carcinoembryonic antigen-related cell adhesion molecule 6	1	2531	N/A	1.5E+07	N/AE+00	6.0	N/A	Homo sapiens	1	10
P31997	Carcinoembryonic antigen-related cell adhesion molecule 8	1	1446	N/A	3.5E+05	N/AE+00	3.4	N/A	Homo sapiens	1	10
Q8WUD6	Cholinephosphotransferase 1	1	668	N/A	2.5E+05	N/AE+00	6.0	N/A	Homo sapiens	1	10
P10909	Clusterin	1	1590	N/A	7.8E+05	N/AE+00	4.4	N/A	Homo sapiens	1	10
P01037	Cystatin-SN	1	1322	N/A	1.4E+06	N/AE+00	6.0	N/A	Homo	1	10

									sapiens		
Q9UGM3	Deleted in malignant brain tumors 1 protein	1	563	N/A	1.2E+06	N/AE+00	6.5	N/A	Homo sapiens	1	10
P24855	Deoxyribonuclease-1	1	1320	N/A	1.0E+07	N/AE+00	7.4	N/A	Homo sapiens	1	10
Q9GZZ8	Extracellular glycoprotein lacritin	1	2804	N/A	1.1E+05	N/AE+00	8.9	N/A	Homo sapiens	1	10
Q08380	Galectin-3-binding protein	1	1750	N/A	4.9E+05	N/AE+00	3.9	N/A	Homo sapiens	1	10
P00738	Haptoglobin	1	2040	N/A	1.5E+05	N/AE+00	2.9	N/A	Homo sapiens	1	10
O60663	LIM homeobox transcription factor 1-beta	1	1899	N/A	4.9E+04	N/AE+00	3.6	N/A	Homo sapiens	1	10
P05164	Myeloperoxidase	1	787	N/A	9.9E+06	N/AE+00	10.5	N/A	Homo sapiens	1	10
Q92886	Neurogenin-1	1	1084	N/A	1.7E+04	N/AE+00	6.0	N/A	Homo sapiens	1	10
P80188	Neutrophil gelatinase-associated lipocalin	1	865	N/A	1.1E+03	N/AE+00	7.4	N/A	Homo sapiens	1	10
Q8WV24	Pleckstrin homology-like domain family A member 1	1	1112	N/A	7.4E+03	N/AE+00	3.6	N/A	Homo sapiens	1	10
P20366	Protachykinin-1	1	1510	N/A	4.2E+06	N/AE+00	3.0	N/A	Homo sapiens	1	10
Q8NCL9	Protein APCDD1-like	1	1123	N/A	1.5E+04	N/AE+00	5.0	N/A	Homo sapiens	1	10
Q96BQ1	Protein FAM3D	1	1232	N/A	1.1E+05	N/AE+00	4.4	N/A	Homo sapiens	1	10
O00472	RNA polymerase II elongation factor ELL2	1	1810	N/A	6.4E+06	N/AE+00	6.3	N/A	Homo sapiens	1	10
P55000	Secreted Ly-6/uPAR-related protein 1	1	1082	N/A	1.4E+04	N/AE+00	6.0	N/A	Homo sapiens	1	10
P19634	Sodium/hydrogen exchanger 1	1	1084	N/A	9.4E+03	N/AE+00	6.8	N/A	Homo sapiens	1	10
P25103	Substance-P receptor	1	2831	N/A	1.0E+06	N/AE+00	6.6	N/A	Homo sapiens	1	10
P00750	Tissue-type plasminogen activator	1	2218	N/A	9.6E+04	N/AE+00	10.9	N/A	Homo sapiens	1	10
Q6ZNK6	TRAF-interacting protein with FHA domain-containing protein B	1	1037	N/A	1.5E+03	N/AE+00	7.4	N/A	Homo sapiens	1	10

P61165	Transmembrane protein 258	1	1943	N/A	4.2E+06	N/AE+00	6.6	N/A	Homo sapiens	1	10
O95807	Transmembrane protein 50A	1	2219	N/A	4.6E+06	N/AE+00	9.1	N/A	Homo sapiens	1	10
P0DTD1	Replicase polyprotein 1ab	7	1512	693.6	7.7E+05	1.17E+06	5.6	2.55	SARS-CoV-2	4	40
P0DTC3	ORF3a protein	2	1420	891.7	1.8E+06	1.98E+06	4.6	1.94	SARS-CoV-2	2	20
P59595	Nucleoprotein	1	2692	N/A	2.3E+06	N/AE+00	5.2	N/A	SARS-CoV-2	1	10
P0C6X7	Replicase polyprotein 1ab	6	2347	799.6	5.4E+06	7.06E+06	6.9	2.02	SARS	6	60
P59594	Spike glycoprotein	1	2105	N/A	1.9E+07	N/AE+00	9.5	N/A	SARS	1	10
P0DUB6	Alpha-amylase 1A	41	1595	658.4	1.2E+07	1.58E+07	5.6	2.14	Homo sapiens	10	100
Q96DR5	BPI fold-containing family A member 2	24	2076	511.1	5.2E+06	6.00E+06	5.5	2.00	Homo sapiens	10	100
P02810	Salivary acidic proline-rich phosphoprotein 1/2	25	1353	553.4	2.5E+07	3.93E+07	8.4	2.80	Homo sapiens	10	100

4.4.3 SARS-CoV-2 proteins

Table 4.4 summarizes the viral SARS-CoV-2 proteins detected using both types of coated SPME blades. Similar to the trends in the untargeted proteomics results reported in the previous section, the porous C18/PAN blades provided the most reliable detection of the viral peptides in 7 of the 10 whole saliva samples. It is important to note that this result does not equate to a 70% detection rate, as the preliminary SARS-CoV-2 genome bank used dates to early 2020,[90] and there are clear differences in the untargeted LC-MS TIC chromatograms (Fig. 4.2). Understandably, higher detection rates are expected when using updated databases in future studies. And importantly, viral peptides were not detected at any meaningful level in healthy control samples via bio-SPME-Tryp-LC-MS/MS.

It is also worth noting that, due to limited access to newer databases and positive cases post-pandemic, this work stands as a proof-of-concept study demonstrating that matrix-compatible SPME devices with porous extraction phases are a viable option for use in peptide analysis. The logistics of personal protective equipment (PPE) for frontline healthcare professionals have improved drastically since the beginning of the pandemic,[105,106] thus paving the way for substantial improvements to the reproducibility and reliability of SPME in clinical settings by enabling direct sampling from the patient's oral cavity. Variabilities accrued during the self-collection, transportation, storage, and treatment of the whole saliva samples will be greatly reduced when sampled directly from the patient. Direct sampling can be implemented using simple modifications such as medical swabs equipped with SPME inserts. For instance, Hu et al. inserted

SPME fibers with various coatings into medical swabs for the direct sampling of participants' oral cavities.[24] One key advantage of performing SPME extraction at the source is that the resultant metabolism quenching prevents viral protein breakdown pre-analysis.[25,86,107] Future studies are encouraged to explore various modifications to the SPME extraction phases, porosity, geometries, and portable detection devices to identify combinations that are best suited for rapid on-site detection.[108] Furthermore, updating the proteomic and metabolomic methodologies and databases will also be critical to the future of rapid and personalized diagnostics.[109] Updated databases will also ensure the validity of MS-based screening techniques and keep up with an evolving virus which, as mentioned above, is an area of limitation for RATs.[90]

Table 4.4 List of samples in which peptides derived from SARS-CoV-2 were identified in whole saliva and whole saliva supernatant samples from COVID-19-positive individuals (n=10) using HLB/PAN and C18/PAN blades coupled with LC-MS/MS.

Sample ID	**HLB/PAN blades**		**Porous C18/PAN blades**				
	Whole saliva		Whole saliva		Whole saliva supernatant		
	Replicase polyprotein 1ab	Mem-brane protein	Replicase polyprotein 1ab	Nucleo-protein	Replicase polyprotein 1ab	Nucleo-protein	ORF3a protein
18	x				x	x	
23	x		x		x		x
28	x		x		x		
29	x			x			
30			x	x			
31			x				
38	x		x		x		
39							x
41							
44	x	X	x				

4.4.4 Peptide characteristics via bio-SPME

The pI and molecular weights of all peptides detected via bio-SPME are shown in Fig. 4.3. Overall, the extracted peptides skew towards acidity. The MWs of all detected SARS-CoV-2 peptides ranged between ~500−2500 Da (Fig. 4.3 a and b). This mass range encapsulates all expected digested SARS-CoV-2 peptides in lieu of SPME.[92] More peptides were extracted via porous C18/PAN blades which was expected based on prior research.[96] Similarly, Fig. 4.3c shows that the vast majority of endogenous and viral peptides identified fell within the ~500−2500 Da range (with the exception of one at closer to 3000 Da), suggesting that bio-SPME can reliably capture peptides up to 2500 Da. Fig. 4.3c is also a good representation of the peptidome coverage of porous C18/PAN-blades as the data were collected from a different and larger cohort (n = 30) of SARS-CoV-2-positive patients. Moving forward from this proof-of-concept study, bio-SPME should explore the possibility of on-site extractions to gain advantages such as improved safety during viral sample transportation (no bulk saliva samples), more representative information (metabolism quenching), and reduced sample variability (reduced steps in sample preparation).[93]

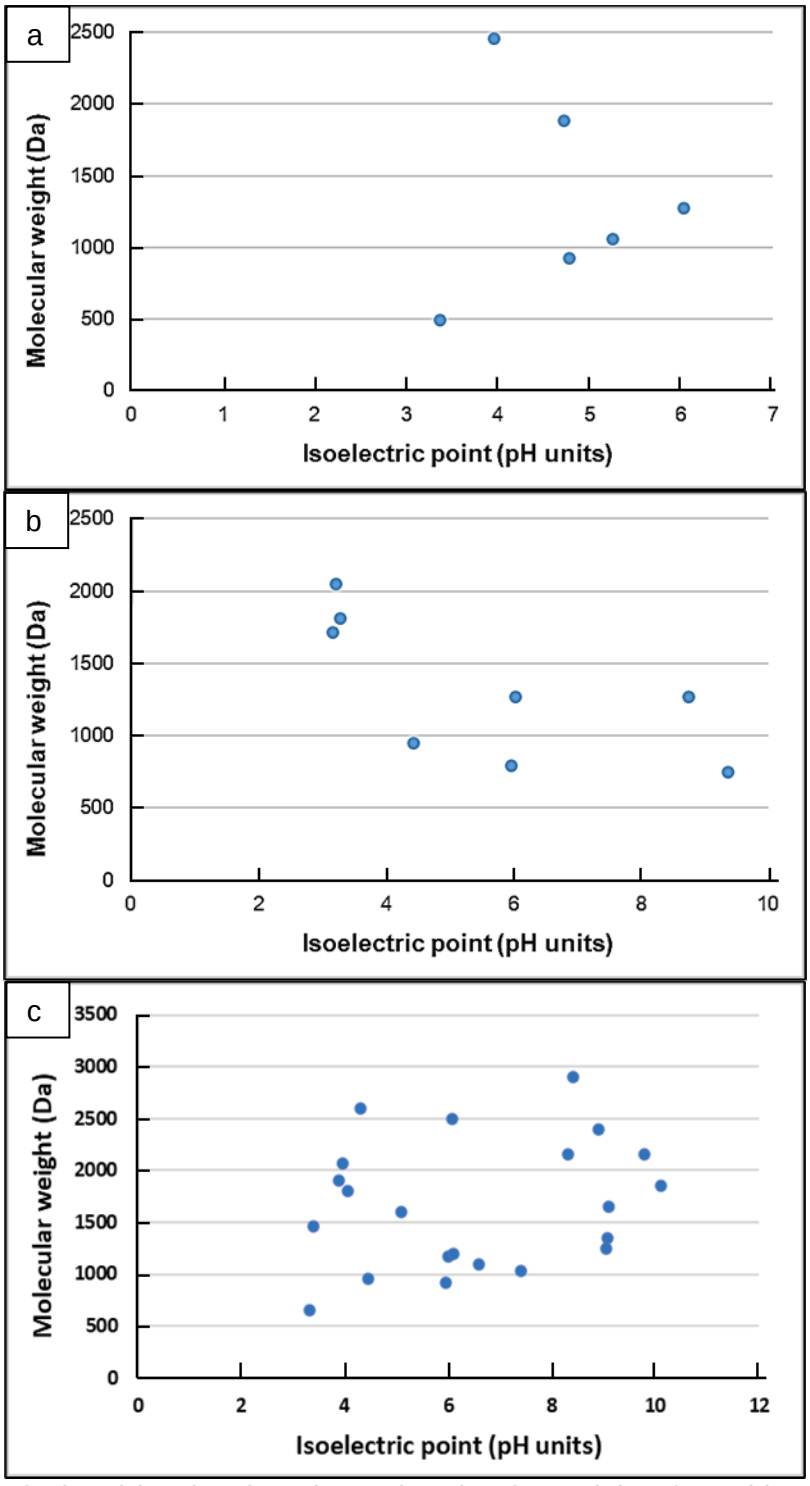


Figure 4.3 Calculated isoelectric point and molecular weight of peptides derived from SARS-CoV-2 proteins identified in whole saliva (n = 10) via (a) HLB\PAN-blades and (b) C18/PAN-blades. (c) pI and MW of all viral and endogenous peptides detected in whole saliva (n = 30) via porous C18/PAN-blades.

4.5 Conclusion

The study presented here contained a clinical application of porous C18/PAN-coated blades for the first time. More specifically, the findings presented herein showed that bio-SPME can extract peptides up to 2.5 to 3.0 kDa range. Trypsin digestion facilitated the extraction of hundreds of peptides and enabled proteomics via SPME which was previously thought to be a highly challenging, if not impossible, task for SPME. The enhanced porous C18\PAN coating enabled the extraction of a wider range of peptides compared to the conventional HLB\PAN coating, which was expected and in agreement with previous studies. When coupled with LC-MS/MS, the proposed bio-SPME was able to obtain peptidomic profiles of saliva samples from and clearly differentiated between healthy and SARS-CoV-2-positive patients following Tryp digestion. This meant that bio-SPME has potential in proteomics investigation of clinical samples. Future studies involving medical applications should investigate patient selection criteria and direct sampling to mitigate variabilities caused by disease severity, sample collection, transportation, storage, and preparation.

Chapter 5. In vivo chemotherapeutic drug monitoring of doxorubicin during in vivo lung perfusion via solid phase microextraction

5.1 Preamble

The clinical findings presented in this chapter were obtained in a collaborative effort between the University of Waterloo and Toronto General Hospital, University Health Network. The theoretical and proof-of-concept findings in this chapter were obtained solely by the author. The clinical data presented in this chapter has been submitted for publication in the *Journal of thoracic oncology* as a result of the collective efforts of the following co-authors: Sahar A. Saddoughi, Jennifer Lister, Vinicius Michaelsen, Aizhou Wang, Runshan Will Jiang, Janusz Pawliszyn, Shaf Keshavjee, Peter Slinger, Juan Camilo Segura Salguero, Abha Gupta, Thomas K Waddell, Albiruni Razak, and Marcelo Cypel. The theoretical and proof-of-concept data on SPME will be prepared for submission at a later date once more clinical data is received. This chapter was written solely by the author of the thesis. Please see Statement of contributions for more information. We would like to thank the following organizations for their generous fundings: Natural Sciences and Engineering Research Council (NSERC) of Canada, Canadian Institutes of Health Research (CIHR), University of Waterloo, and University Health Network.

5.2 Introduction

Pulmonary metastases are amongst the most common secondary cancers, occurring in about 40% of cases following primary cancer. Sarcomas and colorectal carcinomas are two types of primary cancers that exclusively metastasize to the lungs.[110,111] Only surgically resectable pulmonary metastases are curable.[112] While surgical removal of these cancers is the current standard treatment procedure, the 5-year survival rate post-operation remains poor, at about 20 – 50%.[113]

Post-operative recurrence of pulmonary metastases is observed in most patients, most likely due to the presence of micrometastatic tumors, which cannot be observed visually or by any currently available imaging techniques.[114] As such, Intravenous systemic chemotherapy is a common adjuvant treatment for microtumors in patients with resectable pulmonary metastases. However, patient outcome remains poor despite such combinatory treatments; for instance, patients with pulmonary metastases of sarcoma origin developed recurrences at a rate of 41 – 83 % following surgery.[114] This poor patient outcome is suspected to be caused by a combination of drug resistance, limiting dosage due to systemic toxicity, and inadequate distribution of drug concentration within the lungs and tumors.[114] In vivo lung perfusion (IVLP) is a novel technique that enables continuous perfusion of the surgically isolated lungs with high doses of chemoagent without causing systemic toxicity. IVLP also takes advantage of the active perfusion to achieve therapeutic concentrations throughout the organ, which traditional suffusion-based chemotherapy fails to achieve.[51,116]

Current methods to measure local tissue concentration and distribution during IVLP during chemotherapy rely on a sequence of processes including physical biopsies, solvent extraction, protein precipitation, and HPLC detection.[116] While tissue concentrations (in μg/g) can be estimated this way, there are clear drawbacks associated with such methods. Medically, physical biopsy is an invasive technique that causes trauma to the organ; the damage is especially problematic for lung cancer patients with already impaired lung function.[11,117] Analytically, the limiting number of lung biopsies that can be safely performed drastically limits the amount of information obtained. For example, only two biopsies are taken at the baseline and after IVLP, each at a different lobe of the lung.[116] As such, the only information available is the final tissue concentration at the end of the 3-hour long IVLP procedure of a single lobe.[116] Moreover, the current standard assay is time-consuming, as it requires solvent extraction and protein precipitation prior to HPLC detection.[36] A minimally invasive sampling technique that safely enables the acquisition of in vivo tissue concentration during chemotherapy from numerous sampling points with rapid on-site detection is an obvious solution that can provide both temporally and spatially resolved information to the surgical team in real time. Solid phase microextraction (SPME) is one such technique with recent novel animal and human applications demonstrating its feasibility in various in vivo studies.[32,36,50] Preliminary data on the determination of in vivo doxorubicin (DOX) concentrations during IVLP shows quantitative data trends obtained via in vivo SPME are comparable to standard assays involving physical biopsies.[36,118] A few

criteria must be met before SPME can be properly implemented in biomedical applications. First, the SPME device must be inert to the sampled matrix to avoid unwanted changes to the biological system.[119] In this case, a nitinol alloy fiber solid support coated with a biocompatible binder containing the extraction phase is used (Fig. 5.1). Secondly, the extracted analytes must remain stable inside the coating prior to instrumental analysis.[25,119] This is achieved by the porous polyacrylonitrile (PAN) binder, which allows diffusion of small molecules while excluding macromolecules, such as enzymes. Particulates and cells are also rinsed off from the coating surface post-extraction, thus preventing biofouling.[25,119] Thirdly, the extraction phase chemistry must be suitable for the targeted analyte. Here, a silica-based sulfonate-C8 mixed-mode (MM) extraction phase was used for the extraction of DOX. Lastly, the SPME device itself must be physically inert since the autoclave subjects the devices to high temperatures.

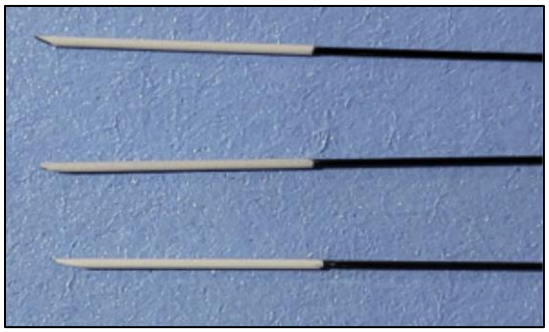


Figure 5.1 SPME probes using sharpened nitinol fibers coated with mixed-mode extraction phase.

In this chapter, extraction characteristics of the nitinol MM SPME probes are investigated for the purpose of clinical applications. Numerous clinical case studies using such devices for in vivo SPME quantification of DOX during IVLP are also presented here. Selected participating patients suffer from resectable

lung metastases of bone or soft tissue sarcomas. In vivo SPME data are directly compared to conventional tissue biopsy-based assays to summarize the advantages and untapped potential of the minimally invasive sampling technique over the conventional practice.

5.3 Methods and materials

5.3.1 Reagents and SPME devices

The information on all reagents used in the experiments presented in this chapter was described in Chapter 2. Nitinol wires with ~200 µm outer diameter coated with mixed mode C8-sulfonate MM extraction phase and PAN binder (to ~240 µm OD) were used for the clinical study, including the ex vivo matrix-matched calibration (MMC). Coated SPME wires were purchased from MilliporeSigma (Burlington, MA, USA), cut to 4.5 cm long fibers, and stripped down to leave 1.5 cm of coating near the tips, which were sharpened by a diamond wheel cutter, as shown in Fig. 5.1. Recessed bio-SPME probes coated with wHLB/PAN were used for a study of the temperature dependence of SPME. All SPME probes were cleaned in a solution made of acetonitrile (ACN), methanol (MeOH), isopropanol (IPA), and water (H_2O) to a ratio of 3:3:3:1 v/v by benchtop vortex mixing at 500 rpm for 30 min, twice. Desorption solution was 7:2:1 MeOH/ACN/H_2O v/v with 0.1% v/v formic acid (FA)

5.3.2 SPME extraction characteristics

Various SPME extraction characteristics were investigated to ensure and improve the accuracy of in vivo SPME. Fresh ovine lung tissue homogenate was

used as model matrix. time profile of DOX from tissue homogenate was obtained at 35°C. Extraction time profiles of various DOAs and DOX were investigated at 17, 36, and 60 °C to understand the temperature-dependence of the in vivo SPME sampling probes. Market Forge Sterilmatic Steam Pressure Sterilizer (Burlington, VT, USA) was used to steam-sterilize (autoclave) SPME devices with 3-L of distilled water at 121 °C for 45 min. Matrix binding kinetics was determined by performing SPME of DOX from homogenized lamb lung tissues at 1, 10, 30, 60, and 120 mins after spiking to two concentrations (50 and 100 ng/kg) at 30 °C.

5.3.3 Matrix-matched calibration (MMC)

Quantitative in vivo DOX concentrations were determined via MMC using ovine lung homogenate, as per the protocol established by Roszkowska et al.[35] Fresh ovine lung was purchased from a local butcher shop, diced up to exclude large bronchi, and homogenized in a blender at 4 °C to avoid heating of the tissue homogenate. The fresh lung homogenate (9 g) was mixed with up to 1 mL of phosphate buffered saline (PBS), in which sub-portions of the 1 mL solution were concentrated DOX spiking solutions in dimethyl sulfoxide (DMSO), so that the final organic solvent was < 5% v/w for the highest concentration, and < 1% v/w for the rest. The following final tissue homogenate concentrations were prepared: 0, 1, 5, 10, 50, 250, 500, 1000 µg/g. Four SPME probes were used to extract from each sample for 20 min while MMC samples were kept inside a 36 °C water bath. Immediately following extraction, each probe was rinsed in ultrapure water with benchtop vortex agitation for 5 seconds to remove blood and

particulates on the surface of the coating, dried with Kimwipes, and stored at -80 °C until (when applicable) desorption and LC-MS analysis.

5.3.4 Patient selection

This study is part of a non-randomized, dose-escalation study approved by the Institutional Review Board. The patient selection inclusion criteria are: 1. Diagnosed with primary soft tissue or osteogenic sarcoma. 2. Secondary lung cancer with bilateral pulmonary metastases. 3. At least 3 lung lesions are present. 4. Between the age range of 18 – 65. 5. No other pulmonary diseases or pneumonitis. Patient exclusion criteria were also employed and are listed elsewhere.[115]

5.3.5 IVLP with DOX

A detailed description of the IVLP procedure is available elsewhere.[51,116] Briefly, the perfusate solutions used during surgery were maintained at 37 °C. Five groups of patients were subjected to 5 different perfusate concentrations: 5, 7, 9, 11, 13 μg/mL perfusate concentrations. Further increments in perfusate DOX concentration took place only if no major toxicity was observed for 30 days with the current highest dosage group. Complications that suggest major toxicity are defined and listed elsewhere.[115] Each patient underwent IVLP of the left lung for up to 3 hours followed by blood reperfusion for up to 30 min.

5.3.6 In vivo SPME

The solvent-cleaned probes were subjected to steam sterilization at 121 °C for 40 min. The autoclaved probes were stored in a sterilized container

until use in the operating room. In vivo SPME took place at 5 sampling time points in each lobe of the lung, with a 20-min extraction time. The same post-sampling procedure described in 5.3.3 was carried out for all fibers following extractions.

5.3.7 Liquid chromatography-Mass spectrometry analysis (LC-MS)

Each probe was desorbed in 100 µL of desorption solution (70:20:10 MeOH/IPA/H_2O, with 0.1% FA). 5 µL of each desorption solution was injected into a Thermo Vanquish UHPLC coupled with a Thermo TSQ Quantiva mass spectrometer (Waltham, MA, USA) for the detection of DOX in positive mode reverse phase LC-MS. A Kinetex UHPLC PFP column (10 cm × 2.1 cm, 1.7 µm) from Phenomenex (Torrence, CA, USA) was used with the following two mobile phases: A) H_2O, 0.1% v/v FA and B) ACN, 0.1% v/v FA. The LC gradient started with a brief (1 min) equilibration stage followed by a simple linear ramp up to 95% B from 10% B at equilibrium over a 5 min period, where it was held at 95% B for 3 min before being brought back down to 10% B in 0.25 min and was held there until the end. The entire method was 10 min long with a 0.4 mL/min flow rate held at 40 °C column temperature. DOX was tuned on the MS to scan for a parent mass of 544.2 m/z with 361.1 m/z and 397.2 m/z as qualifier and quantifier product ions, respectively. Ion source parameters were set to 3500 V spray voltage with 350 °C Heated-ESI vaporizing temperature to accommodate for the high flow rate. All data were processed with Xcalibur 4.0 software and Excel 365.

5. 4 Results and discussion

5.4.1 Extraction time profile of DOX

It is crucial to understand how an SPME device will perform both chemically and physically prior to clinical application. Fundamentally, the amount of analyte extracted depends on a few important variables such as extraction time, rate of diffusion (extraction kinetics), and distribution coefficient between the sample matrix and the extraction phase (extraction thermodynamics), as discussed in Chapter 1. These variables are heavily influenced by practical factors that the experimenter needs to consider and will be discussed in this section.

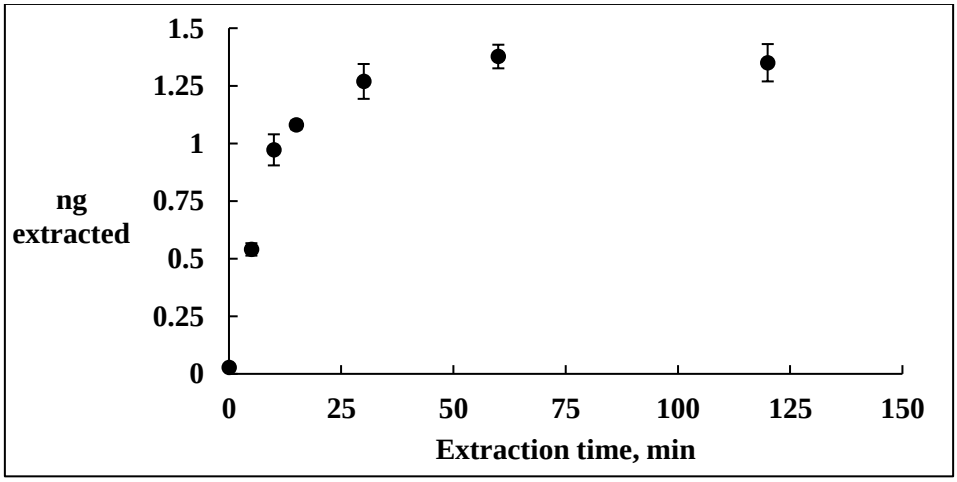


Figure 5.2 Mixed-mode SPME probe extraction time profile of DOX from ovine lung homogenate at 50 µg/g and at 35 °C. Static-mode extraction time = 20 min, 4 replicates (N = 28), RSD < 10% for all data points.

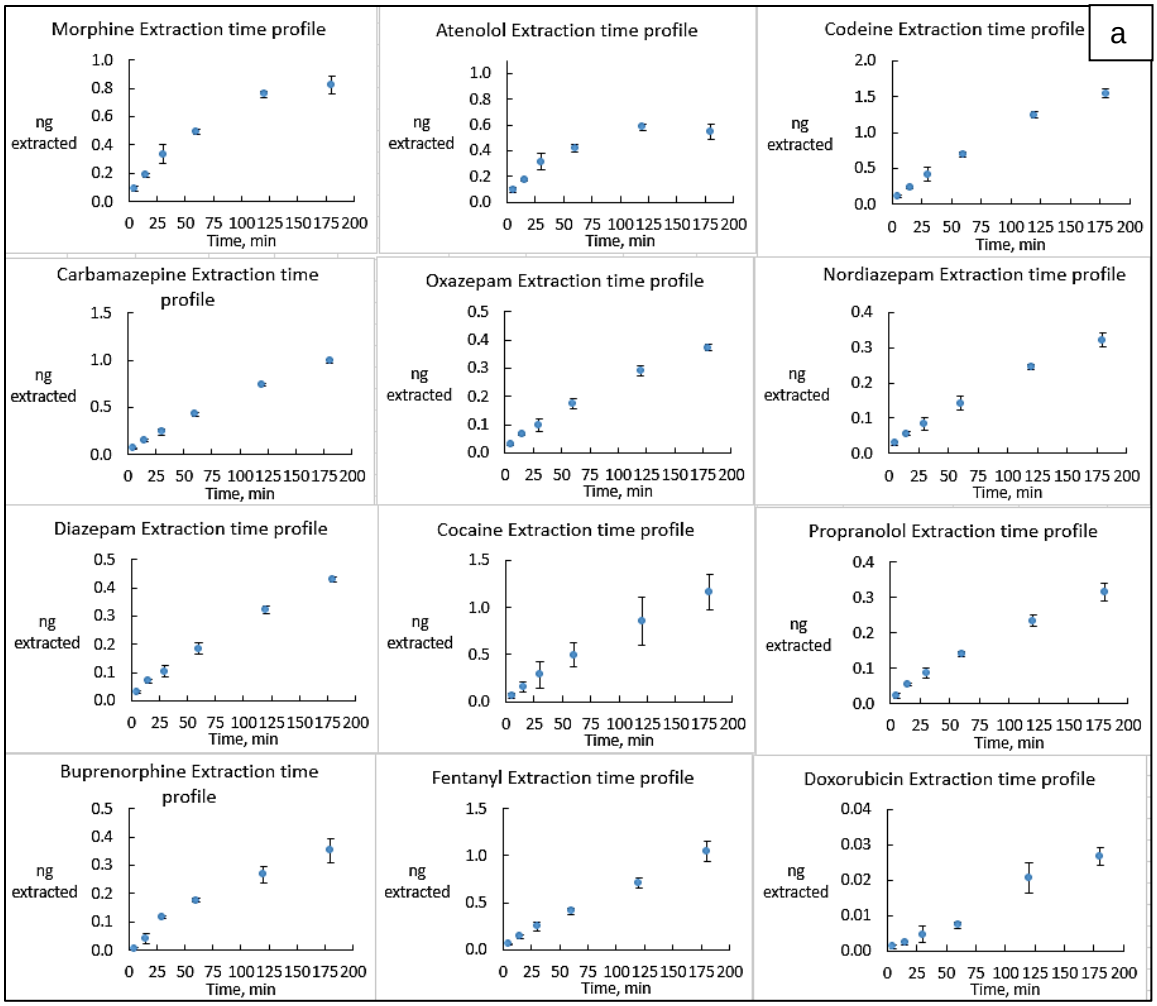
Fig. 5.2 shows a full extraction time profile of DOX using MM SPME probes from homogenized lung tissue. This extraction time profile can be assumed to be representative of the in vivo clinical environment, as Roszkowska et al. showed that ovine homogenized tissue model can be reliably used to mimic

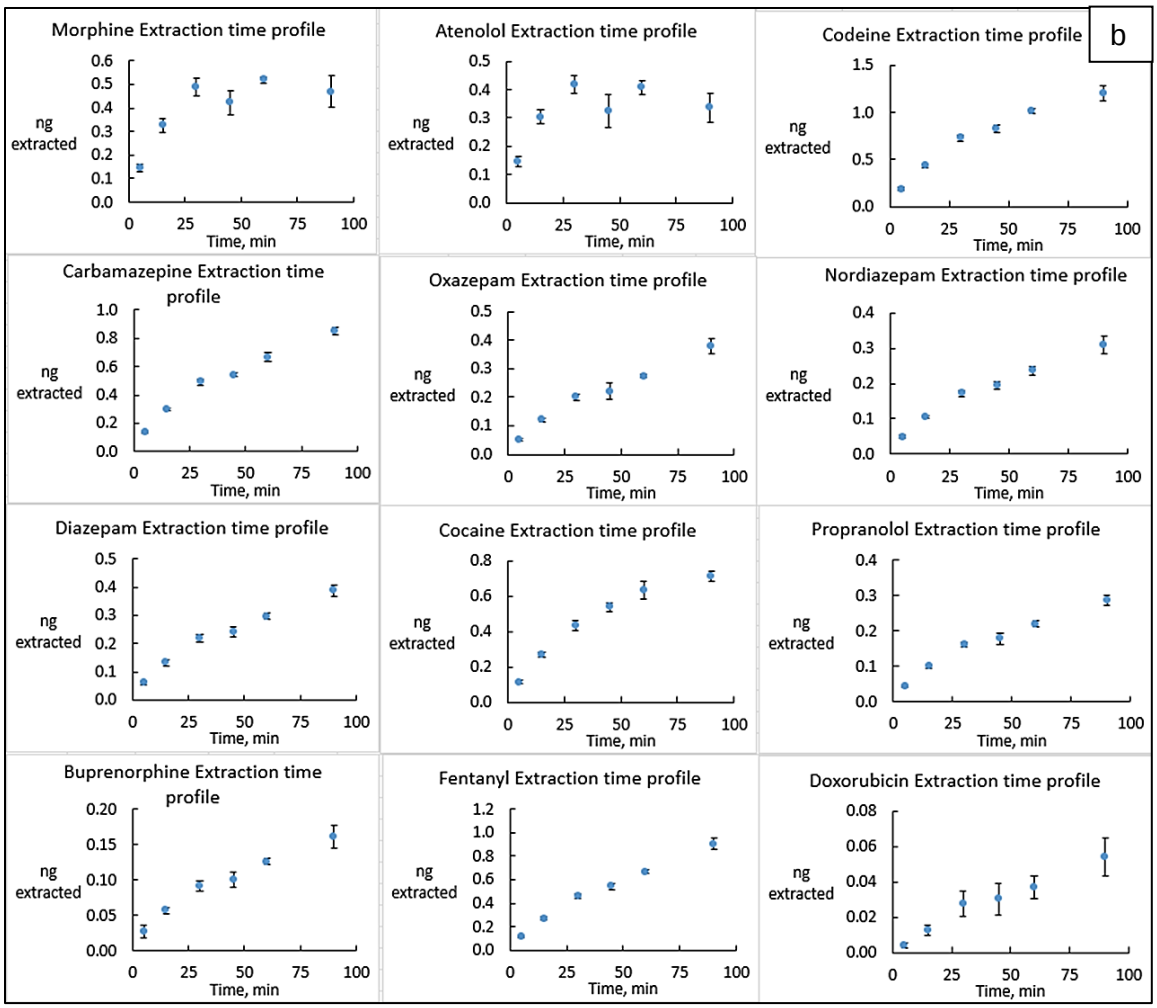
in vivo conditions for DOX.[5.18] Though the 20-minute extraction time is not sufficient to reach extraction equilibrium, this time was a compromise between adequate analytical sensitivity and surgery time constraints. When compared to previous studies, the RSD achieved here is much lower, at 10%.[35,78] This can be attributed to many practical factors such as managing timers, handling of multiple devices, and sample temperature.

5.4.2 Extraction temperature

The extraction efficiency (amount extracted) was much higher (> 2-fold) in this study (Fig. 5.2) compared to prior studies due to the elevated sample temperature at 35 °C, which better represented in vivo conditions.[35] While temperature influences extraction thermodynamics, and thus the distribution coefficient, K_{es}, it has a much greater effect on the extraction kinetics, which is not currently well-understood.

The effect of temperature on extraction kinetics and thermodynamics was observed experimentally, as shown in Figures 5.3 a – c below. As expected, higher amounts of analytes were extracted in shorter times from warmer samples, thus confirming the sizable effect of temperature on the extraction efficiency of bio-SPME. Polar analytes also reached extraction equilibrium more quickly as sample temperature increased. In fact, declines in amount extracted were observed sooner at a high temperature (Fig. 5.3 c) potentially due to a number of reasons, such as the displacement effect and rapid biodegradation of small/polar analytes in the matrix. Future studies should be conducted to explore this phenomenon.


a
Morphine Extraction time profile
Atenolol Extraction time profile
Codeine Extraction time profile
Carbamazepine Extraction time profile
Oxazepam Extraction time profile
Nordiazepam Extraction time profile
Diazepam Extraction time profile
Cocaine Extraction time profile
Propranolol Extraction time profile
Buprenorphine Extraction time profile
Fentanyl Extraction time profile
Doxorubicin Extraction time profile
ng extracted
Time, min


b
Morphine Extraction time profile
Atenolol Extraction time profile
Codeine Extraction time profile
Carbamazepine Extraction time profile
Oxazepam Extraction time profile
Nordiazepam Extraction time profile
Diazepam Extraction time profile
Cocaine Extraction time profile
Propranolol Extraction time profile
Buprenorphine Extraction time profile
Fentanyl Extraction time profile
Doxorubicin Extraction time profile
ng extracted
Time, min

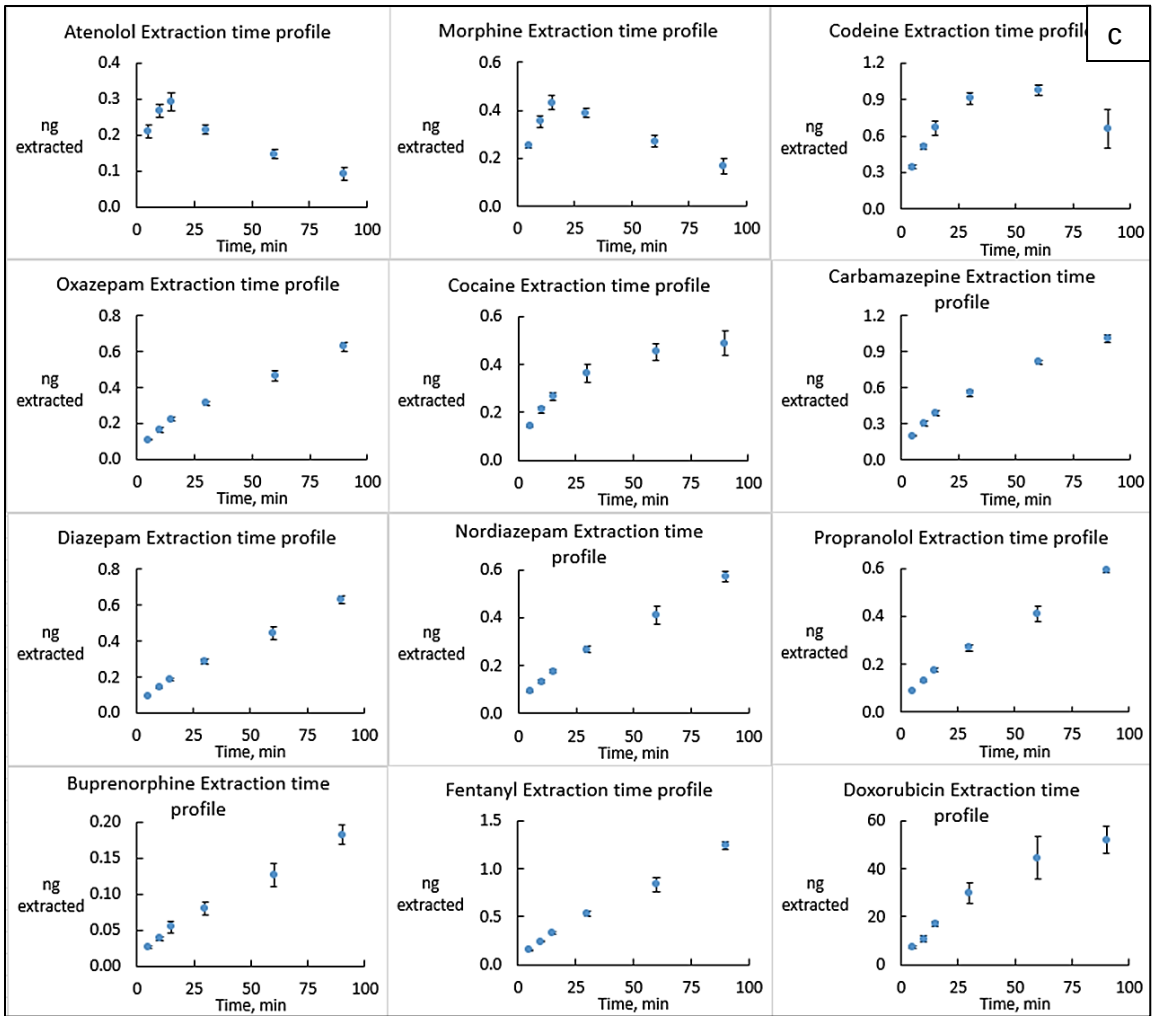


Figure 5.3 Extraction time profiles of 11 DOAs and DOX in homogenized lung tissue at: (a) room temperature (20 °C), (b) physiological temperature (37 °C), and (c) 60 °C. Except for DOX (logP ≈ 1.3), analytes are sorted from top to bottom by decreasing polarity.

5.4.3 Activation-dependent extraction phase performance

In addition to sample temperature, the extraction efficiency of the MM extraction phase is also dependent on whether the coating is properly activated with a high-percentage organic solvent activation solution. This activation-dependent extraction efficiency appears to be strongly correlated with the wettability of the extraction phase particles, as discussed in detail in Chapter 2.

For the purpose of this study, it was imperative to ensure that the MM SPME probes would perform adequately without solvent activation due to the need for autoclave-sterilization immediately prior to surgery.

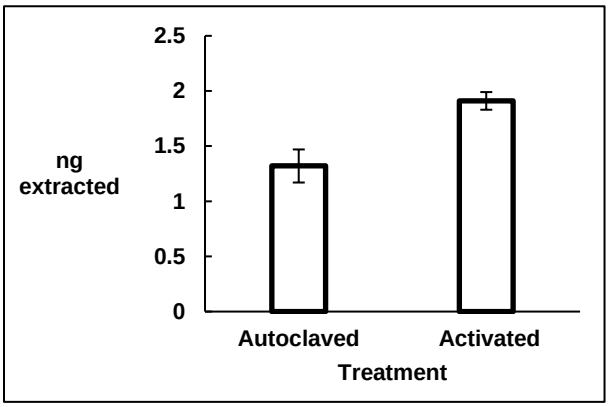


Figure 5.4 Mixed-mode SPME probe extraction efficiency of DOX with and without solvent activation from ovine lung homogenate at 100 µg/g and at 35 °C. Static-mode extraction time = 20 min, 4 replicates (N = 8), RSD < 5% for all data points.

Fig. 5.4 shows that MM SPME probes were able to retain a large portion of their extraction efficiency, albeit deactivated via autoclave-sterilization. This was likely due to the hydrophilic nature of the sulfonate functional group as well as the silica core of the MM coating. Regardless, the decreased extraction efficiency caused by autoclaving was not taken into consideration in prior studies, which contributed to the reported underestimations.[36] This becomes a much bigger issue when implementing a more nonpolar extraction phase. For example, conventional hydrophilic and lipophilic balanced (HLB) organic copolymeric particles with low (% wt.) polar functional groups (n-vinylpyrrolidone) showed greatly diminished extraction efficiency (Fig. 5.5). A detailed comparison of these extraction phases is available in Chapter 2.

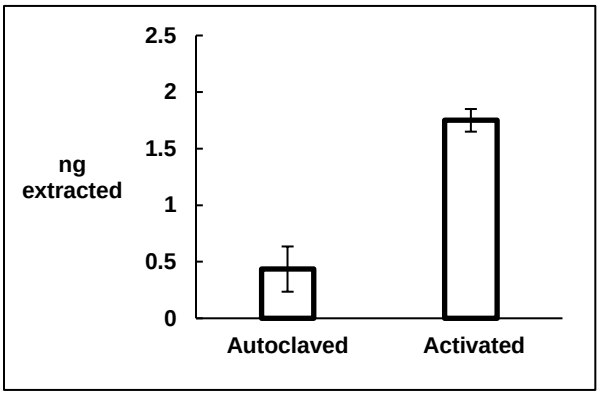


Fig 5.5 In-house HLB SPME probe extraction efficiency of DOX with and without solvent-activation from ovine lung homogenate at 100 µg/g and at 35 °C. Static-mode extraction time = 20 min, 4 replicates (N = 8), RSD < 10% for all data points.

5.4.4 Matrix-matched calibration (MMC)

As the term suggests, MMC is an ex vivo calibration technique that takes advantage of a similar or identical matrix to calibrate for the quantitative analysis of the actual matrix of interest.[120] It is primarily used to compensate for matrix effects that interfere with analytical response, such as ion suppression in mass spectrometry.[121] Furthermore, it can be used to mimic in vivo environments using a more easily accessible model matrix to compensate for tissue binding of targeted analytes.[35] In this case, homogenized ovine lung tissue was used to mimic patient lung tissue during IVLP with DOX. Roszkowska et al. found that MMC was accurate when using homogenized lung tissue to model intact lung tissue via SPME.[35] In a later study by Bojko et al., the same calibration technique was used to obtain comparable trends in temporally resolved in vivo DOX data between in vivo SPME and standard solvent extraction of lung biopsies.[36] However, in vivo SPME data reported in this study were lower (> 2-fold) than expected based on standard solvent extractions. The MMCs from prior studies failed to address a few factors that influence the overall accuracy of this calibration technique, including coating performance, sample temperature, linear

dynamic range (limit of linearity), and biostability (rate of tissue binding vs. metabolism). The following MMC curve and tissue binding kinetics plot were experimentally obtained with considerations to the factors mentioned above.

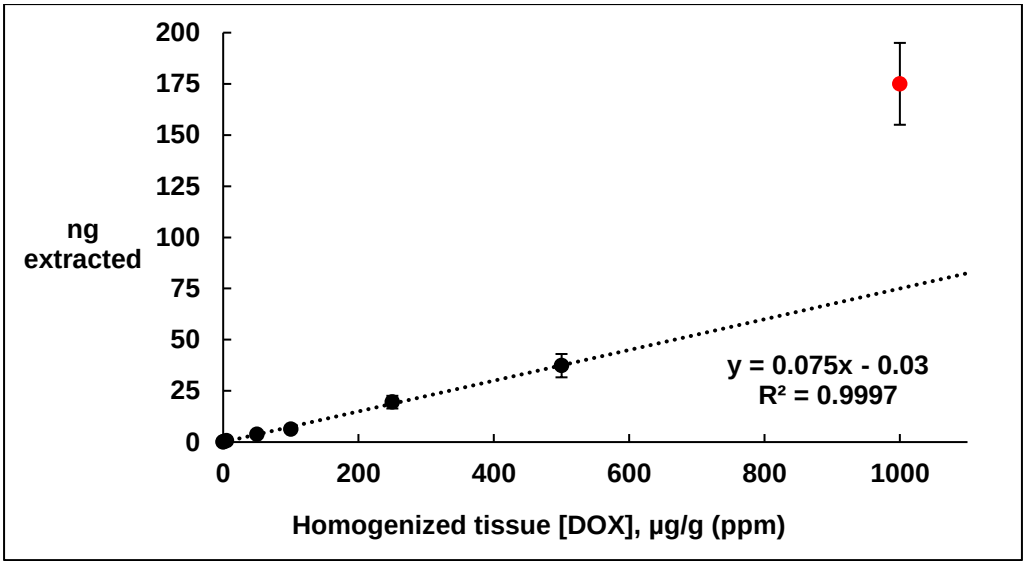


Figure 5.6 Matrix-matched calibration using homogenized ovine lung tissue spiked with doxorubicin via SPME. Static mode extraction time = 20 min, extraction temperature = 35 °C, 4 replicates (N = 32), RSD < 10% for all data points, with the exception of 1000-ppm-level data points.

First, the previous studies stated that the matrix-matched calibration curve could be extrapolated far beyond the highest level of the calibration samples. This assumption was experimentally determined to be false as shown in this MMC curve with an extended concentration range. The ng amount of DOX extracted at 1000 µg-DOX/g tissue concentration far exceeded the linear dynamic range, suggesting that tissue-binding of DOX saturates somewhere below 1000 µg/g. In other words, the extra DOX extracted at the highest concentration can be explained by an abundance of DOX in the “free concentration” resulting from the saturation of tissue-binding. Note the “free concentration” here technically refers to the portion of DOX present only in the

aqueous portion of the interstitial fluid and blood/plasma – which might not be true and a third spike in the slope can be expected with an even high spiking concentration range (assuming the biofluid portion of the tissue matrix possesses higher binding capacity but lower affinity to DOX than tissue). For the most part, the linear dynamic range of the improved MMC technique encapsulates the range of in vivo DOX concentrations expected during IVLP, meaning in vivo SPME is a valid quantitative technique.[36] Secondly, the ng amounts of DOX extracted were much higher (> 2-fold) at every level of the calibration curve as compared to those reported in the previous study. This was most certainly due to the elevated temperature (35°C instead of 20 °C) adopted in the present study. While the trends observed in the temporally resolved data from the previous study are similar to the cases presented in this chapter (Fig. 5.8), the drastically increased amount of DOX extracted at body temperature compared to room temperature (20 °C) would explain the major flaws in the underestimations reported previously.[36]

5.4.5 Analyte matrix-binding and biostability

Authors from previous studies left homogenized tissue samples spiked with DOX overnight to ensure that tissue binding occurred prior to extractions.[35,36] This was also an experimental design flaw as DOX is readily metabolized over time, uncharacteristic of the clinical environment during IVLP.[121] To investigate the kinetics of tissue-binding of DOX, a simple experiment was performed where multiple SPME extractions from DOX spiked homogenized lung

tissue samples took place at 1, 10, 30, 60, and 120 min after spiking at two concentrations.

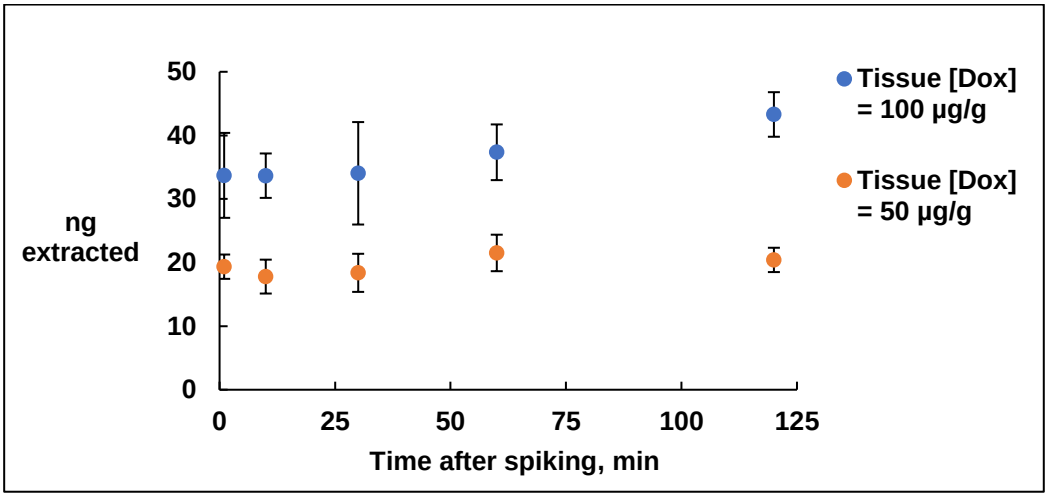


Figure 5.7 Spiking time extraction profile from homogenized ovine lung tissue spiked to 50 and 100 µg/g DOX. Static mode extraction time = 20 min, extraction temperature = 30 °C, 3 replicates (N = 40), RSD < 20% for all data points.

Fig 5.7 shows that tissue-binding of DOX is extremely fast and reaches thermodynamic equilibrium within a minute following spiking as the amounts of DOX extracted via SPME are similar afterwards. This is expected as numerous studies have observed immediate binding between DOX (including DOX-related chemotherapeutic agents) and biological matrices.[122,123] This also means overnight incubation was unnecessary to reach tissue binding equilibrium. Rather, overnight incubation was detrimental to the accuracy of the calibration since DOX has a half-life of about 0.7 days in tissue.[123] The inadequate performance of the extraction coating, an unrepresentative MMC temperature, and the prolonged spiking time would explain the underestimations reported in the previous study.[36]

5.4.6 Quantitative therapeutic drug monitoring via in vivo SPME

From 2017-2022, a total of 8 participating patients were screened for the phase I dose escalation study. Six patients met the inclusion criteria while 2 patients were excluded due to additional pulmonary diseases prior to surgery. Group 1 had 1 patient, who was subjected to 5 µg/mL DOX IVLP; group 2 had 3 patients subjected to 7 µg/mL DOX IVLP; and the last group had 2 patients subjected to 9 µg/mL DOX IVLP. No lung toxicity was observed for the first two groups of patients, whereas some complications were observed at the 9 µg/mL DOX IVLP dosage of chemotherapy. The perfusate and tissue DOX concentrations ([DOX]) determined via the standard procedure as well as in vivo SPME are summarized below in Fig. 5.8 for a direct comparison of the two techniques in therapeutic drug monitoring (TDM) of DOX. Due to unforeseen medical and logistical issues, not every case was investigated with both techniques. Standard procedures were performed for most cases, except for case # 3, whereas in vivo SPME was implemented from case #3 onwards. This means cases 4, 5, and 6 included both drug monitoring techniques. Starting with the IVLP perfusate, results from the standard procedure (Fig. 5.8 A) were drastic overestimations compared to the maximum possible “true value” (maximum [DOX] < initial perfusate [DOX]) – this was likely because solvent extraction, an exhaustive extraction technique, extracts the target analyte (DOX) exhaustively from both the free (aqueous) and matrix-bound (serum) concentrations. On the other hand, SPME extracts non-exhaustively via the free concentration. The non-exhaustive nature of SPME maintains the distribution of DOX between the free

form and the matrix-bound form in serum (K_A). As a result, the undisturbed K_A results in far more accurate and reasonable [DOX] determined for the perfusate solutions (Fig. 5.8 C).[25,78] Tissue [DOX]s determined by the standard procedure (Fig. 5.8 B) were also unrepresentative of the true value during IVLP compared to previous porcine and preliminary human studies.[35,36] This was due to the surgical team's decision to reduce the number of traumatic lung biopsies collected during surgery. Instead, only two lung biopsies were taken – once before IVLP (baseline), once after blood reperfusion (post-IVLP), and none during IVLP. On the other hand, in vivo SPME was safely performed throughout the IVLP operation due to its minimal invasiveness, allowing for data to be collected for the upper and lower lobes of each patient's left lung, as respectively presented in Fig. 5.8 D and E.

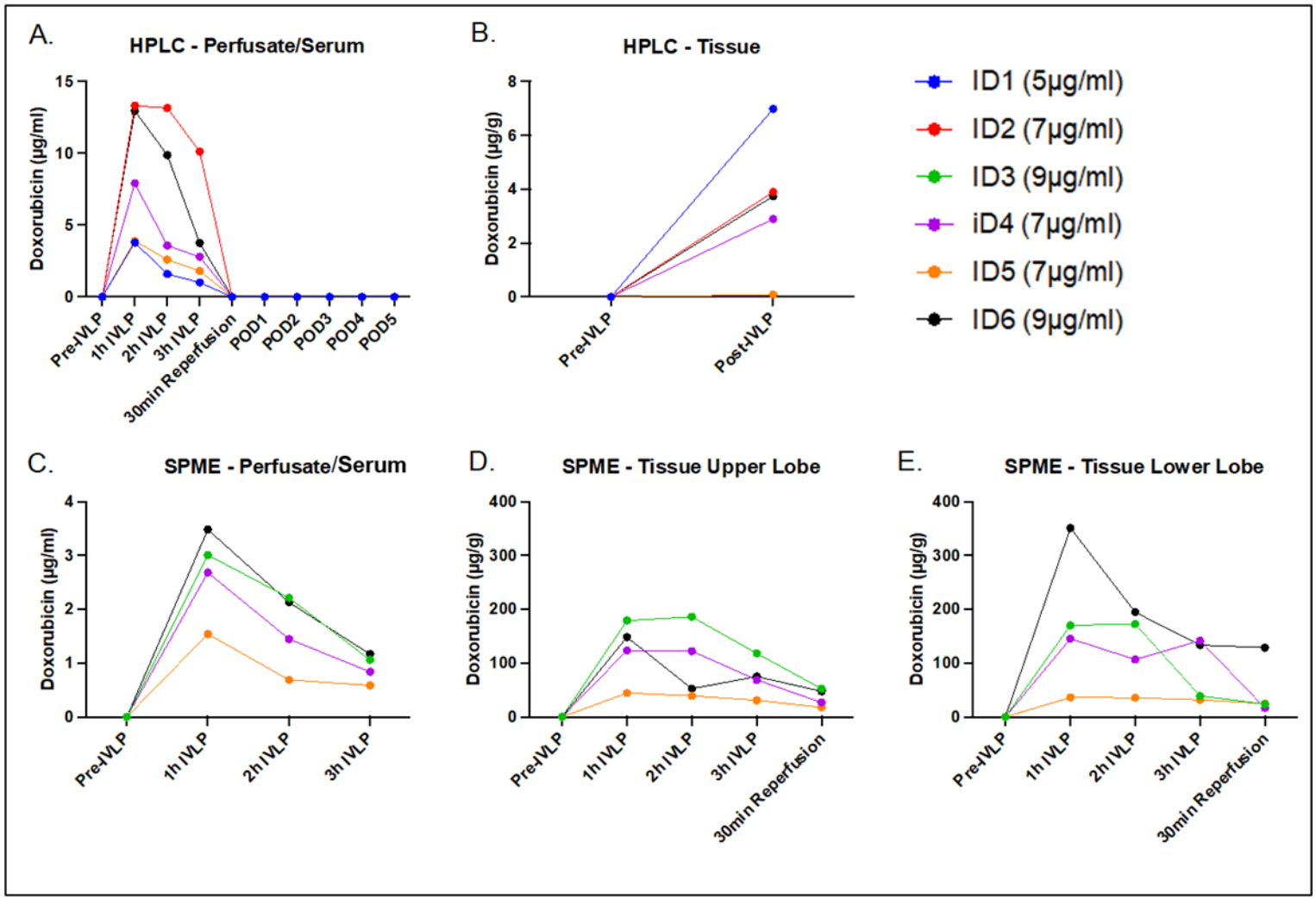


Figure 5.8 Doxorubicin levels in IVLP perfusate (including serum) and tissue. (A – B) determined via standard procedure: solvent extraction of lung tissue biopsies/perfusate, protein precipitation and filtration, HPLC. (C – E) determined by in vivo SPME-LC-MS.

5.5 Conclusion

When implementing novel analytical techniques in clinical applications, many additional considerations must be considered from a medical perspective. Patient safety, surgical complications, and ease of implementation must be satisfied while maintaining analytical accuracy and precision (reliability). In this study, quantitative chemotherapeutic drug monitoring of DOX during open-lung IVLP surgery was easily accomplished with SPME probes in vivo. Few key sampling parameters that had been overlooked in prior studies were addressed in this study; namely, deactivation of the SPME coating via autoclaving, sampling temperature, and analyte biostability were identified as major causes for prior reported underestimations. When applied properly, in vivo SPME is a reliable tool that is drastically simpler and quicker than standard procedures involving protein precipitation and filtration. Rapid analyses have enormous potential in point-of-care diagnostics by providing immediate and accurate feedback, suggesting a promising future for in vivo SPME research.

Chapter 6. Thesis conclusion and future perspectives

6.1 Thesis conclusion

In vivo SPME, the most recent and novel application of SPME technology, continues to observe rapid growth in terms of theoretical and practical considerations as it expands in biomedical fields of applications. This thesis encompassed theoretical, practical, and innovative elements of biomedical applications of SPME with a focus on in vivo applications of bio-SPME. The biggest challenges associated with bio-SPME over conventional fields of SPME applications, such as food and environment, include substantially more complex biological matrices, scarcity of biological (especially clinical) samples, and patient safety (for in vivo SPME). Chapter 1 provided a condensed review of the fundamentals of SPME, including the thermodynamics and kinetics that govern its extraction mechanisms (net mass transfer of analytes from the sample matrix to the extraction phase). Chapter 1 also reviewed key factors that must be considered in in vivo SPME applications for analysis of targeted and untargeted analytes in biological matrices. Namely, minimal invasiveness, physicochemical inertness, biocompatibility, balanced analyte coverage, and a suitable calibration method are key criteria for a successful bio-SPME application. Chapter 2 entails a comprehensive strategy for in vivo SPME applications; a novel recessed bio-SPME chemical biopsy device was developed along with a wettable chemical extraction phase that forgoes solvent activation, thus making it autoclave-compatible. The device can be safely inserted into most types of tissue, exerting minimal damage to the patient organ/tissue, while the extraction sorbent remains

protected from damage within the recess. The bio-SPME probe can also be assembled into a microsyringe capable of aqueous phase extraction to obtain complementary information on highly polar analytes, which often partition poorly to the SPME coating. Promising clinical and preclinical data demonstrated the suitability of the probe for targeted quantifications in vivo. Proof-of-concept studies also revealed the potential for untargeted analysis when employing both wHLB and PBS extraction phases in the format of in vivo push-pull SPME microsyringe. Chapter 3 presented a proof-of-concept study demonstrating the advantages of non-destructive sampling via bio-SPME over conventional destructive sampling techniques such as liquid extraction. Obvious changes to the metabolomic profile were observed when a tissue sample was homogenized to permit liquid extraction. Particularly, the released membrane lipids were detected in great abundance, which is unrepresentative of the physiological environment. As such, minimally invasive in vivo sampling is key to attainment of realistic biological data. In Chapter 4, a proteomics study via bio-SPME was presented for the first time in a clinical application. Numerous Trypsin-digested peptides of endogenous and proteins were consistently extracted via a porous C18/PAN sorbent in all human saliva samples. Tryp peptides of many other endogenous and SARS-CoV-2 proteins were also detected in the majority of samples. In addition, future bio-SPME studies can potentially take advantage of sampling at the source to potentially function as a rapid screening technique for diseases such as COVID-19. Further increasing the porosity of the coating and/or other extraction phases should be investigated to perform

peptidomics/proteomics in lieu of Tryp digestion. By implementing point-of-care extraction in situ, bio-SPME reduces the risk of infection for medical staff who would otherwise need to handle biohazardous biofluids. Lastly, Chapter 5 critically reviewed current in vivo SPME protocols involving therapeutic drug monitoring and MMC and identified major flaws that directly caused erroneous results in prior in vivo SPME studies. SPME sorbent performance, sampling temperature, and analyte biostability were identified as crucial parameters that were overlooked by the authors of prior studies. Updated MMC and new clinical results were in full agreement with conventional laboratory tests presented in prior studies when accounting for the aforementioned extraction parameters. Experiments conducted in Chapters 3-5 took place during the development of the devices presented in Chapter 2, thus different SPME devices were used. The new and improved devices from Chapter 2 shall be used for future biomedical applications. In short, in vivo SPME is a powerful sample preparation and extraction technique for rapid analysis of targeted and untargeted analytes in a plethora of potential biomedical applications. In vivo SPME is truly unique in its ability to extract a multitude of unaltered information while being one of the least invasive sampling techniques.

6.2 Future perspectives

There are currently multiple clinical applications planned or underway using the recessed bio-SPME wHLB/PAN chemical biopsy probe and/or the push-pull SPME microsyringe described in Chapter 2. For example, the current diagnostic practice for malignant hyperthermia (MH) relies on physical biopsies

taken from the patient's thigh muscle to a stress test. However, a sizable portion of the thigh muscle is required to ensure the accuracy of the test.[125] While this novel technique offers the possibility of diagnosing MH prior to surgery, where MH can cause fatality, it is quite traumatic to patients. The recessed bio-SPME probes are therefore a suitable tool to explore the possibility of biomarker screening and diagnostics in lieu of physical biopsies.

Numerous applications of in vivo SPME in brains of live animals and bio-SPME of human brain tumors have been successfully reported,[50,72,95] thus streamlining in vivo SPME in human brains as an expected next step for in vivo SPME. As shown in Chapter 2 of the thesis, the push-pull SPME microsyringe can provide complementary extraction of highly polar biomolecules such as neurotransmitters in addition to the extraction of nonpolar endogenous metabolites in which SPME excels. Certainly, the potential of in vivo SPME in the realm of neuroscience is exciting to contemplate.

In addition to untargeted analyses, targeted monitoring of therapeutic agents as well as known metabolite and peptide biomarkers in screening and diagnostics are also obvious future biomedical applications for in vivo SPME. When coupled with direct-MS and ambient-MS techniques such as MOI, direct analysis in real time (DART),[125] and coated blade spray (CBS),[126] the possibilities for rapid on-site screening via bio-SPME are endless.

On a separate note, applications of the SPME technology, including the devices described in this thesis, lead to environmentally friendly sampling/sample

preparation processes compared to conventional techniques, which aligns with our current trend toward a more sustainable future.

Letter of copyright permission

JA J. Pharm. Anal. <jpasubmit@126.com>
To: Runshan Will Jiang

Dear Dr. Runshan Will Jiang,

Yes. It is permitted. Please clearly show the source of the article.

Best regards
Mengjie Wang
Managing editor
Journal of Pharmaceutical Analysis

---- Replied Message ----

From	Runshan Will Jiang<rwjiang@uwaterloo.ca>
Date	11/10/2023 07:26
To	J. Pharm. Anal.<jpasubmit@126.com>, jpa2011@126.com<jpa2011@126.com>
Subject	Copyright permission for journal

Dear JPA editors,

I am an author for this manuscript published in the Journal of Pharmaceutical Analysis: https://doi.org/10.1016/j.jpha.2022.09.002

And I would like to obtain copyright access to publish contents from this journal article in my PhD thesis, please.

Thank you very much!
Will
--
Runshan (Will) Jiang
PhD Chemistry Candidate
MSc Environment
HBSc Biochemistry and Chemistry

Prof. Janusz Pawliszyn's Research Group
C2-162, ESC - 223
Department of Chemistry, University of Waterloo
200 University Avenue West, Waterloo, ON, Canada (N2L 3G1)

References

1. Ginsburg GS, Willard HF. *Transl. Res.* **2009**, *154* (6), 277-287.
2. Jain KK. *Curr. Opin. Mol. Ther.* **2002**, *4* (6), 548-558.
3. Jain KK. *Technol. Cancer Res. Treat.* **2005**, *4*, 645-650.
4. Chen R, Snyder M. *Curr. Opin. Pharmacol.* **2012**, *12* (5), 623-628.
5. Xu G, Meng Z, Lin J, et al. *Sci. Rep.* **2016**, *6,* 16937.
6. Lord HL, Zhang X, Musteata FM, et al. *Nat. Protocols.* **2011**, *6* (6), 896-924.
7. Singh S, Podder PS, Russo M, et al. *Lab Chip*. **2023**, *23*, 44-61.
8. Gonzalez-Riano C, Dudzik D, Garcia A, et al. *Anal. Chem.* **2020**, *92* (1)*,* 203-226.
9. Dettmer K, Aronov PA, Hammock BD. *Mass. Spectrom. Rev.* **2007**, *26* (1), 51-78.
10. Feider CL, Krieger A, DeHoog RJ, et al. *Anal. Chem.* **2019**, *91* (7), 4266-4290.
11. Grankvist R, Chireh A, Sandell M, et al. *Sci. Rep.* **2020**, *10*, 8029. 11; 5.
12. Hayot M, Michaud A, Koechlin C, et al. *Eur. Respir. J*. **2005**, *25*, 431-440.
13. Newmire DE, Willoughby DS. *Scand. J. Med. Sci. Sports.* **2022**, *32* (11), 1550-1568.
14. Bito L, Davson H, Levin E, et al. *J. Neurochem*. **1966**, *13* (11), 1057-1067.
15. Benveniste H, Huttemeier PC. *Prog. Neurobiol.* **1990**, *35* (3), 195-215.
16. Marchand S, Chauzy A, Dahyot-Fizelier C, et al. *Pharmacol. Res. Commun.* **2016**, *111*, 201-207.

17. Boyaci E, Lendor S, Bojko B, et al. *Chem. Neurosci.* **2020**, *11* (22), 3749-3760.

18. Schafer KC, Denes J, Albrecht K, et al. *Angew.* **2009**, *48* (44), 8240-8242.

19. Dumitru D, Douek M, Benson JR. *Ecancermedicalscience.* **2018**, *12* (795), PMC5804713

20. Hanel L, Kwiatkowski M, Heikaus L, *Future Sci. OA*. **2019**, *5* (3), FSO373.

21. Phelps DL, Balog J, Gildea LF, et al. *Br. J. Cancer.* **2018**, *118* (10), 1349-1358.

22. Haapala I, Karjalainen M, Kontunen A. *J. Neurosurg.* **2019**, *133* (1), 100-106.

23. Pawliszyn J. Handbook of solid phase microextraction. **2011**, *Elsevier*.

24. Vuckovic D, de Lannoy I, Given B, et al. *Angew.* **2011**, *50* (23), 5344-5348.

25. Reyes-Garces N, Gionfriddo E, Gomez-Rios GA, et al. *Anal. Chem.* **2018**, *90* (1), 802-860.

26. Alam MN, Ricardez-Sandoval L, Pawliszyn J. *Ind. Eng. Chem.* **2017**, *56* (13), 3679-3686.

27. Chen Y, Pawliszyn J. *Anal. Chem.* **2004**, *76* (19), 5807-5815.

28. Vuckovic D. *Trends Analy. Chem.* **2013**, *45*, 136-153.

29. Poole JJ, Grandy JJ, Yu M, et al. *Anal. Chem.* **2017**, *89* (15), 8021-8026.

30. Ai J. *Anal. Chem.* **1997**, *69* (6), 1230-1236.

31. Ouyang G, Vuckovic D, Pawliszyn J. *Chem. Rev.* **2011**, *111* (4), 2784-2814.

32. Napylov A, Reyes-Garces N, Gomez-Rios G, et al. *Angew*. **2019**, *59* (6), 2392-2398.

33. Ulvik A, McCann A, Midttun O, et al. *Anal. Chem.* **2021**, *93* (21), 7616-7624.

34. Jiang RW, Jaroch K, Pawliszyn J. *J. Pharm. Anal.* **2023**, *13* (1), 55-62.

35. Roszkowska A, Tascon M, Bojko B, et al. *Talanta*, **2018**, *183* (1), 304-310.

36. Bojko B, Looby N, Olkowicz M, et al. *J. Pharm. Anal.* **2021**, *11* (1), 37-47.

37. Mirnaghi FS, Mousavi F, Rocha M, Pawliszyn J. *J. Chromatogra. A.* **2013**, *1276*, 12-19.

38. Mousavi F, Gionfriddo E, Carasek E, et al. *Metabolomics*. **2016**, *12*, 1-13.

39. Peltenburg H, Bosman IJ, Hermens JLM. *J. Pharm. Biomed. Anal.* **2015**, *115* (10), 534-542.

40. Reyes-Garces N, Boyaci E, Gomez-Rios GA, et al. *J. Chromatogr. A.* **2021**, *1638*, 461862.

41. Khaled A, Gionfriddo E, Acquaro V, et al. *Anal. Chim. Act.* **2019**, *1056*, 34-46.

42. Alam MN, Pawliszyn J. *Anal. Chem.* **2016**, *88* (17), 8632-8639.

43. Wieczorek MN, Zhou W, Pawliszyn J. *Food Chem.* **2022**, *389*, 133038.

44. Risticevic S, Pawliszyn J. *Anal. Chem.* **2013**, *85* (19), 8987-8995.

45. Alam MN, Pawliszyn J. *Anal. Chem.* **2018**, *90* (4), 2430-2433.

46. Kubo T, Furuta T, Johan MP, et al. *Medicine*. **2018**, *97* (29), e11567.

47. Bang JY, Kirtane S, Krall K, et al. *J. Dig. Endosc.* **2019**, *31* (2), 197-202.

48. David A, Rostkowski P. Environmental Metabolomics. **2020**, *Elsevier.*

49. Reyes-Garces N, Bojko B, Hein D, et al. *Anal. Chem.* **2015**, *87* (19), 9722-9730.

50. Lendor S, Hassani SA, Boyaci E, et al. *Anal. Chem.* **2019**, *91* (7), 4896-4905.

51. Dos Santos PR, Sakamoto J, Chen M, et al. *Ann. Thorac. Surg.* **2016**, *101* (6), 2132-2140.

52. Rogers WJ. Steam and dry heat sterilization of biomaterials and medical devices. *Sterilisation of Biomaterials and Medical Devices*. **2012**, *Woodhead Publishing.*

53. Grandy JJ, Singh V, Lashgari M, et al. *Anal. Chem.* **2018**, *90* (23), 14072-14080.

54. Thirukumaran M, Singh V, Arao Y, et al. *Talanta*. **2021**, *231*, 122317.

55. Lewis FM, Walling C, Cummings W, et al. *J. Am. Chem. Soc.* **1948**, *70* (4), 1519-1523.

56. Soh SK, Sundberg DC. *J. Polym. Sci.* **1982**, *20* (5), 1299-1313.

57. Kilambi H, Beckel ER, Berchtold KA, Stansbury JW, et al. *Polymer*. **2005**, *46* (13), 4735-4742.

58. Wei S, Mizaikoff B. *J. Sep. Sci.* **2007**, *30* (11), 1794-1805.

59. Ehrsson H, Wallin I, Yachnin J. *Med. Oncol.* **2002**, *19*, 261-265.

60. Shafirstein G, Bellnier D, Oakley E, et al. *Cancers*. **2017**, *9* (2), 12.

61. Khaled A, Belinato JR, Pawliszyn J. *Talanta*. **2020**, *217*, 121095.

62. Zhou W, Nazdrajic E, Pawliszyn J. *Anal. Chem.* **2023**, *95* (15), 6367-6373.

63. Zou R, Cao W, Chong L, et al. *Anal. Chem.* **2019**, *91* (1), 1157-1163.

64. Sangster JM. Octanol-Water Partition Coefficients: Fundamentals and Physical Chemistry (Vol. 1). **1997**, *John Wiley & Sons.*

65. Nägele T. *Front. Mol. Biosci.* **2014,** *1*, 22.

66. Roszkowska A, Yu M, Bessonneau V, et al. *Sci. Rep.* **2018***, 8* (1), 6980.

67. Yu M, Lendor S, Roszkowska A, et al., *Anal. Chim. Acta.* **2020**, *1136*, 42-50.

68. Hernandes VV, Barbars C, Dudzik D. *Electrophoresis.* **2017**, 38 (18), 2232-2241.

69. Boyaci E, Bojko B, Reyes-Garcés N, et al. *Sci. Rep.* **2018**, *8* (1), 1167.

70. Burlikowska K, Stryjak I, Bogusiewicz J, et al. *Metabolites*. **2020**, *10* (6), 255.

71. Hassani SA, Lendor S, Neumann A, et al. *Biol. Psychiatry. Global open Sci.* **2021**, *3* (1), 68-77.

72. Bogusiewicz J, Burlikowska K, Łuczykowski K, et al. *Sci. Rep.* **2021**, *11* (1), 19522.

73. Musteata F, de Lannoy I, given B, et al. *J. Pharm. Biomed. Anal.* **2008**, *47* (4-5), 907-912.

74. Musteata FM, Musteata ML, Pawliszyn J. *Clin. Chem.* **2006**, *52* (4), 708-715.

75. Gertsman I, Barshop BA. *J. Inherit. Metab. Dis.* **2018**, *41,* 355-366.

76. Thompson JW, Adams KJ, Adamski J. et al. *Anal. Chem.* **2019**, *91* (22), 14407-14416.

77. Zukunft S, Prehn C, Röhring C, et al. *Metabolomics*. **2018**, *14*, 1-12.

78. Huq M, Tascon M, Nazdrajic E, et al. *Anal. Chem.* **2019**, *91* (12), 7719-7728.

79. Law SH, Chan ML, Marathe GK, et al. *Int. J. Mol. Sci*. **2019**, *20* (5), 1149.

80. Indiveri C, Iacobazzi V, Tonazzi A, et al. *Mol. Asp. Med.* **2011**, *32* (4-6), 223-233.

81. North EJ, Osborne DA, Bridson PK, et al. *Bioorg. Med. Chem.* **2009**, *17* (9), 3433-3442.

82. Mansour FR, Wei W, Danielson ND. *Biomed. Chromatogr.* **2013**, *27* (10), 1339-1353.

83. Rinaldo P, Cowan TM, Matern D. *Genet. Med.* **2008**, *10* (2), 151-156.

84. Kaplan MR, Simoni RD. *J. Cell Biol.* **1985**, *101* (2), 441-445.

85. Birjandi AP, Bojko B, Ning Z, et al. *J. Chromatogr. B.* **2017**, *1043*, 12-19.

86. Wu L, Yuan ZC, Yang BC, et al. *Anal. Chim. Acta.* **2021**, *1164*, 338510.

87. Huang C, Wang Y, Li X, et al. *The Lancet.* **2020**, *395* (10223), 497-506.

88. Kim H, Hong H, Yoon SH. *Radiology.* **2020**, *296* (3), E146-E155.

89. Yamayoshi S, Sakai-Tagawa Y, Koga M, et al. *Viruses*. **2020**, *12* (12), 1420.

90. Barrera-Avalos C, Luraschi R, Vallejos-Vidal E, et al. *Front. Public Health.* **2022**, *9*, 780801.

91. Sabino-Silva R, Jardim ACG, Siqueira WL. *Clin. Oral Investig.* **2020**, *24* (4), 1619-1621.

92. Marin LM, Katselis GS, Chumala P, et al. *Clin. Proteom.* **2023**, *20* (1), 30.

93. Pawliszyn J. Handbook of Solid Phase Microextraction. **2009**, *Chemical Industry Press*.

94. Caixeta DC, Oliveira SW, Cardoso-Sousa L, et al. *Front. Public Health.* **2021**, *9*, 589564.

95. Lendor S, Olkowicz M, Boyaci E, et al. *ACS. Chem. Neurosci.* **2020**, *11* (12), 1827-1840.

96. Roy A, De S. *J. Food. Eng.* **2014**, *126*, 7-16.

97. Onat B, Rosales-Solano H, Pawliszyn J. *Anal. Chem.* **2020**, *92* (13), 9379-9388.

98. Prasad B, Johnson K, Billington S, et al. *Drug Metab. Dispos.* **2016**, *44* (12), 1920-1924.

99. Mousavi F, Bojko B, Pawliszyn J. *Anal. Chim. Acta.* **2015**, *892*, 95-104.

100. Rabenau HF, Cinatl J, Morgenstern B, et al. *Med. Microbiol. Immunol.* **2005**, *194*, 1-6.

101. Kozlowski LP. *Biol. Direct.* **2016**, *11* (1), 1-16.

102. Calado G, Behl I, Byrne HJ, et al. *Clinic. Spec.* **2021**, *3*, 100010.

103. de Carvalho Abrão LC, Figueiredo EC. *Analyst*, **2019**, *144* (14), 4320-4330.

104. McBride R, Fielding BC. *Viruses*. **2012**, *4* (11), 2902-2923.

105. Paterson E, Paterson NAB, Ferris LJ. *Anaesthesia*, **2022**, *78* (2), 197-206.

106. Marques-Medeiros AC, Martins RC, Souza LND, et al. *Braz. Oral Res.* **2023**, *37*, e060.

107. Vuckovic D, Risticevic S, Pawliszyn J. *Angew*. **2011**, *50* (25), 5618-5628.

108. Zhou W, Wieczorek MN, Jiang RW, et al. *J. Pharm. Anal.* **2023**, *13* (2), 216-222.

109. Zhan X, Long Y, Lu M. *J. Proteom.* **2018**, *188*, 30-40.

110. Pastorino U, Buyse M, Friedel G, et al. *J. Thorac. Cardiovasc. Surg.* **1997**, *113* (1)*,* 37-49.

111. Predina JD, Puc MM, Bergey MR, et al. *J. Thorac. Oncol.* **2011**, *6* (5), 913-919.

112. Weiser MR, Downey RJ, Leung DH, et al. *J. Am. Coll. Surg.* **2000**, *191* (2), 184-190.

113. Nevala R, Jaamaa S, Tukiainen E, et al. *J. Surg. Oncol.* **2019,** *120* (2), 168-175.

114. Smith R, Pak Y, Kraybill W, et al. *Eur. J. Surg. Oncol. (EJSO).* **2009**, *35* (4), 356-361.

115. Cypel M, Keshavjee S. *Thorac. Surg. Clin.* **2016**, *26* (2), 139-145.

116. dos Santos PR, Iskender I, Machuca T, et al. *J. Thorac. Cardiovasc. Surg.* **2014**, 147 (2), 774-782.

117. Hutchinson JP, McKeever TM, Fogarty AW, et al. *Eur. Respir. J.* **2016**, *48* (5), 1453-1461.

118. Ramadan K, Gomes B, Pipkin M, et al. *J. Thorac. Cardiovasc. Surg.* **2021**, *161* (5), 1626-1635.

119. Vuckovic D, Zhang X, Cudjoe E, et al. *J. Chromatogr. A.* **2010**, *1217* (25), 4041-4060.

120. Hewavitharana AK. *J. Chromato. A.* **2011**, *1218* (2), 359-361.

121. Lin Q, Zhang M, Kong Y, et al. *Heliyon*. **2023**, *9* (3), e13811.

122. Gong J, Yan J, Forscher C, et al. *Drug Des. Devel. Ther.* **2018**, *12*, 777-786.

123. Raoul JL, Heresbach D, Bretagne JF, et al. *Cancer.* **1992**, *70* (3), 585-590.

124. Figueroa L, Kraeva N, Manno C, et al. *Br. J. Anaesth.* **2023**, *131* (1), 47-55.

125. Watt L, Sisco E. *J. Forensic Sci.* **2021**, *66* (1), 172-178.

126. Gomez-Rios GA, Tascon M, Pawliszyn J. *Bioanal.* **2018**, *10* (4), 257-271.

127. Karki I, Li P, Vik EC, et al. *React. Funct. Polym.* **2021**, 163, 104888.

128. Olkowicz M, Rosales-Solano H, Ramadan K, et al. *Cell Dev. Biol.* **2022**, 10, 928152.